

Aus dem Institut für Aktive Polymere Helmholtz-Zentrum Hereon

# Digital tools and bioinspiration for the implementation in science and medicine

zur Erlangung des akademischen Grades

”Doktor-Ingenieur”

(Dr.-Ing.)

in der Wissenschaftsdisziplin

”Materialien in den Lebenswissenschaften”

Kumulative Dissertation

eingereicht an der

Mathematisch-Naturwissenschaftlichen Fakultät der Universität Potsdam

von Johan Dag Valentin Bäckemo

**Tag der Disputation: 02.12.2022**

 **Helmholtz  
Graduate School**  
Macromolecular Bioscience



Day of disputation: 2<sup>nd</sup> of December 2022

1 <sup>st</sup> Supervisor	PD Dr. Axel Neffe	University of Potsdam
2 <sup>nd</sup> Supervisor and reviewer	Prof. Friedrich Jung	Brandenburg Technical University
Reviewers	Prof. Pablo Valdivia	Singapore University of Technology and Design
	y Alvarado Engineering	Product Deelopment, Singapore
	Prof. Jerry Qi	Georgia Institute of Technology
		School of Mechanical Engineering, USA
Thesis committee member	Prof. André Laschewsky	University of Potsdam
Thesis committee chairman	Prof. Andreas Taubert	University of Potsdam

Published online on the  
Publication Server of the University of Potsdam:  
<https://doi.org/10.25932/publishup-57145>  
<https://nbn-resolving.org/urn:nbn:de:kobv:517-opus4-571458>

## Statement of Authenticity

I, Johan Bäckemo, formally submit my PhD dissertation entitled “Digital tools and bioinspiration for the implementation in science and medicine” to the Institute of Chemistry, Faculty of Mathematics and Natural Sciences of the University of Potsdam, Germany, for the acquirement of the academic degree of Doctor of Engineering (Dr.-Ing.).

I hereby declare that the work presented in this dissertation is my own original work based on the research carried out at Helmholtz-Zentrum Hereon, Institute of Active Polymers in Teltow, Germany, from November 2016 to September 2021 under the supervision Prof. Andreas Lendlein and of PD Dr. Axel Neffe. To the best of my knowledge and belief, this dissertation does not contain any work previously published or written by another person, except where due reference is made in it. No portion of this work has been previously submitted in the support of any other degree to another university or institute. Any contribution made by other co-workers to this research is explicitly acknowledged in the dissertation.

Johan Bäckemo

Date and Signature

*14<sup>th</sup> of December 2022*

## List of Abbreviations

**EDM** Electrical Discharge Machining

**SEM** Scanning Electron Microscopy

**CBCM** Chained Beam Constraint Model

**PEVA** Poly[ethylene-*co*-(vinyl acetate)]

**FEA** Finite Element Analysis

**PMMA** poly(methyl methacrylate)

**GI** gastrointestinal tract

**PRBM** Pseudo Rigid Body Model

**BCM** Beam Constraint Model

**AM** Additive Manufacturing

**MEMS** Micro-Electromechanical Systems

**CUDA** Compute Unified Device Architecture

**MRR** Material Removal Rate

**BAFD** Biomimetic Alternative Fixation Device

**GPU** Graphical Processing Unit



## List of Symbols

$V_{SC}$	Expected volume of spherical cap
$V'_{SC}$	Actual volume of spherical cap
$L_{SC}$	Correction height
$x$	Position
$\kappa$	Curvature
$v$	Velocity
$\vec{N}$	Normal vector
$\vec{T}$	Tangent vector
$S$	Path in $2D$ and Surface in $3D$
$C$	Curve
$p$	Point
$\vec{t}$	Tangent unit vector
$\vec{n}$	Normal unit vector
$\vec{k}_n$	Normal curvature vector
$\vec{k}_g$	Geodesic curvature vector
$\alpha$	Initial slope value
$\omega$	Deflection in the $y$ -direction
$I$	Second moment of inertia
$E$	Young's modulus
$G$	Shear modulus
$\kappa_t$	Timoshenko shear coefficient

## List of Figures

1	Electrical Discharge Machining (EDM) schematic . . . . .	2
2	Scanning Electron Microscopy (SEM) image of an EDM treated surface . . . . .	3
3	Schematic of impact model for EDM process . . . . .	4
4	Curvature schematic $\in \mathbb{R}^2$ . . . . .	4
5	Schematic of a plane surface $\in \mathbb{R}^3$ . . . . .	5
6	Vector-valued function $r(u, v)$ on surface $S$ . . . . .	6
7	Parts of the <i>Taenia Solium</i> . . . . .	9
8	Euler and Timoshenko beam theories . . . . .	11
9	Bi-stable shuttle . . . . .	13
10	EDM volume correction . . . . .	25

# Contents

<b>List of Abbreviations</b>	<b>iv</b>
<b>List of Symbols</b>	<b>v</b>
<b>List of Figures</b>	<b>vi</b>
<b>Acknowledgements</b>	<b>ix</b>
<b>Abstract</b>	<b>xi</b>
<b>Zusammenfassung</b>	<b>xiii</b>
<b>1 Introduction</b>	<b>1</b>
1.1 Electrical Discharge Machining (EDM)	1
1.1.1 Physical principles	1
1.1.2 Modelling of EDM	1
1.2 Curvature	2
1.2.1 Curvature Analysis	2
1.2.2 Curvature in three dimensions	3
1.3 Biomimicry	7
1.3.1 Venus flytrap	8
1.3.2 Tapeworm	8
1.4 Bi-stable mechanics	10
1.4.1 Euler and Timoshenko beam theories	10
1.4.2 Bi-stability models	12
<b>2 Motivation, Aims and Strategy</b>	<b>14</b>
2.1 Motivation	14
2.2 Aims and Hypotheses	14
2.3 Strategies and concept	15
<b>3 Organization of thesis</b>	<b>17</b>
<b>4 Predictive topography impact model for Electrical Discharge Machining (EDM) of metal surfaces</b>	<b>18</b>
4.1 Summary	18
4.2 Contribution to the publication	18
4.3 Publication - Appendix I	19

<b>5 Bio-inspired and computer-supported design of modulated shape changes in polymer materials</b>	<b>20</b>
5.1 Summary . . . . .	20
5.2 Contribution to the publication . . . . .	20
5.3 Publication - Appendix II . . . . .	21
<b>6 A Biomimetic Alternative bi-modular bi-stable fixation Device (BAFD)</b>	<b>22</b>
6.1 Summary . . . . .	22
6.2 Contribution to the publication . . . . .	22
6.3 Publication - Appendix III . . . . .	23
<b>7 Discussion</b>	<b>24</b>
7.1 EDM models . . . . .	24
7.2 Curvature analysis . . . . .	25
7.3 Bioinspired design . . . . .	26
7.3.1 Design methodology . . . . .	26
7.3.2 Applications of design . . . . .	27
7.3.3 Challenges of manufacturing . . . . .	28
7.4 Compliant mechanisms . . . . .	29
7.4.1 Non-linear mechanical models . . . . .	29
7.5 Application of compliant mechanisms . . . . .	30
7.6 Programming challenges . . . . .	30
<b>8 Summary and conclusion</b>	<b>32</b>
<b>9 References</b>	<b>34</b>
<b>Appendix I Predictive topography impact model for Electrical Discharge Machining (EDM) of metal surfaces</b>	<b>44</b>
<b>Appendix II Bio-inspired and computer-supported design of modulated shape changes in polymer materials</b>	<b>57</b>
<b>Appendix III A Biomimetic Alternative bi-modular bi-stable fixation Device (BAFD)</b>	<b>70</b>
<b>Appendix IV Programmatic implementation</b>	<b>107</b>
<b>Appendix V CV</b>	<b>108</b>
<b>Appendix VI List of Publications</b>	<b>108</b>

## Acknowledgements

I would first like to acknowledge Prof. Andreas Lendlein for supervising the work of my thesis from November 2016 to September 2021, and I would like to thank my first supervisor PD Dr. Axel Neffe who supervised me for the remainder of the thesis and provided support during submission. I would also like to thank Hereon; an institution that fosters scientific excellence and provides world-class facilities. To my second supervisor and previous department leader at Hereon, Prof. Friedrich Jung, I would like to thank for the great working environment you created in your department and the interesting discussions you led. I always felt respected as an equal and to have someone like you to appreciate my work and to review it means a lot.

In addition I would also like to thank Prof. Jerry Qi and Prof. Pablo Valdivia y Alvarado for agreeing to review my thesis. To Prof. Qi I would like to say that I found your scientific research and your visit in Teltow a highlight, and your work regarding new implementations of additive manufacturing really inspiring. To Prof. Valdivia I would like to thank you for your interesting talks and discussions we had meeting in Teltow and the MRS 2019 Winter conference in Boston. Your work in soft robotics and biomimicry gave me the push to keep on working on my topics. Furthermore I would like to thank Prof. Andreas Taubert for agreeing to be the head of the thesis committee and aiding me together with PD DR. Axel Neffe in the slightly challenging submission process. Also, a big thank you to Prof. André Laschewsky agreeing to being on my thesis committee.

To work at Hereon there were at times taxing periods, but there were some people that made the time so much more enjoyable and have also become long-time friends in the process. Dr. Markus Reinthaler thank you for the great insight into the clinic and the energy you brought to the work. Dr. Manfred Gossen, thank you for your effort to help me navigate myself through my thesis. I would want to thank Dr. Matthias Heuchel for having great personal and scientific discussions, to me you were like a mentor. Dr. Victor Izraylit, Dr. Natalia Tarazona, and Dr. Rainhard Machatschek - you have given me a lot of scientific advice throughout the years and made laugh out loud more than I can count. Mark Schröder, you have been my office mate throughout the years and you have always been there to help when it came to any engineering problems and always provided support. Dr. Johannes Großhauser, you were the postdoc mentor I never had but wish I would have - your insight, industrial knowledge and positive attitude really spurred me on. Dr. Yue Liu, thank you for being a great scientific partner. Dr. Steffen Braune, I thank you for being a great mentor and for creating a scientific climate which was focused on respect and discourse - you set the standard high. Richard Alfranseder, Cristiane Henschel, Nino Chirico, Dr. Marisa Assunção, and Dr. Nadia Brunacci you were all there from the beginning and

have been through it all, I am very lucky to have such compassionate and lovely friends in my life.

To my family in-laws the Seitz family: Ulrike, Thorsten, Björn, Sonja, Arno and Annabell, you have provided so much love, empathy and support throughout these years when you are near I feel like I am at home. To my dad Klas Johansson, to my mother Margareta Bäckemo and to my sister Louise Bäckemo-Johansson you have literally, figuratively, and emotionally been through it all and without you there would be no thesis - I love you all so much.

To you Franziska Bäckemo. You have seen all the happy, stressful, ugly, devastating, and joyous moments throughout this whole thing. With you by my side, you have meant everything. You are the one who has more than once spurred me on to not give up, and to push on to finish at the most critical of moments. When you are near music is all around. I love you.

## Abstract

Biomimicry is the art of mimicking nature to overcome a particular technical or scientific challenge. The approach studies how evolution has found solutions to the most intricate problems through the permutations and mutations of different species. This makes it a powerful method for science. In combination with the rapid development of manufacturing and information technologies into the digital age, structures and material combinations that seemed to be unrealistic a few decades ago can now be realized. This doctoral thesis had as its primary goal to investigate how digital tools, such as programming, modelling, 3D-Design tools and additive manufacturing, in conjunction with a design strategy founded in biomimicry, could lead to new analysis methods and devices to be applied in science and medicine. This will be demonstrated by the following three projects:

The Electrical Discharge Machining (EDM) process is applied commonly to deform or mold hard metals that are cumbersome or implausible to manufacture or process with other subtractive manufacturing processes. A work-piece submerged in an electrolyte is deformed while being in close vicinity to an electrode. When high voltage is put between the work-piece and the electrode it will cause sparks that create cavitations on the substrate which in turn removes material and is flushed away by the electrolyte. In order to further the topographical analyses usually applied to EDM-treated substrates, such as roughness analysis, this work investigates how a novel curvature analysis method could characterize the deformed state of the substrate and the topographical changes during the process. A phenomenological model based on the EDM process was devised that deformed the substrate through an impact model, which allowed to quasi-temporally analyse the substrate and how it changes over time by applying the curvature analysis method. Using this approach the model produced surfaces similar to that of actual deformed samples with a crater and a ridge of material formed from ejected material which re-solidified. The curvature analysis showed that the parameter reduced peak concavity curvature  $S_{pk}$  reached an equilibrium between  $10^3$  and  $10^4$  impacts. In terms of potential applications, curvature analysis may be used to evaluate fatigue limits for machined parts and it has been seen that curvature may play an important role in blastocyst formation and this analysis could also be applied for substrates to be used for cell culture purposes.

By analysing the closing of the lobes of the Venus flytrap one could see that non-linear mechanics enabled the lobes to quickly snap shut after being stimulated. By applying the non-linear mechanical model Chained Beam Constraint Model (CBCM) for the development of a bi-stable structure, there were two truncated tetrahedral structures devised - one with a slope angle of  $30^\circ$  which was predicted to be mono-stable and one with a slope angle of  $45^\circ$  predicted to be bi-stable. The predictions were confirmed from mechanical tests and the

bi-stable structure showed a characteristic bi-stable behaviour with three equilibrium points, two stable and one unstable. Developing this idea further, by using the shape-memory polymer Poly[ethylene-co-(vinyl acetate)] (PEVA), the 30° structure was programmed to have a 45° slope angle. This enabled the structure to be bi-stable below the switching temperature of 70°C. Above this switching temperature, the structure changed its shape to a slope angle of 30° and became mono-stable. Here, we illustrated that a structure could achieve multi-functional properties by using geometrical properties to achieve bi-stability and material properties to switch between bi-stability and mono-stability.

The tapeworm is a parasite habiting in the intestine of mammals and birds. The tapeworms of the order of Cyclophyllidea are most commonly found in domesticated animals and are equipped with suckers on their sides to attach themselves to the villi of the intestine. Some species of the Taeniidae family are equipped with hooks on their scolex (head) which can be in- or evaginated. For the purpose of constructing medical devices in minimally invasive medicine, these two attachment mechanisms are interesting due to the nature of the attachments: suction (temporary) and penetration of hooks (permanent). In this work the switching between the two attachment mechanisms could be achieved through a bi-stable mechanism predicted by the CBCM. By using additive manufacturing, combining different materials and geometry could be used to tune the bi-stable mechanism. Here, the bi-stability was achieved through creating a truncated cone and by using digital polymer materials with a Young's modulus ranging from  $E = 2$  to 40 MPa (Shore A40 - A95) and a thickness variation of 0.5, 1.0, and 1.5 mm. From experimental work, the combination of the material with  $E = 10$  MPa (Shore A70) and a thickness of 1.0 mm was used. A prototype was devised and showed that, relative to gauge pressure, a pressure of  $\Delta P = 20$  kPa only achieved suction on the substrate. A pressure of  $\Delta P = 50$  kPa penetrated the hooks into the porcine tissue. This work illustrates the high applicability potential of a discrete two-step controlled attachment mechanism for use in minimally invasive medicine.

In summary, these three projects in this thesis display how digital tools and bioinspiration can work symbiotically to analyse, break down, and overcome scientific challenges and aiding the development of novel medical devices.



## Zusammenfassung

Der Begriff der Biomimetik bezeichnet das Vorgehen, bestimmte technische oder wissenschaftliche Problemstellungen durch Nachahmen der Natur zu lösen. Die Biomimetik untersucht, wie die Evolution durch Permutationen und Mutationen verschiedener Spezies Lösungen für komplexe Probleme gefunden hat. Das macht sie zu einer leistungsfähigen Methode für die Wissenschaft. In Verbindung mit der rasanten Entwicklung der Fertigungs- und Informationstechnologien im digitalen Zeitalter können heute Strukturen und Materialkombinationen realisiert werden, die vor einigen Jahrzehnten noch unrealistisch schienen. Diese Doktorarbeit untersucht anhand dreier Beispiele, wie digitale Werkzeuge wie Programmierung, Modellierung, 3D-Konstruktions-Werkzeuge und additive Fertigung in Verbindung mit einer auf Biomimetik basierenden Designstrategie zu neuen Analysemethoden und Produkten führen können, die in Wissenschaft und Medizin Anwendung finden.

Mit dem Verfahren des Electrical Discharge Machining (EDM) kann man harte Metalle verformen, die sich schwer mit anderen subtraktiven Fertigungsverfahren herstellen oder bearbeiten lassen. Ein Werkstück wird in einen Elektrolyten eingetaucht und verformt, und es wird eine Hochspannung zwischen dem Werkstück und der Elektrode angelegt. Dadurch entstehen Funken und es kommt durch Kavitation zu Materialabtrag. Üblicherweise werden die Oberflächen der so behandelten Werkstücke mittels topographischer Methoden analysiert (zum Beispiel Rauheitsanalyse). Diese Arbeit untersucht, wie eine neuartige Methode zur Krümmungsanalyse den verformten Zustand des Werkstücks und dessen topografische Veränderungen während des Prozesses charakterisieren kann. Es wurde ein phänomenologisches Modell auf der Grundlage des EDM-Prozesses entwickelt, bei dem das Werkstück durch ein Aufprallmodell verformt wird, das eine quasi-temporale Analyse des Werkstücks und seiner zeitlichen Veränderungen durch Anwendung der neuartigen Methode zur Krümmungsanalyse ermöglicht. Mit diesem Ansatz erzeugte das Modell Oberflächen, die denen von tatsächlich verformten Proben ähnelten: mit einem Krater und einem Kraterrand, der sich aus ausgestoßenem und wieder erstarrtem Material bildete. Die Krümmungsanalyse zeigte, dass der Parameter der reduzierten Spitzenkonkavitätskrümmung  $S_{pk}$  ein Gleichgewicht zwischen  $10^3$  und  $10^4$  Einschlägen erreichte. Was mögliche Anwendungen betrifft, so kann die Krümmungsanalyse zur Bewertung der Ermüdungsgrenzen für bearbeitete Werkstücke verwendet werden. Es hat sich außerdem gezeigt, dass die Krümmung eine wichtige Rolle bei der Blastozystenbildung spielen kann, und, dass diese Analyse auch für Substrate in der Zellkultur angewendet werden könnte.

Bei der Analyse des Schließmechanismus der Blätter der Venusfliegenfalle konnte man feststellen, dass die nichtlineare Mechanik es ermöglicht, dass die Blätter nach einer

Stimulation schnell zuschnappen. Mithilfe des nichtlinearen mechanischen Modells Chained Beam Constraint Model (CBCM) für die Entwicklung einer bistabilen Struktur wurden zwei abgestumpfte Tetraederstrukturen entwickelt: eine monostabile mit einem Neigungswinkel von  $30^\circ$  und eine bistabile mit einem Neigungswinkel von  $45^\circ$ . Die Vorhersagen wurden durch Versuche am mechanischen Modell bestätigt und die bistabile Struktur zeigte ein charakteristisches, bistabiles Verhalten mit drei Gleichgewichtspunkten: zwei stabilen und einem instabilen. In Weiterentwicklung dieser Idee wurde die 30-Grad-Struktur unter Verwendung des Formgedächtnispolymers Poly-(ethylen-co-vinylacetat) (PEVA) so programmiert, dass sie einen Neigungswinkel von  $45^\circ$  aufweist. Dadurch wurde die Struktur unterhalb der Schalttemperatur von  $70^\circ$  Grad Celsius bistabil. Oberhalb dieser Schalttemperatur änderte die Struktur ihre Form zu einem Neigungswinkel von  $30^\circ$  und wurde monostabil. Damit wurde gezeigt, dass eine Struktur multifunktionale Eigenschaften haben kann, indem sie sowohl geometrische Eigenschaften nutzt, um Bistabilität zu erreichen, als auch Materialeigenschaften, um zwischen Bistabilität und Monostabilität zu wechseln.

Die Bandwürmer der Ordnung Cyclophyllidea kommen am häufigsten bei Haustieren vor und sind mit Saugnäpfen an den Seiten ausgestattet, mit denen sie sich an den Darmzotten festsetzen. Einige Arten aus der Familie der Taeniidae haben Haken an ihrem Scolex (Kopf), die ein- oder ausgefahren werden können. Für die Konstruktion von Medizinprodukten in der minimalinvasiven Medizin sind diese beiden Mechanismen aufgrund der Art der Befestigung interessant: dem Saugen (vorübergehend) und Eindringen der Haken (dauerhaft). In dieser Arbeit konnte der Wechsel zwischen den beiden Befestigungsmechanismen durch einen bistabilen Mechanismus erreicht werden, der durch das CBCM vorhergesagt wurde. Mithilfe additiver Fertigung wurden verschiedene Materialien und Geometrien kombiniert, um den bistabilen Mechanismus zu optimieren. Die Bistabilität wurde durch die Schaffung eines Kegelstumpfs und die Verwendung von Materialien mit einem Elastizitätsmodul von  $E = 2$  bis  $40$  MPa (Shore A-Wert von 40-95) und einer Dicke von  $0,5$ ,  $1,0$  und  $1,5$  mm erreicht. Für die Experimente wurde ein Material mit  $E = 10$  MPa (Shore A 70) und einer Dicke von  $1,0$  mm verwendet. Damit wurde ein Prototyp gebaut, der sich bei einem Unterdruck von  $P = 20$  kPa an einer Oberfläche festsaugte. Eine Erhöhung des Unterdrucks auf  $P = 50$  kPa ließ die Haken in das Schweinegewebe eindringen. Diese Arbeit verdeutlicht das hohe Anwendungspotenzial eines diskreten, zweistufig gesteuerten Befestigungsmechanismus für den Einsatz in der minimalinvasiven Medizin.

Die drei vorgestellten Projekte zeigen beispielhaft wie Biomimetik, digitale Modellierung und neuartige additive Fertigungsverfahren eine leistungsfähige Kombination darstellen, die zur Weiterentwicklung wissenschaftlicher Berechnungs- und Analysemethoden sowie neuer Medizinprodukte beiträgt.

# 1 Introduction

## 1.1 Electrical Discharge Machining (EDM)

### 1.1.1 Physical principles

With any machining process the surface of the workpiece is modified to a certain extent; whether its waviness, cracks, or roughness, and they occur at different scales or orders [1]. In many cases this may be undesirable as fitting of work pieces usually depends on workpieces being machined exactly with smooth finishes. However, surface roughness may be desirable in fields such as dental and orthopedic implants to promote osseointegration [2] and has shown to improve implant fixation over time [3, 4, 5]. For surface roughness treatment there are many different options ranging from mechanical methods such as lathing, milling, threading, and sandblasting to chemical and electrochemical methods such as alkaline/acid etching, passivation, electropolishing, and anodization [6]. Electrical Discharge Machining (EDM) is an electro-chemical process which is able to deform metallic substrate with a high hardness value, such as Titanium, which is a significant advantage for medical equipment. An electrode, which is within close vicinity of the metallic surface has current flowing through the gap which builds up charge until a certain time point, at which the current is switched off and a spark is created. This occurs several thousands or millions of times during the process. There are many variations to the EDM process such as wire-EDM, die-sinking-EDM, and hole drilling-EDM. This thesis focuses on die-sinking-EDM. The spark in effect removes material from the metallic surface and the debris is removed by the flowing dielectric fluid [7] (see Figure 1). The process is usually initiated setting a desired roughness value. The process time is set so that the repeated removal of material through EDM sparks reached said roughness value. A significant benefit of the process, is that no physical contact is made between workpiece and electrode which removes any problems with mechanical stresses or vibrations [8]. Depending on the electrical input parameters (current, voltage, electrolyte) one can vary the final surface roughness [9]. The location of each spark on the surface can be assumed to be stochastic, and thus a model of the EDM process should imitate that.

### 1.1.2 Modelling of EDM

In order to optimize the surface treatment of EDM, modelling of the process would be beneficial. The resulting deformation on a metallic workpiece consists of three key events: (i) material removal, (ii) overlapping craters, and (iii) shape of the impact. For material removal (i): The resulting deformation on a metallic surface after the impact of one spark consists of heating of the material, loss of material that is washed away by the dielectric fluid, and the melted material debris left on the periphery which can be seen in Fig. 2. In addition, another crucial point is (ii)

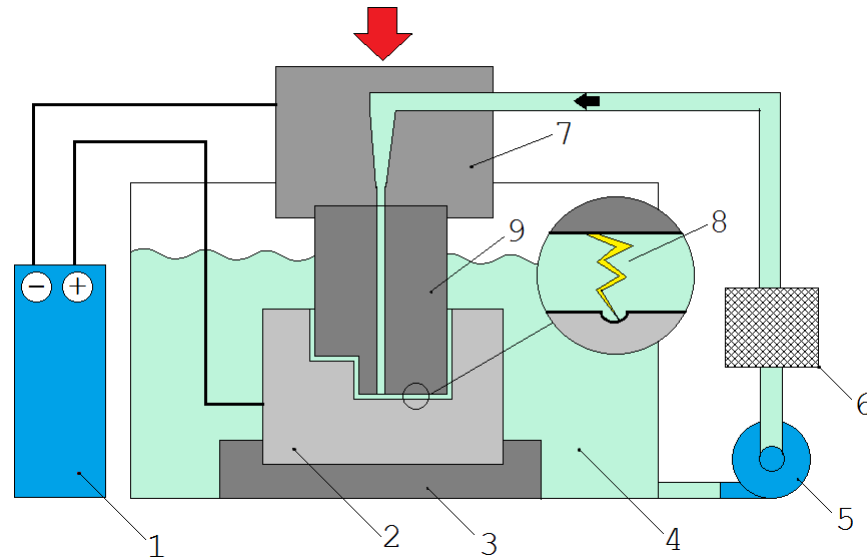


Figure 1: A schematic of the EDM process. 1 Pulse generator (DC), 2 Workpiece, 3 Fixture, 4 Dielectric fluid, 5 Pump, 6 Filter, 7 Tool holder, 8 Spark, 9 Tool. Image source: *"Electrical Discharging Machining scheme"* by Frank50 licensed under CC BY-SA 4.0

the overlapping of craters. There have been simpler anode-cathode models [10] which tries to find the optimum processing parameters with respect to cathode material, and there are thermal Finite Element Analysis (FEA) models [11, 12] that only consider single spark events. Overlapping craters have a direct impact on surface roughness [13] and thus, to model the substrate outcome of an EDM treatment, successive impacts should be included. Another aspect is (iii) the shape of the cross-section of the deformation after a single spark removes materials. Throughout an EDM process there may be millions of such impacts, which are compounded over time and creates a rough topography. Previously, researchers have used an ellipsoidal model [14], however there have also been simulation studies that have considered a more spherical shape with a bulging rim [15, 16]. The latter was used in order to consider the aspects that some material is ejected whereas some portion of the material melts but remains on the surface. This will be referred to as an impact model, which is illustrated in Figure 3. For a successive model, all three aspects have to be considered.

## 1.2 Curvature

### 1.2.1 Curvature Analysis

Considering the vast amount of options and methods there are to analyse roughness, there are equally many for considering curvature. Curvature,  $C$ , in 1-D space is defined as the deviation from some line, such as the curving of a circle. This could be defined as the reciprocal of some

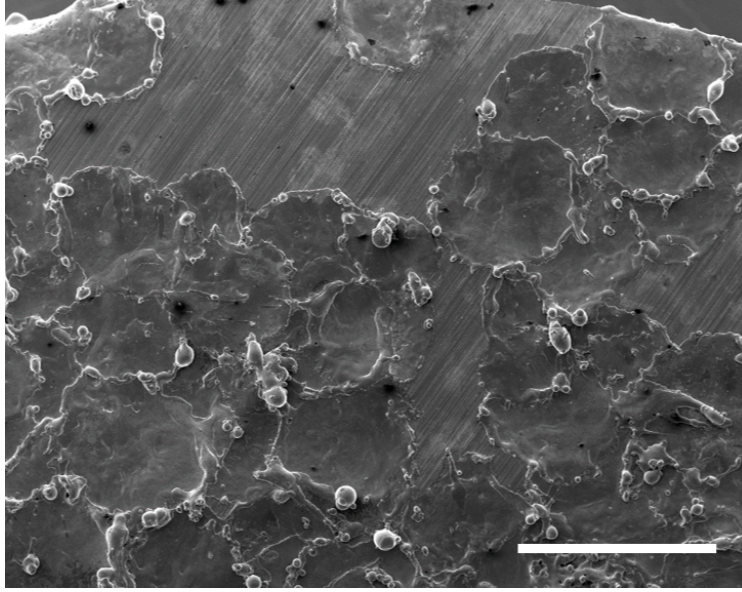


Figure 2: Scanning Electron Microscopy (SEM) image of an EDM treated surface. The appearance of crater-like structures is evident, as well as the unremoved material at the periphery of each impact. Scale bar = 1000  $\mu\text{m}$

radius  $r$

$$K = \frac{1}{r} \quad (1)$$

Consequently the units of curvature are in inverse length  $[L]^{-1}$ . It could be thought of the velocity of a point  $\in \mathbb{R}^2$ . Initially at timepoint  $t_0$  the point is at coordinate  $A$  with velocity  $v$ , and at a later timepoint  $t_1$  the point is at coordinate  $B$  with velocity  $v'$  (Fig. 4). If  $S$  denotes the path the point travels between  $A$  and  $B$  then curvature can be defined as:

$$\frac{d\vec{N}(S)}{dS} = \kappa\vec{T}(S) \quad (2)$$

Where  $\vec{N}$  denotes the normal perpendicular to the velocity vector, and  $\vec{T}$  is the tangent vector. Effectively at the limit for  $\frac{d\vec{N}}{dS}$  the direction will be  $\vec{N}$  and the speed of the rotation of the frame is  $\kappa$ . For points and curves  $\in \mathbb{R}^2$  the curvature is defined and its calculation is trivial. However, for planes and bodies  $\in \mathbb{R}^3$  the definition of curvature becomes more intricate.

### 1.2.2 Curvature in three dimensions

To consider curvature in 1D or 2D space is without greater ambiguity. When analysing planes and bodies  $\in \mathbb{R}^3$  one must take more parameters into consideration. First lets consider a 2D plane  $\in \mathbb{R}^3$ . A surface  $S$  exists in 3D space:  $S \in \mathbb{R}^3$  (See Fig. 5). On this surface consider a point  $p$

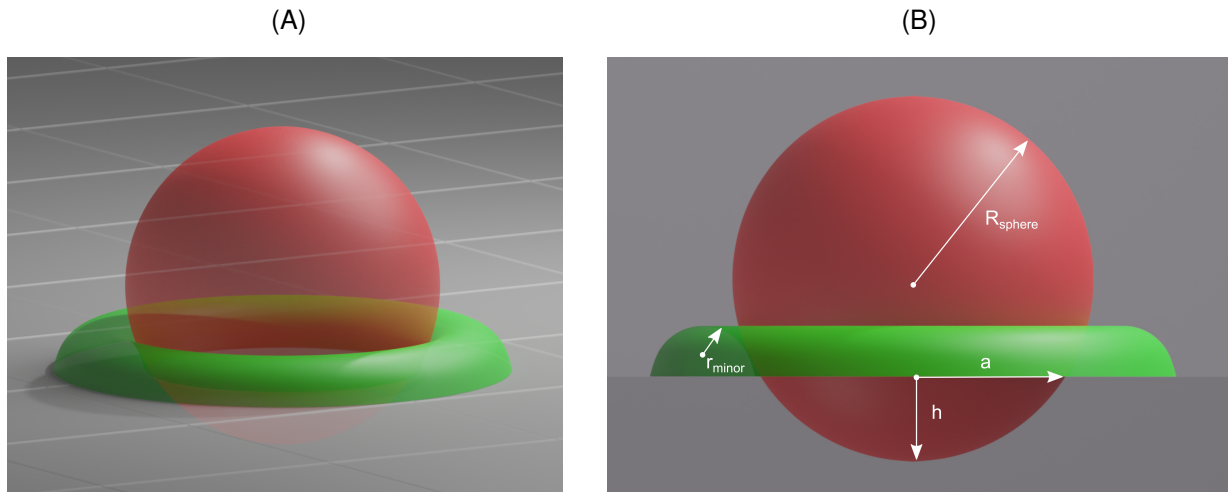


Figure 3: Schematic showing the impact model for a spark hitting a metallic surface during the EDM process. The colours denote material to remove (red) and to add (green). A) Profile view. B) Annotated view showing the relevant parameters.

that lies on this surface, and a curve  $C$  that goes through  $p$  on  $S$  in direction  $t$  which is defined as the unit tangent vector. Perpendicular to  $t$  and defined as the normal of  $S$  at  $p$  is the normal vector  $N$ . Furthermore,  $t$  and  $n$ , the unit normal vector of  $C$  at  $p$ , are related through the following expression:

$$\vec{k} = \frac{d\vec{t}}{dS} = \kappa\vec{n} = \vec{k}_n + \vec{k}_g \quad (3)$$

Where  $\vec{k}_n$  is the normal curvature vector parallel to the normal  $\vec{N}$ , and  $\vec{k}_g$  is the geodesic curvature vector, parallel to the tangent plane which is perpendicular to the normal  $\vec{N}$ . These are the

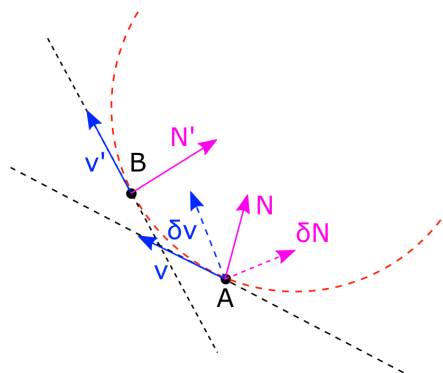


Figure 4: Schematic of a velocity vector changing direction in space



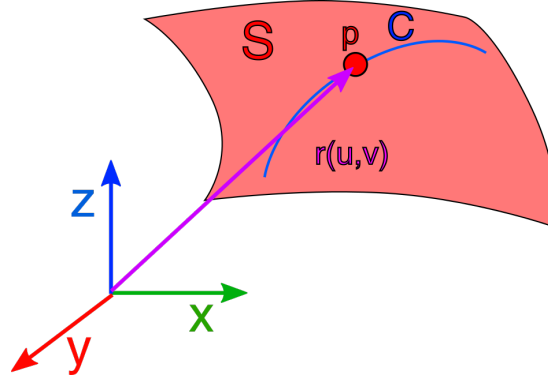


Figure 6: Schematic showing the vector-valued function  $r(u, v)$  defining the location of point  $p$  as a function of the lagrangian surface coordinates  $u$  and  $v$  pointing from the origin to point  $p$  within  $S$ .

$C$ , then  $\frac{d\vec{r}}{dS}$  must be equal to the tangent vector  $\vec{t}$  i.e.:

$$\vec{t} = \frac{d\vec{r}}{dS} \quad (10)$$

Thus the expression for normal curvature  $\kappa_n$  is:

$$\kappa_n = -\frac{d\vec{r}}{dS} \cdot \frac{d\vec{N}}{dS} = -\frac{d\vec{r} \cdot d\vec{N}}{d\vec{r} \cdot d\vec{r}} \quad (11)$$

And this can be rewritten as:

$$\kappa_n = \frac{Ldu^2 + 2Mdudv + Ndv^2}{Edu^2 + 2Fdudv + Gdv^2} \quad (12)$$

Where

$$\begin{aligned} L &= \vec{r}_{uu} \cdot \vec{N} & E &= \vec{r}_u \cdot \vec{r}_u \\ M &= \vec{r}_{uv} \cdot \vec{N} & F &= \vec{r}_u \cdot \vec{r}_v \\ N &= \vec{r}_{vv} \cdot \vec{N} & G &= \vec{r}_v \cdot \vec{r}_v \end{aligned}$$

The parameters  $E, F, G$  are coefficients of the first fundamental form ( $I$ ) and  $L, M, N$  are coefficients of the second fundamental form ( $II$ ). Rewriting eq. (12) for direction one gets

$$\kappa_n = \frac{L + 2M\lambda + N\lambda^2}{E + 2F\lambda + G\lambda^2} = \frac{II}{I} \quad (13)$$

Where  $\lambda = \frac{du}{dv}$  which is the direction in the tangent plane at point  $p$  on  $S$ . This enables one the mathematical operation to calculate normal curvature at any given point on  $S$  in any direction in the tangent plane. Furthermore, for any point there are two principal directions in which  $\kappa_n$  reaches a maximum and minimum respectively. These are referred to as maximum and minimum curvature



$k_{max} = k_1$  and  $k_{min} = k_2$ . Evaluating these two parameters one can compute the average  $H$  and Gaussian  $G$  curvature:

$$H = \frac{k_1 + k_2}{2} \quad (14)$$

$$G = k_1 \cdot k_2 \quad (15)$$

These calculations of curvature were classically worked through by Gauss in his *Theorema Egregium*, but were developed further by Weingarten [17].

### 1.3 Biomimicry

Coming up with new ideas in science always commences with the first question of: *where do you start?* It could start with a need as with John Wesley Hyatt, who was commissioned with creating billiard balls not using ivory, as they were prone to crack during play. He came up with a new material referred to as “Celluloid” which with a new method he invented would later be patented by himself as the first injection molding machine [18]. Or it could start with serendipity, as with Sir Harold Ridley who noticed that the eyes of some pilots after World War II who had gotten plastic shards implanted in their eyes after their windshield of their planes shattered, had healed without any sign of further infection. This led to the discovery that poly(methyl methacrylate) (PMMA), which the airplane windshields were made of, were in fact tolerated by biological tissue and no foreign body reaction was observed, or in other words “biocompatible” [19]. It could start with insight, as in the case of George de Mestral noticing how burrs got stuck in his dog’s fur while walking in the forest. This later became the idea of the hook-and-loop fastening system which we know today as Velcro [20]. Once an idea has been formed, a natural progression would be to consider the strategy to realize the idea. It may be to understand a process, such as a manufacturing process, or to understand how a biological system works mechanically. To use nature as inspiration for the creation of new medical devices becomes ever more present in literature. Other examples include the development of new tissue adhesives inspired by the van der Waal’s interactions between Gecko feet and substrates. The bottom surface of a gecko foot consists of many smaller repeated structures known as *setae*, which is an architectural structure that branches into even smaller long thin structures called *spatulae*. These structures enable the gecko to make use of the van der Waal’s forces, and climb vertical and inclined surfaces. For this example the group constructed a micropillar-structured biodegradable array using a photolithographic method and optimized for geometrical parameters [21].

In the Karp lab at the Brigham’s and Women’s hospital there are many examples. To come up with new syringe and needle designs, they looked at porcupine quills and saw that their design and mechanical performance allowed for easy tissue penetration [22]. The long thin shape with

backward-facing barbs contributed to this design, and from decoding this information they came up with a design that required less force to penetrate skin than a barb-less design. There are many other examples like the superhydrophobic effect from the lotus plant [23], dry vaccine development from tardigrades [24], and cacti-like tendrils for robotic arm development [25]. In this thesis, it will be examined how digital methods such as modelling, functional programming, in combination with bioinspiration, may be used as a powerful set of tools to overcome scientific challenges. There will be focus on two particular species: the Venus flytrap and the tapeworm.

### 1.3.1 Venus flytrap

The Venus flytrap, *Dionaea muscipula*, is a plant which is able to lure prey into its two lobes and snap shut within 100 - 300 ms [26]. This finely tuned mechanical system still is under scrutiny and debate as to what mechanisms constitute this rapid shutting of the lobes. It is known that the lobes consist of two layer of cells [27, 28] and that there is movement of water from the inner to the outer lobes [29, 30]. The shape-change of the Venus flytrap lobes is also something characteristic of a bi-stable behaviour - the buckling of the lobes is what allows the lobes to "snap" shut. In the work from Speck and Poppinga, they argue that not only displacement of water is necessary for the function but also that pre-stress plays an important role [31], and refer to this as a "ready-to-snap" state. This species has been previously implemented as a fluidic origami device [32] and snapping hydrogel assembly [33]. Here, it would be interesting to see whether it would be possible to devise a polymeric structure that is able to activate and de-activate its bi-stable behaviour, which could potentially be used as an energy storage.

### 1.3.2 Tapeworm

Tapeworms, or the sub-class *Eucestoda* from the class *Cestoda*, are parasitic worms found in the intestine of living species. The order *Cyclophyllidea* encompasses all tapeworms that are found in terrestrial vertebrates [34]. For larger mammals such as cattle, one can find the family *Taeniidae*, which is also commonly spread and found in humans. Some common species of this family are *Taenia Solium* (pork tapeworm), *Taenia saginata* (beef tapeworm) and *Echinococcus granulosus*. The main feature of such species is the use of suction and hook attachment to attach their bodies to gastrointestinal tract (GI) (See Figure 7). Tapeworms of the order *cyclophyllidea* are identified by having four suckers located laterally on the scolex (head) of the tapeworm (See Figure 7). For the species *T. Solium* the size of its suckers is around 400  $\mu\text{m}$  [36]. With the suckers the tapeworm can temporarily attach itself to host tissue, presumably to probe a potential landing location. As can be seen in the figure, there is an extendable section inside the scolex called the rostellum which is a flexible pouch that can be evaginated. The mechanism with which the tapeworm attaches is a result of specifically designed hooks coordinated by a fine tuned muscular system. The rostellum

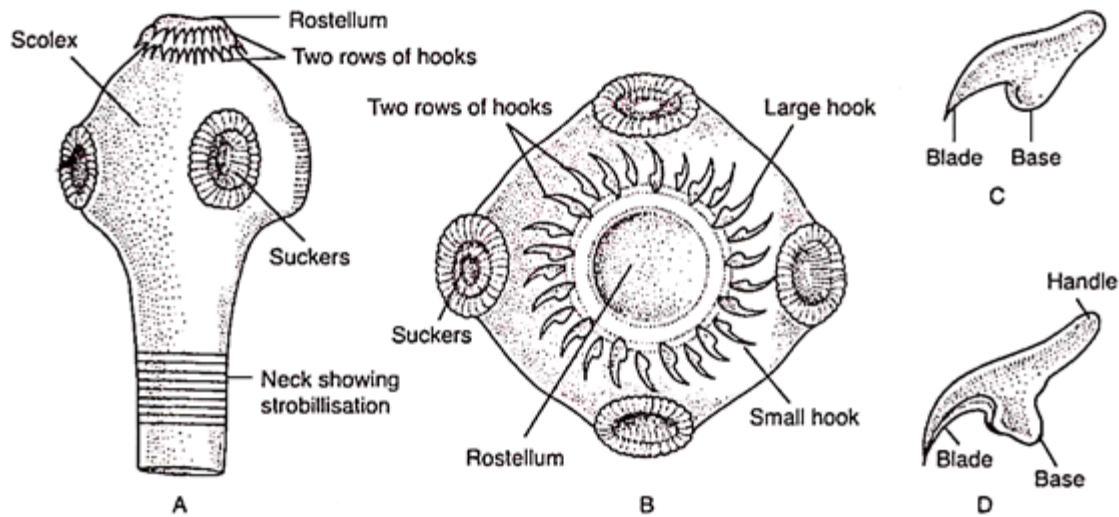


Figure 7: Parts of the *Taenia Solium*. Image taken from *Taenia Solium cysticercosis: from basic to clinical science* [35].

can be described as a muscular pouch which comprises circular muscle fibres which are located a small distance above the suckers. This forms a sphincter which is believed to be contracted when the hooks are invaginated keeping them inert. This sphincter is located above the hooks when they are invaginated and below the hooks when they are evaginated. The rostellum is also separate from the rest of the scolex tissue by the rostellar capsule [37]. Two muscle layers form the rostellar capsule; an inner circular layer and an outer longitudinal layer. Basal lamina separates these two layers. The interface between the tapeworm and the host is called the tegument, and is a metabolically active structure providing protection, absorption and secretion [38]. The rostellum extends for a certain length, and subsequently the rostellar pad bends through the extension of the apical rostellum, which increases the angle between the rostellar hooks and the longitudinal axis of the worm. Lastly, the rostellar region posterior to the hooks contracts and the worm securely anchors into the host's tissue. Analysing the attachment steps of the tapeworm one can conclude that once roaming the host in the GI tract, one can see that initially the tapeworm may probe probable locations for attachment by using its suckers. Through evolution the shape and mechanistic functions of the suckers and hooks have made it so that *Taenia Solium* is able to attach to several villi simultaneously in the GI tract [39]. Once such a location is deemed suitable for the tapeworm it evaginates its hooks and penetrates the mucosal wall. It has been observed that the latter mode of attachment is irreversible, meaning that this attachment serves as an anchoring mechanism [40] - the tapeworm would spend the rest of its life cycle firmly attached to the GI tract of its host. This fact serves a good blueprint for a medical device where the attachment is divided into two steps: temporary attachment (suckers) and permanent attachment (anchoring through

hooks).

## 1.4 Bi-stable mechanics

### 1.4.1 Euler and Timoshenko beam theories

Before explaining bi-stable mechanics, one first has to explain classical mechanics based on beam theory from Euler-Bernoulli and Timoshenko principles. From the Euler-Bernoulli theory, we are given that for a static beam

$$\frac{d}{dx^2}(EI \frac{dw^2}{dx^2}) = q(x) \quad (16)$$

Where  $x$  denotes a point along the beam,  $E$  the Young's modulus,  $I$  the second moment of inertia, and  $w$  is the deflection along the beam in the  $y$ -direction, and  $q$  is the distributed load along the beam. If the beam is made from a homogenous material and the thickness is constant along the beam, the equation can be simplified to

$$EI \frac{dw^4}{dx^4} = q(x) \quad (17)$$

In the case of a clamped cantilever beam, with one fixed end and one free end where the load  $F$  is applied, the neutral axis of the beam is perpendicular to the cross-sectional beam as can be seen in Figure 8A. In other words one could say that the rate of deflection  $\frac{dw}{dx}$  is equal to the cross-sectional angle  $\phi$  with respect to the coordinate system

$$\frac{dw}{dx} = \phi \quad (18)$$

This fact is not the case for the Timoshenko beam theory. The theory is formulated by two coupled ordinary differential equations

$$q(x) = \frac{d}{dx^2} \left( EI \frac{d\phi}{dx} \right) \quad (19)$$

$$\frac{dw}{dx} = \phi - \frac{1}{\kappa_t AG} \frac{d}{dx} \left( EI \frac{d\phi}{dx} \right) \quad (20)$$

Where  $A$  is the cross-sectional area,  $G$  is the shear modulus, and  $\kappa$  is the Timoshenko shear coefficient dependant on the shape of the beam. For a rectangular cross-section of the beam Timoshenko set  $\kappa_t = \frac{2}{3}$  [41], but later he used values dependant on Poisson's ratio  $\nu$ :  $\kappa_t = (5 + 5\nu)/(6 + 5\nu)$  [42]. And again if the material of the beam is homogenous and the cross-section is constant then Eq. 19 can be rewritten as

$$EI \frac{d}{dx^2} \left( \frac{d\phi}{dx} = q(x) \right) \quad (21)$$

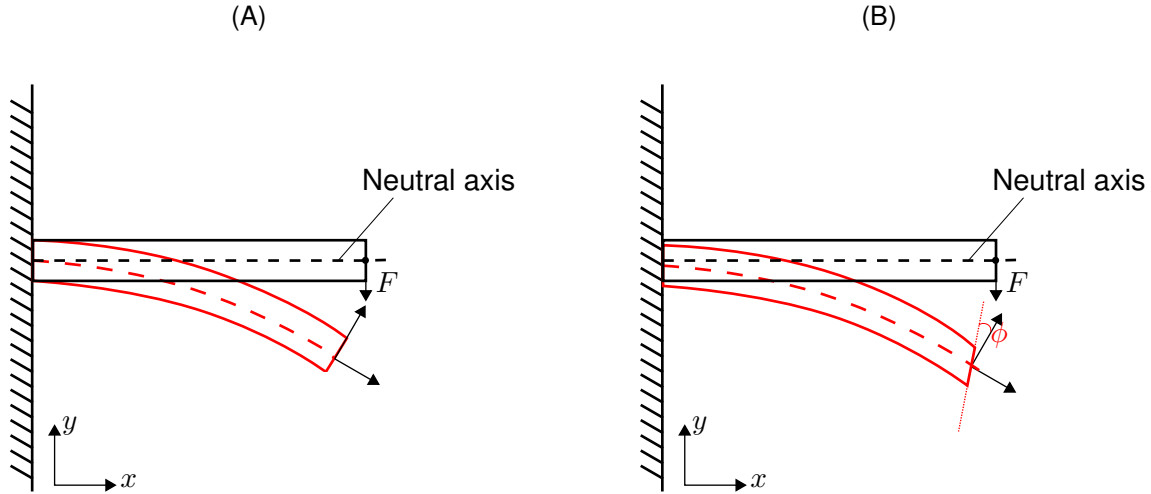


Figure 8: The deformation response according to (A) Euler-Bernoulli beam theory and (B) Timoshenko-Ehrenfest beam theory. For Euler-Bernoulli beam theory the mid-line of the beam is always perpendicular to the free-end plane of the beam, and for Timoshenko beam theory there may be an angle  $\phi$  between the free-end plane and the midline

By derivating Eq. 19 with respect to  $x$  and substituting Eq. 21

$$\frac{dw^2}{dx^2} = \frac{d\phi}{dx} - \frac{1}{\kappa_t AG} \frac{d^2}{dx^2} \left( EI \frac{d\phi}{dx} \right) \quad (22)$$

$$\frac{dw^2}{dx^2} = \frac{d\phi}{dx} - \frac{1}{\kappa_t AG} \cdot q(x) \quad (23)$$

And then by derivating again twice with respect to  $x$  and re-arranging and substituting Eq. 21.

$$\frac{dw^4}{dx^4} = \frac{d\phi^3}{dx^3} - \frac{1}{\kappa_t AG} \cdot \frac{d^2 q}{dx^2} \quad (24)$$

$$\frac{dw^4}{dx^4} = \frac{q(x)}{EI} - \frac{1}{\kappa_t AG} \cdot \frac{d^2 q}{dx^2} \quad (25)$$

$$EI \frac{dw^4}{dx^4} = q(x) - \frac{EI}{\kappa_t AG} \cdot \frac{d^2 q}{dx^2} \quad (26)$$

Which gives us the ordinary differential equation for the deflection of the beam  $w$  along the beam  $x$  for a given distributed load  $q$ . When considering Eq. 20, when neglecting the second term the two equations 19-20 reduces to the Euler-Bernoulli theorem equation Eq. 17.

$$\frac{dw}{dx} = \phi - \frac{1}{k_t A G} \frac{d}{dx} \left( EI \frac{d\phi}{dx} \right) \quad (27)$$

$$\frac{dw}{dx} = \phi \quad (28)$$

$$\frac{d}{dx} \left( EI \frac{d^2 w}{dx^2} \right) = q(x) \quad (29)$$

$$EI \frac{d^4 w}{dx^4} = q(x) \quad (30)$$

There is not a definite consensus when the Euler-Bernoulli theorem could be used instead of the Timoshenko theorem, as the Euler-Bernoulli theorem is easier to compute, but generally when dealing with beams with a lower aspect ratio,  $L/t < 10$  where  $L$  and  $t$  are the length and thickness of the beam respectively, shear forces become more dominant and the Timoshenko theory produces more reliable results [43].

#### 1.4.2 Bi-stability models

There are however more complex mechanics that are difficult, or even impossible to determine analytically and other models or numerical methods need to be implemented. One such example is bi-stable mechanics which is defined as having two stable positions during deformation, usually in its rested state and at some deformation distance  $d$  (Figure 9). To accurately predict such deformations the Euler-Bernoulli theorem is insufficient as it neglects transverse strain and the Poisson effect [43] because these effects become prominent with large deformations. The Timoshenko beam theory accommodates these effects, but for complex geometry as for curved beams there is a coupling between tangential and transverse deformations as well as an induced rotation due to curvature [44]. Therefore, analytical solutions are often not found in closed-form. Other models divide the beams into separate segments and use Timoshenko beam theory to solve them, similar to an FEA approach. Some proposed models use elliptical integrals and numerical approximation such as the Pseudo Rigid Body Model (PRBM) from Howell [45, 46]. Other solutions such as as the Beam Constraint Model (BCM) from Awtar [47] and the extension CBCM from Chen [48] are two models that provide more accurate results for curved beams. The PRBM is a numerical approximation of the non-linear bending of complex shapes and reduces beams into torsional springs with characteristic radii which results in non-linear algebraic expressions which can be more easily solved [49, 50]. This model provides a tool which to easily design complex behaviour with relatively little computation power, however with the allowance for errors. Furthermore, the parameters based on elliptical integrals must be recalculated for each load case [51]. The BCM is a model based a generalized beam fixed at one end with set boundary conditions which results in hyperbolic functions for parameters relating back to the stiffness directions of a

beam. These parameters are then approximated by a Taylor's expansion and truncated for higher order terms, to create a closed-form system of equations of six equations and six unknowns [47]. This model was later extended by Chen et al. as the CBCM which divides up the beam into  $N$  segments, implementing a *quasi*-FEA approach [48]. The BCM assumes linear curvature along the beam since the contribution of non-linear curvature within a deformation of 10 % beam length results in <1 % error [51], and thus for beams with varying curvature and larger than 10 % beam length deformation the CBCM should provide more accurate results depending on the number  $N$  of segments.

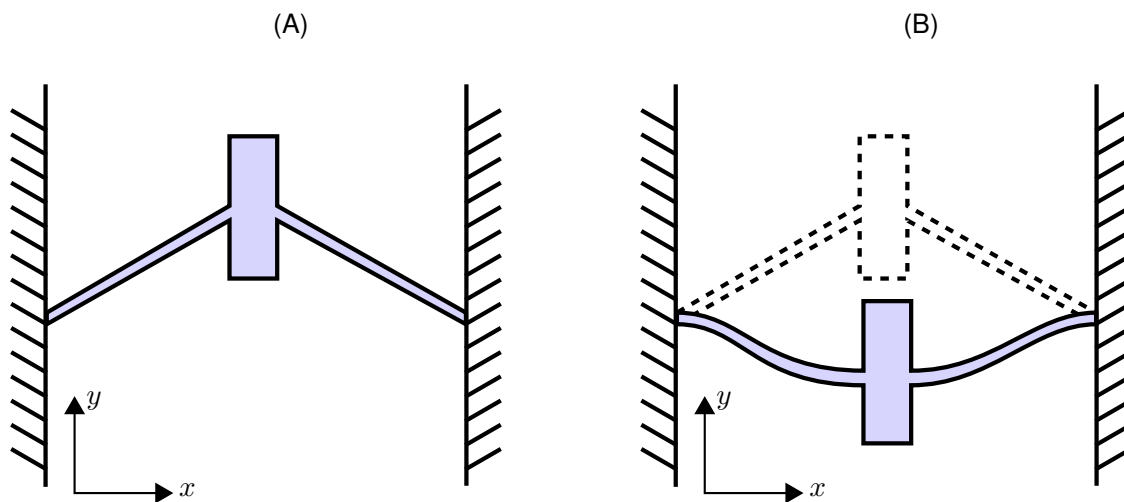


Figure 9: The bi-stable behaviour of a shuttle with two fixed supports. In its undeformed state (A) the shuttle is stabilized by two arms at an angle to the horizontal. Due to this angle, when deformed in the negative  $y$ -direction the beams will start to buckle and at a certain buckling point for both beams, a static equilibrium is reached (B) and is stable until further acted upon.

## 2 Motivation, Aims and Strategy

### 2.1 Motivation

For EDM modelling, many of the models proposed are either labour intensive or based on thermal FEA models. With the focus on the actual geometrical shapes with which a workpiece is deformed with, and use a more phenomenological approach may provide a more predictive approach of the actual surface structure for a large region of interest. Furthermore, when analysing EDM-treated surfaces, they are usually characterized through roughness parameters defined by ISO norm 25178-2:2012 [52]. However for certain milled parts, it has been found that curvature analysis can be used to predict fatigue limits [53]. Therefore, to use curvature analysis to see how the EDM process changes the surface may provide useful insights.

With the readily available methods of Additive Manufacturing (AM), realization of complex multi-material parts has become facile and an important cornerstone in research and development. In addition, more intricate models for non-linear bending to create compliant mechanisms has opened up great potential to create designs with pre-defined deformation modes. Compliant principles have been implemented in many areas such as in Micro-Electromechanical Systems (MEMS) and solar sails for the ISS, and with the development of more sophisticated models and manufacturing methods, compliant mechanisms have been implemented to create flexure hinges, robotics, and organic designs. An area, in which compliant mechanisms have yet to be applied is in minimally invasive medicine, and due to the need for more control with laparoscopic procedures bi-stable may be a useful tool in medical device design. By combining the above mentioned principles together with a biological design approach, this thesis explores how novel medical devices could be conceptualized.

### 2.2 Aims and Hypotheses

The aims for this thesis are to use a combined approach of (i) modelling, (ii) biological design, and (iii) bi-stable mechanics solve challenges for science and medical device design. An important part is to use AM and mechanical testing to realize and validate predicted designs respectively.

**Hypothesis (i): Modelling of the EDM process can be realized by using an iterative impact model**

Using an iterative model which implements an impact model to model the material removal and debris remains from a single EDM spark event which is repeated  $N$  number of times with varying sizes of crater impacts and debris heights should be able to represent the EDM process.



**Hypothesis (ii): Curvature analysis can be implemented as a topographical analysis tool**

By using a curvature analysis method with respect to scale and direction, a surface can be characterized analogous to that of surface roughness parameters.

**Hypothesis (iii): Using bioinspired designs will improve design functionality**

Observing nature and how species mechanistically work will create designs that are intricate and has improved functionality

**Hypothesis (iv): Using the CBCM will predict bi-stable behaviour in 3D**

Conceptualizing new medical devices will be made possible by using the CBCM predict bi-stable behaviour in 3D.

**2.3 Strategies and concept**

In order to realize the modelling part of the thesis, the algorithms were written in Python 3 with standard libraries being implemented, such as NumPy, SciPy, Matplotlib, and proprietary packages such as Numpy-Stl to create STL-files, for more details see Appendix IV. For designing prototypes and bespoke testing rigs two AM methods were used: Multi-Jet printing for multi-material parts, and stereolithographical printing for heat-resistant parts. Mechanical testing and validation of results were done using tensile testing machines and bespoke 3D-printed parts.

**Strategy (i): Modelling of the EDM process and subsequent curvature analysis accelerated by Compute Unified Device Architecture (CUDA) implementation**

The modelling of the EDM process is based on that a substrate starts initially as a smooth surface and iteratively becomes deformed using an impact model that is applied randomly on the substrate for  $N$  number of times. In addition, the substrates through defined impact number points are analysed through curvature analysis to follow the change in topographical information. The curvature analysis can be adapted by applying a scale length and to look in certain directions. The programmatic implementation is accelerated by using Compute Unified Device Architecture (CUDA) cores, for more details see Appendix IV.

**Strategy (ii): Analysis and review of species for bi-stable behaviour and attachment principles**

In order to choose an appropriate biological system for the application, a two-step biological analysis is used. Initially, a general review is first made to identify families or order of species

that may serve as a good blueprint. Once a species or family of species is identified, a more detailed literature review is done to understand the underlying physical principles and feasibility for realization.

### **Strategy (iii): Prediction and realization of designs using digital methods**

To predict the bending and bi-stable behaviour of complex geometry the CBCM will be used, and various design variations will be tested to find the optimum design. To realize the predicted designs, CAD-models will be created and manufactured using AM methods. To validate the results and find the optimum design, bespoke mechanical tests were conducted using a mechanical tensile tester.

### **3 Organization of thesis**

This cumulative dissertation aims use the strategies of modelling and additive manufacturing as digital tools, together with bio-inspiration to solve scientific challenges regarding surface topography parameters and engineering new medical devices. A short description of the contents of each section is outlined below.

Section 1 contains the introduction to the subject matters of each included manuscript

Section 2 contains the overall motivation, aims, and strategy for each included manuscript

Section 3 contains the organization of the thesis

Section 4 contains the manuscript titled: "Predictive topography impact model for Electrical Discharge Machining (EDM) of metal surfaces"

Section 5 contains the manuscript titled: "Bio-inspired and computer-supported design of modulated shape changes in polymer materials"

Section 6 contains the manuscript titled: "A Biomimetic Alternative bi-modular bi-stable fixation Device (BAFD)"

Section 7 contains the discussion of the three included manuscripts

Section 8 contains the summary, drawn conclusions, and future prospects of the thesis work

Section 9 contains the reference list

## 4 Predictive topography impact model for Electrical Discharge Machining (EDM) of metal surfaces

### 4.1 Summary

This paper investigates how an iterative model for the EDM process can be made using an impact model and some simple boolean operations over a pre-defined smooth substrate. The motivation is to conduct this iterative model over several thousand so-called impacts. Through a new curvature analysis method suggested in the paper, we observe how this substrate changes as impact number increases and eventually reaches an equilibrium. This change is presented through the comparison of standard normed roughness parameters and visualized through Abbott-Firestone curves based on the novel curvature analysis method.

### 4.2 Contribution to the publication

- Literature Study
  - Review of current and existing EDM models
  - Review of curvature analysis methods
  - Research on how to make Python code runtime faster
- Study design in active discussion with co-authors
  - Choice of impact model to be implemented
  - How to iteratively conduct the simulation
  - Choice of curvature analysis method and numerical implementation
  - At what impact number points to conduct curvature analysis
- Experimental work
  - Code writing and troubleshooting for EDM simulation
  - Code writing and troubleshooting for the curvature analysis method
  - Abbott-Firestone analysis of simulated surfaces
- Manuscript
  - Manuscript structure in coordination with the co-authors
  - Figure creation, text writing of all sections, and discussion points of experimental work
  - Revision and finalization together with comments from co-authors and peer reviewers

### 4.3 Publication - Appendix I

Bäckemo, J., Heuchel, M., Reinthaler, M., Kratz, K. and Lendlein, A., 2020. Predictive topography impact model for Electrical Discharge Machining (EDM) of metal surfaces. *MRS Advances*, 5(12-13), pp.621-632.

## 5 Bio-inspired and computer-supported design of modulated shape changes in polymer materials

### 5.1 Summary

Here a bioinspired approach is used to come up with a design that is based on the Venus Flytrap. The Venus Flytrap is working through a finely tuned mechanical system which is driven by two main processes: water displacement and pre-stress. The snapping function is aided through the curved lobes which creates a bi-stable structure that is able to quickly snap shut. In the paper the bi-stable behaviour of a bio-inspired design is predicted by the Chained Beam Constraint Model (CBCM) which is tested for two different design variations of a truncated tetrahedron. In addition, this bi-stable behaviour can be turned off by using a shape-memory polymer and by a programming step using heat-resistant molds. The bi-stable and mono-stable behaviour is validated through functional and mechanical tests.

### 5.2 Contribution to the publication

- Literature Study
  - Review of natural species with bi-stable mechanical behaviour
  - Review of non-linear mechanics for predicting bi-stable behaviour
  - Review of previously implemented compliant mechanisms
  - Researching of algorithms for implementing compliant mechanism theories
- Study design in active discussion with co-authors
  - Choice of 3D-design to be used
  - Design of experimental setup for the mechanical evaluation
  - Choice of bi-stable mechanical model
- Experimental work
  - CAD-Design of prototypes and mechanical test jigs
  - Manufacturing of prototype molds and mechanical test jigs using Additive Manufacturing (AM)
  - Code writing and implementation of the CBCM
  - Mechanical testing of manufactured prototypes
- Manuscript

- Manuscript structure in coordination with the co-authors
- Figure creation, text writing of all sections, and discussion points of experimental work
- Revision and finalization together with comments from co-authors and peer reviewers

### **5.3 Publication - Appendix II**

Bäckemo, J., Liu, Y. and Lendlein, A., 2021. Bio-inspired and computer-supported design of modulated shape changes in polymer materials. *MRS Communications*, 11(4), pp.462-469.

## 6 A Biomimetic Alternative bi-modular bi-stable fixation Device (BAFD)

### 6.1 Summary

In this work, a combined approach of bioinspired design and digital methods is used to devise a new design strategy for minimally invasive medical devices. A comprehensive review of different medical devices were done to observe what the current challenges in the clinic are. Subsequently, an investigation of different attachment systems with widely different physical principles were conducted to identify a species with a novel attachment system. The tapeworm poses an interesting and applicable attachment strategy as it is divided into two steps: temporary and permanent attachment. Suckers on its sides stabilizes the species in the gut of its host, and hooks penetrate tissue to permanently attach the parasite to host tissue. This design was converted into a design concept which is actuated by one stimulus which is vacuum, and the two different modes of attachment is aided by bi-stable mechanics and strength of the vacuum. With this approach, one stimulus can control the mode of attachment. A bi-stable column design was created with 18 different design variations which were mechanically evaluated to find an optimum design. These results were then verified by a suction test. Finally, a full prototype was created and tested on porcine tissue to illustrate the proof-of-concept.

### 6.2 Contribution to the publication

- Literature Study
  - Review of different minimally invasive devices for cardiovascular medicine
  - Review of various attachment systems in nature
  - Systematic study of physical principles of attachment systems for selected species
  - Review of non-linear mechanics for predicting bi-stable behaviour
- Study design in active discussion with co-authors
  - Choice of species based on systematic study to be implemented in a design concept
  - Choice of design steps of mechanical and functional testing
  - Choice of bi-stable mechanical model
- Experimental work
  - CAD-Design of multi-material prototypes and mechanical test jigs
  - Manufacturing of prototypes and mechanical test jigs using Additive Manufacturing (AM)



- Code writing and implementation of the CBCM
- Mechanical testing of manufactured prototypes
- Suction tests with printed bi-stable columns and prototypes
- Manuscript
  - Manuscript structure in coordination with the co-authors
  - Figure creation, text writing of all sections, and discussion points of experimental work
  - Revision and finalization together with comments from co-authors and peer reviewers

### **6.3 Publication - Appendix III**

A Biomimetic Alternative bi-modular bi-stable fixation Device (BAFD), J. Bäckemo, M. Reinthaler, A. Lendlein. [Unpublished work]

## 7 Discussion

The discussion will consist of the work and findings of the publications shown in Sections 4-6. The work comprises the modelling of the EDM process with a novel curvature analysis method, and a bioinspirational approach combined with digital methods such as modelling, AM, and non-linear mechanics. In the first part of the introduction the EDM modelling will be briefly discussed, following the comparison of different curvature analysis methods and its position as a predictive tool. In the following section, bioinspiration as a design philosophy will be discussed in relation to literature and what developments have been made in the last decade in terms of AM and how this has changed design possibilities in comparison to traditional manufacturing. Also, non-linear mechanics and in particular the prediction of bi-stable behaviour will be discussed and the differences between the different models and how they may be used in different applications. Finally, as all three publications included in this thesis have a central focus on the application of programming to analyse and to solve non-linear equations, this also will be discussed.

### 7.1 EDM models

As mentioned in the Introduction there are various approaches to model the EDM process, whether a theoretical model in relation to roughness parameters, a thermal FEA-based model, or with an impact-model. In the work presented in this thesis an impact model was used which consisted of a crater part that removed material and a surrounding ridge part that added material on the perimeter of the crater, which represented debris of molten material not flushed away by the dielectric fluid. Here the craters formed show clearly that a crater forms with a surrounding bulging rim, and from simulation results is due to debris which is either molten or shortly suspended in the dielectric fluid before settling around the crater. This is also shown by other researchers [54, 55, 56]. Other models focuses on the Material Removal Rate (MRR) of the metallic workpiece, dependent on changing the electrical input parameters like current, voltage, duty cycle, and pulse duration [57, 58]. This may be useful in applications where the deformation over the whole workpiece of important, however an impact model or an FEA-approach gives more information about the deformation on the micro-scale. Another aspect would be to consider the anode wear rate, which if too high requires frequent replacement of the anode material which is undesirable [58]. For theoretical modelling cathode erosion [10], anode erosion [59] and plasma channel formation [60, 61, 62] are of main interest. The impact model in our work is based on simple inequalities and boolean operations. A trivial statement but albeit important, is that every subsequent impact has precedence over any previous impact. If a ridge is created from an previous impact, and a subsequent impact occurs in that ridge, it is removed. For forming the ridge a factor  $F$  was set to represent how much material is removed and how much debris would remain to form the ridge. In

addition, a volume correction factor was calculated to adjust for actual material removed compared to the theoretical maximum removed (Figure 10). In our work, the shape of the cross-section of the ridge to be semi-circular, other researchers have used thermal models that results in a more parabolic shape [56]. The benefit of a phenomenological model is that it can be quickly computed and easily changed to see how small variations in the impact model changes the overall surface deformation. Concerning limitations, the model is not based on more common thermal flux models and does not simulate material ejection.

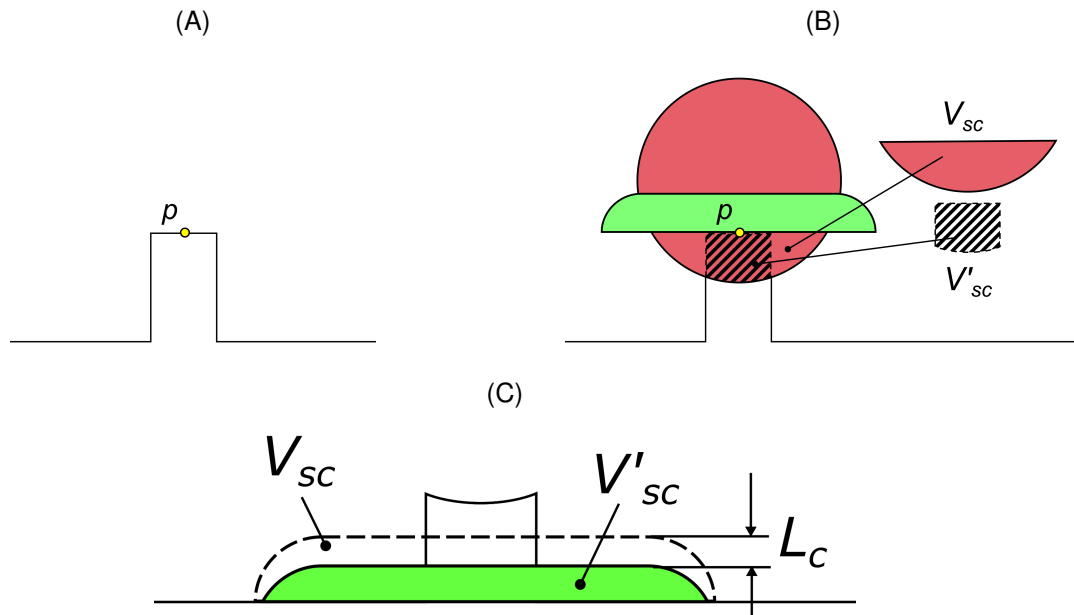


Figure 10: A-C) Series of images illustrating the difference between volume of the spherical cap  $V_{sc}$  and the actual removed volume  $V'_{sc}$ . In order to accommodate for the discrepancy the ridge is shifted downwards by a length of  $L_c$

## 7.2 Curvature analysis

Connected with EDM-modelling, is the evaluation of substrate topography through curvature analysis. As explained in the introduction, curvature and roughness are two similar surface characterisations. Both roughness and curvature depend on scale, i.e. different orders of substrate changes. Curvature is important not only for machined surface analysis but also for segmentation [63], denoising [64], partial shape matching [65], and many more areas. Based on the differential geometry calculations from Weingarten [17], curvature can be directly calculated from mathematical principles. However, this requires the substrate to be exactly differentiable at each point of a substrate. The substrate model created exists in a 3D-format, an .stl format, which contains discrete points which are connected that make up the substrate. For actual EDM-treated

surfaces these .stl. models are acquired by  $\mu$ -CT machines which has an intrinsic resolution. Furthermore, there is no scale factor per say in the curvature calculations, one could achieve a sense of scale by down-sizing the substrate 3D-model in question. More recent work has been to extend the principles by Weingarten to make them continuous on triangulated surfaces (such as common 3D .stl files). Here a tensor is devised to make curvature measurements within one single triangle (or face) based on vertex normals, and by averaging the values for every adjacent triangles (faces) a continuous calculation over the whole surface could be made [66]. A similar approach calculated the normals for a triangle, and used the least squares fitting method to for the curvature between adjacent vertices of the face (1-ring neighbours) [67]. One of the main problems in calculating on discrete surfaces is the lack of information in between vertices, and the discontinuity between faces. Therefore, the curvature inside a triangle (face) needs to be interpolated and the curvature between triangles need to be made continuous, either through averaging or fitting. Another group, instead of averaging on adjacent triangles defined appropriate neighbourhoods from the point of interest and fitted their curvature tensor, with which it is more reliable against noise and outliers [68]. Another approach may be to use a pre-defined geodesic distance, i.e. the distance along a curved surface, from a vertex being analysed to define the region of interest being used to calculate curvature [69]. In the work we presented, a three-point curvature method based on Heron's formula was devised. The three points used for the curvature calculation were set apart at a distance  $L$  which could be changed. In addition no averaging was performed for the calculation. Using curvature analysis for EDM-treated surfaces has been performed by Bartkowiak et al. [70]. Their research showed that curvature analysis, and distributions, over the whole surface of treatment had a strong correlation with discharge energy. Furthermore, in other fields of research such as biology, curvature may have an important role. It can be seen that curvature is important for blastocyst formation for stem cells [71, 72].

## 7.3 Bioinspired design

### 7.3.1 Design methodology

To apply designs, inspired by the complex and specific designs from nature have in the last 10-20 years seen a great interest. As such, 'bioinspired design' comes in many other formulations such as, 'biomimicry', 'biomimetics', 'bionics', and 'bioinspiration'. However, in the last years an ISO-standard defines subtle, yet specific, differences between these terms [73]. The most widely known example, must be that of George de Mestral being inspired of the hooks from Burr's getting stuck in his dogs fur which ultimately led to the invention of the closing system known as Velcro. The general challenge, however, is that to convert a biological system to an engineering or scientific solution often is difficult and without significant simplifications may not be realizable but at the same time will remove the inspired design from the biological system. There is no clear

method to transfer biological information to solve challenges, and there is significant friction in interdisciplinary work [74]. There are methodological approaches developed. BioTRIZ (Theory of Inventive Problem Solving) is an analytical approach [75] which established 39 design parameters and 40 inventive principles to analyse a biological system. From these parameters a so-called conflict matrix can be devised to establish how one can systematically analyse a natural system and draw parallels to a desired engineering system, i.e the design needs to be mechanically strong but has to be light in mass. Other approaches may deal with big databases of gathered information. AskNature.org from the Biomimicry institute is a huge curated database, with organized biological data according to function [76]. A biomimetic taxonomic system where focus was put on function was developed by the researchers, and included descriptive examples of how other groups have implemented bioinspired design. This is one of more than 40 different design tools with focus on biomimicry [77]. Here, the authors sort the different methodological or algorithmic processes to facilitate biomimetic design and saw that over three out of four tools have been analysed in theoretical and practical case studies, to illustrate their value in the design process. The TRIZ methodology has been extended for biomimetic designs realizable with AM to create new gear designs [78].

### 7.3.2 Applications of design

For all design tools, the first question is whether to start top-down or bottom-up: does the technology pull from nature, or does nature govern what technical applications could be made [79]. A problem-driven approach takes the scientific problem and tries to fit a biological design to it; a top-down approach. For the work inspired by the tapeworm *Taenia Solium* is an example of a problem-driven approach: an issue or challenge is detected in minimally invasive medicine regarding control *in situ*, and an appropriate biological solution in nature is found by dividing up attachment in two modes. The implication here is that the biological inspiration is fitted to the problem. One could argue that this is not bioinspired, but that it is biomimetic in that it is following the mechanism of the tapeworm closely. Another paradigm is a solution-based approach, a bottom-up approach. The work based on the Venus flytrap is an example of such an approach. The mechanism of the lobes of the flytrap snapping shut; an example of a bi-stable mechanism, and its stimulus through sensing and water displacement is seen as a design rationale. Here, in contrary, a problem or challenge is sought after that could be solved by such a design. Another example of this approach is from Valdivia et al., in which the group looked at underwater bio-locomotion [80]. The extracted design uses distributed mass, and anisotropic materials in order to achieve a kinematic locomotion much similar to that of the stingray. In addition, comparing two prototypes where one uses one polymer and another that used two polymers (one for the front half, another for the body and the back half) showed that the prototype with better distributed mass density, more

similar to the stingray itself, showed better performance. As a counter example, a solution-based approach is that of Tardigrades. These creatures are able to dry out themselves, while still preserving their biological material and suffer no damage until they are re-hydrated. This research area is referred to as anhydrobiosis, essentially life without water. A research group found that the ability of Tardigrades to undergo such extreme dryness under a prolonged period of time, may aid in developing medicines, e.g. for dry vaccines where sufficient cool conditions cannot be maintained [81]. Furthermore, the technology could be further developed to have 'slow release' which would make the need for boosters of vaccines obsolete.

### 7.3.3 Challenges of manufacturing

When looking at biomimetic parts to be used for a mechanical purpose; to actuate in some way - organic design does not lend itself to classic manufacturing. Here in order to follow organic design with curved shapes and struts, and thin free-flowing structures AM has been a definite accelerator [82]. In the work for a minimally invasive design, bioinspired from the Tapeworm, the bi-stable column is printed as one part but with two different materials to achieve two parts with varying stiffness and flexibility. Creating such a part from classical milling, CNC-machines, or injection moulding may be difficult, time-consuming and costly. However, AM suffers from other issues and challenges. Small angled parts may suffer from the staggered "stair-step" artifact, downward-facing surfaces usually display rougher surface quality, parts with a low angle with respect to the printing bed requires support [83]. Furthermore, the post-processing step may also be a cumbersome affair but sometimes more important than the actual part creation. For the Stratasys Connex 3 Objet 260 the support material which is Polyethylene Glycol- and Propylene Glycol-based encases the printed part and must be either removed physically through tools or a water jet, or by dissolving the whole part in a caustic soda bath. This of course, makes hidden parts in a design encased with support that may not be removable. For an STL-based approach, the post-processing may consist of several steps such as material curing steps and material removal through isopropanol baths. Here, the curing steps have a crucial impact on part strength, however due to elevated temperature may cause thin parts to distort. As a general remark, there is a degree of anisotropy to all printed parts as they are a layer-by-layer manufacturing principle - the orientation with the highest strength will be perpendicular to the layer surface [84]. Parts created through AM are generally weaker due to the layer-by-layer process than one-shot manufacturing processes such as injection molding, however AM parts enable more outlandish designs and allow the integration of elements not possible by injection molding, e.g. hollow spaces. Another challenge, is that of meso-manufacturing. The meso-scale sits in between the macro-scale in the mm-range and the micro-scale in the micrometer range. The problem is that manufacturing in the meso-scale which ranges from a few micrometers to many hundred micrometers [85] is difficult

to manufacture with common manufacturing methods, and on to large of a scale for micro-meter scale manufacturing. One example which works in this scale is EDM which deforms hard metals, however this is limited to basic shapes and requires the negative shape for die-sink EDM. The main challenges at this scale is that grain size becomes an important factor, and the tolerances of machined parts need to be extremely small [86]. In order to further minimally invasive medicine, AM progress in the meso-scale is necessary as more medical devices are down-sized. A recent example of medical devices moving toward minimally invasive surgery at the time of writing of this thesis is the Aveir VR lead-less pacemaker from Abbott which has transformed the pacemaker from consisting of a battery housing, leads, and electrodes to one single device which can be inserted through a catheter [87].

## 7.4 Compliant mechanisms

### 7.4.1 Non-linear mechanical models

To forecast the behaviour of non-linear mechanics in a mechanical structure, one would first have to define what kind of non-linearity is referred to. Non-linear behaviour can refer to the material behaviour, that the material has a changing response depending on the strength of the deformation or a transient response depending on the speed of deformation. This can be thought of as a material science aspect - however when geometry applied, there is non-linear behaviour appearing because of phenomena such as buckling, kinematic and elastokinematic effects, and large deflections. There are many various models to forecast such behaviour such as the FEA, the circular arc method [88], Adomian decomposition method [89], the chain algorithm [90], the global coordinate model with an incremental linearization approach [91], elliptical integral solutions [92, 93], and Gauss-Chebyshev quadrature formulation [94], or the CBCM [48]. For designing compliant mechanisms there is an interesting approach called the PRBM [45].

The PRBM is a model which gives the user a graphical and mathematical prediction of how their structure will deform. In the example of a cantilever beam, the beam will be divided up into two segments: one rigid and one flexible element. The elements are connected by a pin joint and a torsional spring. The location of the pin joint estimates the deflection arc of the beam, and the torsional spring is analogous to the stored elastic energy in the beam. This model is an estimation to the analytical solutions involving elliptic integrals [95], and for each structure the exact location of the pin joints as well as the torsional spring constant need to be calculated. With  $L$  being the length of the beam, the location of the pin joint is  $0.17L$  for angles  $\theta < 15^\circ$  and  $0.15L$  for angles  $\theta > 45^\circ$  [45]. The estimated constants 0.15 and 0.17 are calculated from trial and error to find the smallest error, and for an applied angle of  $180^\circ$  the relative error reaches a relatively low value of 7% [96]. As a result, it does not provide an exact solution but rather the emphasis is on

actually coming up with new designs in an easily accessible way. Using the PRBM provides a way to compute kinematic equations for a mechanical design which is easily solved from trigonometric equations. This can also be applied to beams which are initially curved before deformation, with a constant radius of curvature. In effect the location of the pin joint increases in value as the curvature of the beam increases. Furthermore, the model and its calculated constants are based on isotropic materials and constant cross-section beams, any deviation from these assumptions and the constants need to be recalculated.

In comparison the CBCM is computationally more cumbersome as open-form equations are involved. A similar point is that the formulation of the model is based on isotropic materials and constant cross-section beams. The main difference between the PRBM and CBCM is the latter can handle beams with changing curvature, and piecewise equations for the beam profile. For the bi-stable columns created for the Biomimetic Alternative Fixation Device (BAFD), the profile are based on three piece-wise equations and the focus lay on the accuracy of the results, hence the CBCM was chosen. The benefits of the model is in addition that the amount of elements can be equally or unequally discretized, meaning that customization can be made and more elements can be inserted at critical points along the beam.

## 7.5 Application of compliant mechanisms

As previously discussed with bio-inspired design, compliant mechanisms are characterized by slender members or the combination between thick and thin elements. Therefore AM lends itself well to produce compliant mechanisms. In this work, compliant mechanisms have been used as switch that can also be turned off with the aid of shape-memory polymers, and as an actuating switch for a minimally invasive device. Compliant mechanisms have been used in countless fields such as airplane wing designs [97], a bio-inspired wrist [98], prosthetic fingers [99], MEMS [100, 101], or even bicycle brakes [102]. The further compliant mechanisms, and bi-stable mechanics, can be developed and computed with better analytical tools and models the more applications in medicine will be developed in the coming decade.

## 7.6 Programming challenges

For all three projects, programming was one shared components across all works. For the EDM-modelling and curvature analysis the challenge was to overcome speed of computation. For a generated substrate measuring 1000 x 1000 points, there are  $10^6$  points to be considered, and as the substrate was deformed a new substrate was generate - however not saved as this would have caused massive amounts of data saved on the harddrives. Here in order to speed up the coding, and seeing that most of the calculations required were matrix-based, as in the curvature



deformation was intrinsically a matrix filter applied around a central point of impact - however the size of the matrix changed depending on the chosen radius of the impact. The curvature analysis suffered from the same challenge as in order to fully calculate the curvature for a point 18 unique directions, i.e. 18 calculations per point were needed. In theory there were 36 directions considered, but due to symmetry this could be reduced to 18. Here the CUDA cores were aiding in the computation, the Python code functions needed to be wrapped into a C-based environment which then only allowed matrix-like and boolean operations, which can be implemented quicker on GPUs due to its high parallelization and high-volume data throughput [103]. As a rough comparison, when applying  $10^6$  impacts on a 1000 x 1000 substrate, the simulation would take about 3 days of computation, and with the CUDA cores it took 6 hours. This is due to Python having to interpret variables dynamically and not using parallelization. In contrast C variable types as well as matrix shape input and outputs for functions need to be declared. In addition work load can be parallelized over several CUDA cores. In comparison, for the bi-stable mechanics model CBCM the issue was not speed but stability. The model takes  $6N$  parameters, three geometrical and three mechanical per  $i$ -th element [48]. For each elements it introduces another DOF and thus the possibilities for bending modes increases exponentially. In early implementation of the model the prediction for one  $\Delta d_1$  state could have a widely different shape to another prediction of a  $\Delta d_2$  state. As such there needed to be a continuity between  $\Delta d_1$  and  $\Delta d_2$ . This was solved by taking the initial guess for solving the system of equations of the previously calculated matrix of parameters as the guess for the next prediction - in this way continuity could be achieved as the weight of finding a solution is dependant on the initial guess - the algorithm searches for an appropriate solution within the dimensional space of the initial guess and then proceeds further away as the algorithm increases its iterations. These parameters were also fine-tuned to not allow to outlandish guesses. In summary, for these three projects it was illustrated how modelling and digital tools can aid in solving complex challenges, either when it is modelling mechanical systems and processes or implementing topographical analyses.

## 8 Summary and conclusion

Using modelling, biomimicry and non-linear mechanics are strategies that are well-suited strategies to solve scientific and engineering challenges. Through better computational models and analytical tools, processing and surface parameters could be better understood and elucidated. As can be seen curvature analysis may be another avenue to extract important surface features, which normed surface parameters may not be able to detect adequately. In addition, curvature analysis also captures direction and scale for any given surface point which gives more dimensions to be considered for analysis. As thoroughly described in this work, biomimicry has been useful in guiding design but also to create elaborate but distinct features. By observing species in the animal kingdom and performing systematic analysis of their mechanical features and processes this thesis shows that one could extract design rationales for minimally invasive devices and new mechanical storage systems.

For the EDM modelling project, a phenomenological model was created to imitate the impacts made on a substrate from the EDM process. By using an impact model with a spherical cap and a shifting half-torus depending on actual volume removed created substrates that were comparable to actual substrates treated with EDM. The combination of using curvature analysis with Abbott-Firestone to characterize treated surfaces illustrates a new analysis method. It shows that the reduced concavity curvature  $K_{pk}$  followed an exponential trend until reaching a plateau with increasing impact number. This illustrates that the impact model is deforming the substrate up until a certain point; an equilibrium, where from a perspective of curvature the substrate does not change a lot beyond this point.

In terms of bioinspired design, the Venus flytrap and the tapeworm *Taenia Solium* have proven as two species that have enabled novel designs. For the Venus flytrap it was understood that from rigorous literature research that the snapping behaviour is activated by water displacement and pre-stress, and actuated by bi-stable mechanics. By modelling the bi-stable mechanics for a particular design it was found that a beam profile with an slope angle of  $30^\circ$  showed mono-stable behaviour and an angle of  $45^\circ$  showed bi-stable behaviour. By exploiting the shape-memory properties of PEVA, the bi-stable behaviour could also be de-activated mimicking the dehydrated state of a Venus flytrap. For the tapeworm it was essential how suction and penetration work in concert with each other to enable secure attachment in the small intestine and gut of their host animals. By understanding the well-tuned structure of the *rostellum* and its *scolex*, and how the hooks are evaginated was key to convert the idea to a CAD-design. Understanding how this behaviour could be translated to a polymeric structure aided by AM was one of the major challenges, and through several manufacturing steps was made possible. By using a combination

of VeroWhitePlus and TangoBlack as digital materials, it was found that the combination giving a Young's modulus of  $E = 10 \text{ MPa}$  (Shore A70) gave the best results in terms of required force to trigger the second bi-stable point for the BAFD.

The modelling of bi-stable behaviour by utilizing non-linear mechanical models like the CBCM was key in order to identify the critical stable and unstable static equilibria. In addition, the programming of solving such a system and interpreting the mathematical model was an engineering challenge in itself. As a result, once the model had been set, any type of piecewise equation could be evaluated as a beam profile. Compared to the mechanical tests, the forces for a 3D-model of a bi-stable column were either over- or under-estimated but the displacement points at which the equilibria were located were correctly identified. This was in part due to the viscoelastic nature of the used materials for the prototypes. To incorporate a function in the CBCM to allow for non-constant beam cross-sections and anisotropic material properties would be the next step to further develop the model.

With more intricate mathematical models to more accurately predict bending behaviour in complex organic designs, the opportunities to use compliant mechanisms to replace joints, screws and functions actuated by motors become more apparent and applicable. To sum up the work conducted in this thesis show of digital engineering tools like modelling, CAD-design, and AM, and bioinspiration can work symbiotically to devise new smart functions to be applied to solve scientific challenges, and to design new prototypes for minimally invasive medical devices.

## 9 References

- [1] P. G. Benardos and G.-C. Vosniakos, "Predicting surface roughness in machining: a review," *International Journal of Machine Tools and Manufacture*, vol. 43, no. 8, pp. 833–844, 2003.
- [2] L. Le Guéhennec, A. Soueidan, P. Layrolle, and Y. Amouriq, "Surface treatments of titanium dental implants for rapid osseointegration," *Dental Materials*, vol. 23, no. 7, pp. 844–854, 2007.
- [3] D. Buser, R. Schenk, S. Steinemann, J. Fiorellini, C. Fox, and H. Stich, "Influence of surface characteristics on bone integration of titanium implants. a histomorphometric study in miniature pigs," *Journal of biomedical materials research*, vol. 25, no. 7, pp. 889–902, 1991.
- [4] K. Gotfredson, A. Wennerberg, C. Johansson, L. T. Skovgaard, and E. Hjørting-Hansen, "Anchorage of tio<sub>2</sub>-blasted, ha-coated, and machined implants: An experimental study with rabbits," *Journal of biomedical materials research*, vol. 29, no. 10, pp. 1223–1231, 1995.
- [5] A. Wennerberg, T. Albrektsson, B. Andersson, and J. Krol, "A histomorphometric study of screw-shaped and removal torque titanium implants with three different surface topographies," *Clinical oral implants research*, vol. 6, no. 1, pp. 24–30, 1995.
- [6] R. Krishna Alla, K. Ginjupalli, N. Upadhyaya, M. Shamma, R. Krishna Ravi, and R. Sekhar, "Surface roughness of implants: A review," vol. 25, no. 3, 2011.
- [7] H. Tsai, B. Yan, and F. Huang, "Edm performance of cr/cu-based composite electrodes," *International Journal of Machine Tools and Manufacture*, vol. 43, no. 3, pp. 245–252, 2003.
- [8] K. Ho and S. Newman, "State of the art electrical discharge machining (edm)," *International Journal of Machine Tools and Manufacture*, vol. 43, no. 13, pp. 1287–1300, 2003.
- [9] Sanjeev Kumar, Rupinder Singh, T. P. Singh, and B. L. Sethi, "Surface modification by electrical discharge machining: A review," 2009.
- [10] D. D. DiBitonto, P. T. Eubank, M. R. Patel, and M. A. Barrufet, "Theoretical models of the electrical discharge machining process. i. a simple cathode erosion model," *Journal of Applied Physics*, vol. 66, no. 9, pp. 4095–4103, 1989.
- [11] A. K. Tiwari, A. Dvivedi, and K. Pal, "Thermal modelling of edm process using fea and parametric study of mrr," in *MATERIALS, MECHANICS & MODELING (NCMMM-2020)*, AIP Conference Proceedings, p. 040042, AIP Publishing, 2021.

- [12] J. Marafona and J. Chousal, "A finite element model of edm based on the joule effect," *International Journal of Machine Tools and Manufacture*, vol. 46, no. 6, pp. 595–602, 2006.
- [13] P. C. Tan and S. H. Yeo, "Modelling of overlapping craters in micro-electrical discharge machining," *Journal of Physics D: Applied Physics*, vol. 41, no. 20, p. 205302, 2008.
- [14] H. Ding, X. Li, X. Wang, L. Guo, and L. Zhao, "Research on the topography model of micro wire electrical discharge machining surface," 2016.
- [15] X. Yang, J. Guo, X. Chen, and M. Kunieda, "Molecular dynamics simulation of the material removal mechanism in micro-edm," *Precision Engineering*, vol. 35, no. 1, pp. 51–57, 2011.
- [16] J. Tao, J. Ni, and A. J. Shih, "Modeling of the anode crater formation in electrical discharge machining," *Journal of Manufacturing Science and Engineering*, vol. 134, no. 1, p. 011002, 2012.
- [17] J. Weingarten, "Ueber eine klasse auf einander abwickelbarer flächen.," *Journal für die reine und angewandte Mathematik*, vol. 59, pp. 382–393, 1861.
- [18] N. Williams, "The invention of injection molding." <http://harknessindustries.com/invention-injection-molding-2/>, 2017. Accessed: 28th July 2021.
- [19] B. D. Ratner, *Biomaterials science: an introduction to materials in medicine*, ch. A history of Biomaterials. Elsevier, 3 ed., 2013.
- [20] VELCRO®, "About velcro® brand." <https://www.velcro.com/about-us/our-brand/>. Accessed: 20th July 2021.
- [21] A Mahdavi, L Ferreira, C Sundback, J W Nichol, E P Chan, D J Carter, C J Bettinger, S Patanavanich, L Chignozha, E Ben-Joseph, A Galakatos, H Pryor, I Pomerantseva, P T Masiakos, W Faquin, A Zumbuehl, S Hong, J Borenstein, J Vacanti, R Langer, and J M Karp, "A biodegradable and biocompatible gecko-inspired tissue adhesive," *Proc Natl Acad Sci U S A*, vol. 105, no. 7, pp. 2307–2312, 2008.
- [22] W. K. Cho, J. A. Ankrum, D. Guo, S. A. Chester, S. Y. Yang, A. Kashyap, G. A. Campbell, R. J. Wood, R. K. Rijal, R. Karnik, R. Langer, and J. M. Karp, "Microstructured barbs on the north american porcupine quill enable easy tissue penetration and difficult removal," *Proceedings of the National Academy of Sciences of the United States of America*, vol. 109, no. 52, pp. 21289–21294, 2012.
- [23] Sanjay S. Latthe, Chiaki Terashima, Kazuya Nakata, and Akira Fujishima, "Superhydrophobic surfaces developed by mimicking hierarchical surface morphology of lotus leaf," 2014.

- [24] Steffen Hengherr, Arnd G. Heyer, Heinz R. Köhler, and Ralph O. Schill, "Trehalose and anhydrobiosis in tardigrades - evidence for divergence in responses to dehydration," *FEBS Journal*, vol. 275, no. 2, pp. 281–288, 2008.
- [25] Anil K. Bastola, Nadia Rodriguez, Marc Behl, Patricia Soffiatti, Nick P. Rowe, and Andreas Lendlein, "Cactus-inspired design principles for soft robotics based on 3d printed hydrogel-elastomer systems," *Materials and Design*, vol. 202, 2021.
- [26] Y. Forterre, "Slow, fast and furious: understanding the physics of plant movements," *Journal of experimental botany*, vol. 64, no. 15, pp. 4745–4760, 2013.
- [27] H. N. Mazingo, P. Klein, Y. Zeevi, and E. R. Lewis, "Venus's flytrap observations by scanning electron microscopy," *American Journal of Botany*, vol. 57, no. 5, pp. 593–598, 1970.
- [28] T. Iijima and T. Sibaoka, "Movements of  $K^+$  during shutting and opening of the trap-lobes in *aldrovanda vesiculosa*," *Plant and Cell Physiology*, vol. 24, no. 1, pp. 51–60, 1983.
- [29] A. G. Volkov, T. Adesina, V. S. Markin, and E. Jovanov, "Kinetics and Mechanism of *Dionaea muscipula* Trap Closing," *Plant Physiology*, vol. 146, pp. 323–324, 12 2007.
- [30] W. H. Brown, "The mechanism of movement and the duration of the effect of stimulation in the leaves of *dionaea*," *American Journal of Botany*, pp. 68–90, 1916.
- [31] R. Sachse, A. Westermeier, M. Mylo, J. Nadasdi, M. Bischoff, T. Speck, and S. Poppinga, "Snapping mechanics of the venus flytrap (*dionaea muscipula*)," *Proceedings of the National Academy of Sciences of the United States of America*, vol. 117, no. 27, pp. 16035–16042, 2020.
- [32] S Li and K W Wang, "Fluidic origami with embedded pressure dependent multi-stability: a plant inspired innovation," *J R Soc Interface*, vol. 12, no. 111, p. 20150639, 2015.
- [33] Qian Zhao, Xuxu Yang, Chunxin Ma, Di Chen, Hao Bai, Tiefeng Li, Wei Yang, and Tao Xie, "A bioinspired reversible snapping hydrogel assembly," *Materials Horizons*, vol. 3, no. 5, pp. 422–428, 2016.
- [34] Eric P. Hoberg, "Taenia tapeworms: Their biology, evolution and socioeconomic significance," *Microbes and Infection*, vol. 4, no. 8, pp. 859–866, 2002.
- [35] G. Singh and S. Prabhakar, *Taenia solium cysticercosis: from basic to clinical science*. Cabi, 2002.
- [36] A. Verster, "Redescription of *taenia solium* linnaeus, 1758 and *taenia saginata* goetze, 1782," *Zeitschrift für Parasitenkunde*, vol. 29, no. 4, pp. 313–328, 1967.

- [37] H. Kumazawa and K. Yagyu, "Rostellar gross anatomy and the ultrastructural and histochemical characterization of the rostellar tegument-related structures in *hymenolepis nana*," *International journal for parasitology*, vol. 18, no. 6, pp. 739–746, 1988.
- [38] T. C. Cheng, *General parasitology*. Elsevier, 2012.
- [39] Marie Therese Merchant, Laura Aguilar, Guillermina Avila, Lilia Robert, Ana Flisser, and Kaethe Willms, "Taenia solium: description of the intestinal implantation sites in experimental hamster infections," *The Journal of Parasitology*, pp. 681–685, 1998.
- [40] N. Pospekhova and S. Bondarenko, "Morpho-functional characteristics of the scolex of *wardium chaunense* (cestoda: Aploparaksidae) penetrated into host intestine," *Parasitology research*, vol. 113, no. 1, pp. 131–137, 2014.
- [41] S. P. Timoshenko, "Lxvi. on the correction for shear of the differential equation for transverse vibrations of prismatic bars," *The London, Edinburgh, and Dublin Philosophical Magazine and Journal of Science*, vol. 41, no. 245, pp. 744–746, 1921.
- [42] S. P. Timoshenko, "X. on the transverse vibrations of bars of uniform cross-section," *The London, Edinburgh, and Dublin Philosophical Magazine and Journal of Science*, vol. 43, no. 253, pp. 125–131, 1922.
- [43] S. F. Hosseini, A. Hashemian, B. Moetakef-Imani, and S. Hadidimoud, "Isogeometric analysis of free-form timoshenko curved beams including the nonlinear effects of large deformations," *Acta Mechanica Sinica*, vol. 34, no. 4, pp. 728–743, 2018.
- [44] K.-Q. Pan and J.-Y. Liu, "Geometric nonlinear dynamic analysis of curved beams using curved beam element," *Acta Mechanica Sinica*, vol. 27, no. 6, pp. 1023–1033, 2011.
- [45] Larry L. Howell, Spencer P. Magleby, and Brian M. Olsen Howell, *Handbook of Compliant Mechanisms*. Wiley & Sons, Ltd., 2013.
- [46] Larry L. Howell, *21st Century Kinematics: Compliant Mechanisms*. Springer, 2013.
- [47] S. Awtar, *Analysis and synthesis of planer kinematic XY mechanisms*. PhD thesis, Sc. D. thesis, Massachusetts Institute of Technology, Cambridge, MA, 2004.
- [48] Guimin Chen, Fulei Ma, Guangbo Hao, and Weidong Zhu, "Modeling large deflections of initially curved beams in compliant mechanisms using chained beam constraint model," *Journal of Mechanisms and Robotics*, vol. 11, no. 1, p. 11002, 2019.
- [49] M. H. Dado, "Limit position synthesis and analysis of compliant 4-bar mechanisms with specified energy levels using variable parametric pseudo-rigid-body model," *Mechanism and Machine Theory*, vol. 40, no. 8, pp. 977–992, 2005.

- [50] B D Jensen, L L Howell, and L G Salmon, "Design of two-link, in-plane, bistable compliant micro-mechanisms," *Journal of Mechanical Design*, vol. 121, no. 3, pp. 416–423, 1999.
- [51] S. Awtar and S. Sen, "A generalized constraint model for two-dimensional beam flexures: Nonlinear load-displacement formulation," *Journal of Mechanical Design*, vol. 132, no. 8, 2010.
- [52] "Geometrical Product Specification (GPS) – Surface Texture: Areal – Part 2: Terms definitions and surface texture parameters," standard, International Organization for Standardization, Geneva, CH, 2012.
- [53] M. Vulliez, M. A. Gleason, A. Souto-Lebel, Y. Quinsat, C. Lartigue, S. P. Kordell, A. C. Lemoine, and C. A. Brown, "Multi-scale curvature analysis and correlations with the fatigue limit on steel surfaces after milling," *Procedia CIRP*, vol. 13, pp. 308–313, 2014.
- [54] T. Tamura and Y. Kobayashi, "Measurement of impulsive forces and crater formation in impulse discharge," *Journal of Materials Processing Technology*, vol. 149, no. 1-3, pp. 212–216, 2004.
- [55] E. Weingärtner, F. Kuster, and K. Wegener, "Modeling and simulation of electrical discharge machining," *Procedia CIRP*, vol. 2, pp. 74–78, 2012.
- [56] J. Tang and X. Yang, "A novel thermo-hydraulic coupling model to investigate the crater formation in electrical discharge machining," *Journal of Physics D: Applied Physics*, vol. 50, no. 36, p. 365301, 2017.
- [57] H. Beravala and P. M. Pandey, "Modelling of material removal rate in the magnetic field and air-assisted electrical discharge machining," *Proceedings of the Institution of Mechanical Engineers, Part C: Journal of Mechanical Engineering Science*, vol. 234, no. 7, pp. 1286–1297, 2020.
- [58] S. S. Habib, "Study of the parameters in electrical discharge machining through response surface methodology approach," *Applied Mathematical Modelling*, vol. 33, no. 12, pp. 4397–4407, 2009.
- [59] M. R. Patel, M. A. Barrufet, P. T. Eubank, and D. D. DiBitonto, "Theoretical models of the electrical discharge machining process. ii. the anode erosion model," *Journal of applied physics*, vol. 66, no. 9, pp. 4104–4111, 1989.
- [60] P. T. Eubank, M. R. Patel, M. A. Barrufet, and B. Bozkurt, "Theoretical models of the electrical discharge machining process. iii. the variable mass, cylindrical plasma model," *Journal of applied physics*, vol. 73, no. 11, pp. 7900–7909, 1993.



- [61] W. Natsu, M. Shimoyamada, and M. Kunieda, "Study on expansion process of edm arc plasma," *JSME International Journal Series C Mechanical Systems, Machine Elements and Manufacturing*, vol. 49, no. 2, pp. 600–605, 2006.
- [62] S. Dhanik and S. S. Joshi, "Modeling of a single resistance capacitance pulse discharge in micro-electro discharge machining," 2005.
- [63] B. Lévy, S. Petitjean, N. Ray, and J. Maillot, "Least squares conformal maps for automatic texture atlas generation," *ACM transactions on graphics (TOG)*, vol. 21, no. 3, pp. 362–371, 2002.
- [64] M. Meyer, M. Desbrun, P. Schröder, and A. H. Barr, "Discrete differential-geometry operators for triangulated 2-manifolds," in *Visualization and mathematics III*, pp. 35–57, Springer, 2003.
- [65] T. D. Gatzke and C. M. Grimm, "Estimating curvature on triangular meshes," *International journal of shape modeling*, vol. 12, no. 01, pp. 1–28, 2006.
- [66] Holger Theisel, Christian Rössl, Rhaleb Zayer, and Hans Peter Seidel, "Normal based estimation of the curvature tensor for triangular meshes," *Proceedings - Pacific Conference on Computer Graphics and Applications*, pp. 288–297, 2004.
- [67] S. Rusinkiewicz, "Estimating curvatures and their derivatives on triangle meshes," in *Proceedings. 2nd International Symposium on 3D Data Processing, Visualization and Transmission, 2004. 3DPVT 2004*, pp. 486–493, IEEE, 2004.
- [68] E. Kalogerakis, P. Simari, D. Nowrouzezahrai, and K. Singh, "Robust statistical estimation of curvature on discretized surfaces," *Proceedings of the fifth Eurographics symposium on Geometry processing*, no. November 2006, pp. 13–22, 2007.
- [69] T. Gatzke, C. Grimm, M. Garland, and S. Zelinka, "Curvature maps for local shape comparison," in *International Conference on Shape Modeling and Applications 2005 (SMI'05)*, pp. 244–253, IEEE Comput. Soc, 2005.
- [70] T. Bartkowiak and C. A. Brown, "A characterization of process–surface texture interactions in micro-electrical discharge machining using multiscale curvature tensor analysis," *Journal of Manufacturing Science and Engineering*, vol. 140, no. 2, p. 021013, 2018.
- [71] S. Anani, S. Bhat, N. Honma-Yamanaka, D. Krawchuk, and Y. Yamanaka, "Initiation of hippo signaling is linked to polarity rather than to cell position in the pre-implantation mouse embryo," *Development (Cambridge, England)*, vol. 141, no. 14, pp. 2813–2824, 2014.

- [72] L. Canty, E. Zarour, L. Kashkooli, P. François, and F. Fagotto, "Sorting at embryonic boundaries requires high heterotypic interfacial tension," *Nature communications*, vol. 8, no. 1, p. 157, 2017.
- [73] "Biomimetics — Terminology, concepts and methodology," standard, International Organization for Standardization, Geneva, CH, Apr. 2015.
- [74] J. F. V. Vincent, O. A. Bogatyreva, N. R. Bogatyrev, A. Bowyer, and A.-K. Pahl, "Biomimetics: its practice and theory," *Journal of the Royal Society, Interface*, vol. 3, no. 9, pp. 471–482, 2006.
- [75] M. W. Glier, J. Tsenn, D. A. McAdams, and J. S. Linsey, "Methods for supporting bioinspired design," *ASME 2011 International Mechanical Engineering Congress and Exposition*.
- [76] J.-M. Deldin and M. Schuknecht, "The asknature database: Enabling solutions in biomimetic design," in *Biologically Inspired Design* (A. K. Goel, D. A. Mcadams, and R. B. Stone, eds.), pp. 17–27, London: Springer London, 2014.
- [77] K. Wanieck, P.-E. Fayemi, N. Maranzana, C. Zollfrank, and S. Jacobs, "Biomimetics and its tools," *Bioinspired, Biomimetic and Nanobiomaterials*, vol. 6, no. 2, pp. 53–66, 2017.
- [78] T. Kamps, M. Gralow, G. Schlick, and G. Reinhart, "Systematic biomimetic part design for additive manufacturing," *Procedia CIRP*, vol. 65, pp. 259–266, 2017.
- [79] T. A. Lenau, A.-L. Metze, and T. Hesselberg, "Paradigms for biologically inspired design," in *Bioinspiration, Biomimetics, and Bioreplication VIII* (A. Lakhtakia, ed.), p. 1, SPIE, 04/03/2018 - 08/03/2018.
- [80] P. Valdivia y Alvarado, S. Chin, W. Larson, A. Mazumdar, and K. Youcef-Toumi, "A soft body under-actuated approach to multi degree of freedom biomimetic robots: A stingray example," in *2010 3rd IEEE RAS & EMBS International Conference on Biomedical Robotics and Biomechatronics*, pp. 473–478, IEEE, 2010.
- [81] Ralph O. Schill, Brahim Mali, Thomas Dandekar, Martina Schnölzer, Dirk Reuter, and Marcus Frohme, "Molecular mechanisms of tolerance in tardigrades: New perspectives for preservation and stabilization of biological material," 2009.
- [82] A. Du Plessis, C. Broeckhoven, I. Yadroitsava, I. Yadroitsev, C. H. Hands, R. Kunju, and D. Bhate, "Beautiful and functional: A review of biomimetic design in additive manufacturing," *Additive Manufacturing*, vol. 27, pp. 408–427, 2019.

- [83] S. Moylan, J. Slotwinski, A. Cooke, K. Jurrens, and M. A. Donmez, “An additive manufacturing test artifact,” *Journal of research of the National Institute of Standards and Technology*, vol. 119, pp. 429–459, 2014.
- [84] M. W. Barclift and C. B. Williams, “Examining variability in the mechanical properties of parts manufactured via polyjet direct 3d printing,” in *International Solid Freeform Fabrication Symposium*, pp. 6–8, 2012.
- [85] “Materials Degradation and Detection (MD2): Deep Dive Final Report,” technical report, U.S. Department of Energy, Springfield, USA, Feb. 2013.
- [86] T. Dow and R. Scattergood, “Mesoscale and microscale manufacturing processes: challenges for materials, fabrication and metrology,” in *Proceedings of the ASPE winter topical meeting*, vol. 28, pp. 14–19, Citeseer, 2003.
- [87] Abbott, “Why the aveir vt leadless pacemaker — abbot.” <https://www.cardiovascular.abott/us/en/hcp/products/cardiac-rhythm-management/pacemakers/aveir-vr-leadless-pacemaker/why.html>. Accessed: 15th May 2022.
- [88] L. F. Campanile and A. Hasse, “A simple and effective solution of the elastica problem,” *Proceedings of the Institution of Mechanical Engineers, Part C: Journal of Mechanical Engineering Science*, vol. 222, no. 12, pp. 2513–2516, 2008.
- [89] A. Banerjee, B. Bhattacharya, and A. K. Mallik, “Large deflection of cantilever beams with geometric non-linearity: Analytical and numerical approaches,” *International Journal of Non-Linear Mechanics*, vol. 43, no. 5, pp. 366–376, 2008.
- [90] A. Midha, I. Her, and B. A. Salamon, “A methodology for compliant mechanisms design: Part i — introduction and large-deflection analysis,” in *18th Design Automation Conference: Volume 2 — Geometric Modeling, Mechanisms, and Mechanical Systems Analysis*, pp. 29–38, American Society of Mechanical Engineers, 09131992.
- [91] C.-C. Lan, “Analysis of large-displacement compliant mechanisms using an incremental linearization approach,” *Mechanism and Machine Theory*, vol. 43, no. 5, pp. 641–658, 2008.
- [92] G. L. Holst, G. H. Teichert, and B. D. Jensen, “Modeling and experiments of buckling modes and deflection of fixed-guided beams in compliant mechanisms,” *Journal of Mechanical Design*, vol. 133, no. 5, 2011.
- [93] A. Zhang and G. Chen, “A comprehensive elliptic integral solution to the large deflection problems of thin beams in compliant mechanisms,” *Journal of Mechanisms and Robotics*, vol. 5, no. 2, 2013.

- [94] A. Saxena and S. N. Kramer, "A simple and accurate method for determining large deflections in compliant mechanisms subjected to end forces and moments," *Journal of Mechanical Design*, vol. 120, no. 3, pp. 392–400, 1998.
- [95] R. Frish-Fay, *Flexible Bars*. London: Butterworth, 1962.
- [96] C. P. Lusk, "Quantifying uncertainty for planar pseudo-rigid body models," in *Volume 6: 35th Mechanisms and Robotics Conference, Parts A and B*, pp. 67–73, ASMEDC, 2011.
- [97] S. Kota, J. A. Hetrick, R. Osborn, D. Paul, E. Pendleton, P. Flick, and C. Tilmann, "Design and application of compliant mechanisms for morphing aircraft structures," p. 24.
- [98] P. Bilancia, M. Baggetta, G. Berselli, L. Bruzzone, and P. Fanghella, "Design of a bio-inspired contact-aided compliant wrist," *Robotics and Computer-Integrated Manufacturing*, vol. 67, p. 102028, 2021.
- [99] P. Steutel, G. A. Kragten, and J. L. Herder, "Design of an underactuated finger with a monolithic structure and largely distributed compliance," in *Volume 2: 34th Annual Mechanisms and Robotics Conference, Parts A and B*, pp. 355–363, ASMEDC, 2010.
- [100] W. Zeng, F. Gao, H. Jiang, C. Huang, J. Liu, and H. Li, "Design and analysis of a compliant variable-diameter mechanism used in variable-diameter wheels for lunar rover," *Mechanism and Machine Theory*, vol. 125, pp. 240–258, 2018.
- [101] R. M. Gouker, S. K. Gupta, H. A. Bruck, and T. Holzschuh, "Manufacturing of multi-material compliant mechanisms using multi-material molding," *The International Journal of Advanced Manufacturing Technology*, vol. 30, no. 11-12, pp. 1049–1075, 2006.
- [102] B. M. Olsen, L. L. Howell, and S. P. Magleby, "Compliant mechanism road bicycle brake: A rigid-body replacement case study," in *Volume 6: 35th Mechanisms and Robotics Conference, Parts A and B*, pp. 245–254, ASMEDC, 2011.
- [103] J. D. Owens, M. Houston, D. Luebke, S. Green, J. E. Stone, and J. C. Phillips, "Gpu computing," *Proceedings of the IEEE*, vol. 96, no. 5, pp. 879–899, 2008.
- [104] J. Hao and T. K. Ho, "Machine learning made easy: a review of scikit-learn package in python programming language," *Journal of Educational and Behavioral Statistics*, vol. 44, no. 3, pp. 348–361, 2019.
- [105] M. Lovrić, J. M. Molero, and R. Kern, "Pyspark and rdkit: moving towards big data in cheminformatics," *Molecular informatics*, vol. 38, no. 6, p. 1800082, 2019.

- [106] R. T. Yarlagadda, "Python engineering automation to advance artificial intelligence and machine learning systems," *INTERNATIONAL JOURNAL OF INNOVATIONS IN ENGINEERING RESEARCH AND TECHNOLOGY [IJIERT]*, 2018.
- [107] S. Cass, "The 2018 top programming languages," *IEEE Spectrum*, vol. 31, 2018.
- [108] S. Raschka, J. Patterson, and C. Nolet, "Machine learning in python: Main developments and technology trends in data science, machine learning, and artificial intelligence," *Information*, vol. 11, no. 4, p. 193, 2020.
- [109] L. Oden, "Lessons learned from comparing c-cuda and python-numba for gpu-computing," in *2020 28th Euromicro International Conference on Parallel, Distributed and Network-Based Processing (PDP)*, pp. 216–223, IEEE, 2020.
- [110] S. Van Der Walt, S. C. Colbert, and G. Varoquaux, "The numpy array: a structure for efficient numerical computation," *Computing in science & engineering*, vol. 13, no. 2, pp. 22–30, 2011.
- [111] S. K. Lam, A. Pitrou, and S. Seibert, "Numba: A llvm-based python jit compiler," in *Proceedings of the Second Workshop on the LLVM Compiler Infrastructure in HPC*, pp. 1–6, 2015.

## **Appendix I Predictive topography impact model for Electrical Discharge Machining (EDM) of metal surfaces**



## Predictive topography impact model for Electrical Discharge Machining (EDM) of metal surfaces

Johan Bäckemo<sup>1,2</sup>, Matthias Heuchel<sup>1</sup>, Markus Reinthaler<sup>1,3</sup>, Karl Kratz<sup>1</sup>, and Andreas Lendlein<sup>1,2,\*</sup>

<sup>1</sup>*Institute of Biomaterial Research and Berlin-Brandenburg Center for Regenerative Therapies, Helmholtz-Zentrum Geesthacht, Kantstrasse 55, 14513 Teltow, Germany*

<sup>2</sup>*Institute of Chemistry, University of Potsdam, Karl-Liebknecht-Str. 24/25, 14476 Potsdam, Germany*

<sup>3</sup>*Department of Cardiology, Campus Benjamin Franklin, Charité Berlin, Berlin, Germany*

\* To whom correspondence should be addressed:

Prof. Dr. Andreas Lendlein, email: andreas.lendlein@hzg.de

### ABSTRACT

*Electrical discharge machining (EDM) is a method capable of modifying the microstructure of metal surfaces. Here, we present a predictive computer supported model of the roughness generated on the surface by this process. EDM is a stochastic process, in which charge generated between a metallic substrate and an electrode creates impacts, and thus is suitable for modeling through iterative simulations. The resulting virtual, modified surface structures were evaluated for roughness. Curvatures were analyzed using Abbott-Firestone curves. Three radii of impacts (10, 20, 30  $\mu\text{m}$ ) and two values for the depth to radius ratio (0.1, 0.3) were used as input parameters to compute a total of six simulations. It was found that the roughness parameters followed an inverse exponential trend as a function of impact number, and that the strongly concave curvatures reached equilibrium at an earlier impact number for lower depth to radius ratios.*

## INTRODUCTION

Electrical Discharge Machining (EDM) is a process in which a metallic substrate is brought into close vicinity with an electrode and subjected to repeated sparks, which iteratively removes material – ultimately creating a rough surface [1]. This process is commonly used for difficult-to-machine materials, tooling of complex parts and especially highly accurate micro parts [2]. The roughness of the surface is dependent on many variables such as electrical parameters (voltage, pulse duration, and dielectric influence [3]) and duration of treatment. EDM is a random process, and a probable statistical distribution governs the geometrical parameters and must be taken into account – but as a first approximation the parameters were fixed for each impact for a given simulation. The size of each individual impact is dependent on the charge built up before each spark [3] which is a function of the said electrical parameters, and the number of sparks is dependent on the duration of treatment. Thus, the size of impact and duration of treatment were considered for simulation in this paper. It is of interest to researchers who wish to create surfaces with not only a specific roughness profile, but also a curvature profile. It has previously been discussed that to determine fatigue limits for milled surfaces roughness parameters are not sufficient but that curvature parameters show good correlation for this application [4]. For this purpose, it would be important to see how these parameters differ with each iteration, i.e. impact from spark. Our aim is to get a better understanding for how this iterative process changes the surface topographically with respect to processing time, and that we can relate the output parameters of roughness and curvature to the input parameters. Thus, our hypothesis is that this kind of process could be modeled by an iterative approach, where each iteration subjects the surface to an additional impact from a spark. The motivation and purpose for this study is to be able to manufacture surfaces with defined topographical parameters that are later intended for technical (e.g. aerospace materials [5]) or medical applications, such as orthopedic and dental implant surfaces [6] – and to be able to anticipate these parameters by means of simulation

Considering there is no preference for the location of each impact it can be assumed that this process is stochastic. To model this process by using randomly chosen points on a surface would therefore be suitable. In order predict how surfaces topographically change with each impact, it may be of interest to look at how roughness and curvature changes throughout the process. More importantly, a salient point would be to determine if, at a certain number of iterations, these output parameters reach an equilibrium and do not significantly change with subsequent impacts.

## METHODS

### Model

The generation of a crater with a surrounding rim by a combined spherical cap and half-torus is modeled, as shown in Fig. 1 (A-B). The model used for calculating the deformation was assumed to be ellipsoidal in a previous report [7], however such craters of a concave bowl with bulging rim have been found in simulation studies of simple spark impacts considering both heating and material ejection [8,9]. The spherical cap creates a crater and the torus creates a ridge. The grey line shows the surface datum line, which is initially a flat plane. A point is chosen on that line, which is the point of impact.



The points that fall within the region of the inner and outer circles are deformed accordingly. Overlapping behavior was also considered. It was assumed that a ridge would be formed for each impact due to the physical removal of material for an EDM process, i.e. a ridge could be formed inside of the crater from a previous impact. For each iteration, the volume ( $V$ ) was calculated and removed and a fraction thereof,  $F$ , was used to build the ridge (see equations 1-4).  $F$  was set to 0.5 as preliminary results from visual inspection of an actual EDM-treated surface indicated that this may be a good first approximation (see Figure ). It has previously been shown that electrical discharge energy has a direct influence on average diameter and maximum depth, and that the relationship appears to follow a logarithmic trend [7]. Bartkowiak and Brown also showed that surface discharge energy influences curvature calculation strongly at smaller scales, but showed little variance at larger scales [10]. Others have also reported that crater size increases with increasing current supplied to the EDM [11].

The model was applied to an initially flat surface measuring 1000 x 1000 points with a distance of 1  $\mu\text{m}$  in between each point. The simulation ran iteratively up to 10,000 impacts. Two input parameters were used to determine the extent of changing surface parameters on the surface: radius of impact  $a$ , and the ratio between  $h$  and  $a$ . The values chosen for  $a$  were fixed to 10, 20, and 30  $\mu\text{m}$ , and for the  $h/a$  ratio, 0.1 and 0.3, and were kept constant for each simulation. The radius of the ridge formed were calculated as 2, 4, 6  $\mu\text{m}$  for each value of  $a$ . Equations (1)-(4) give the relation between the model parameters ( $a$ ,  $h$ ,  $F$ ) and the crater radius and respective volume calculations.

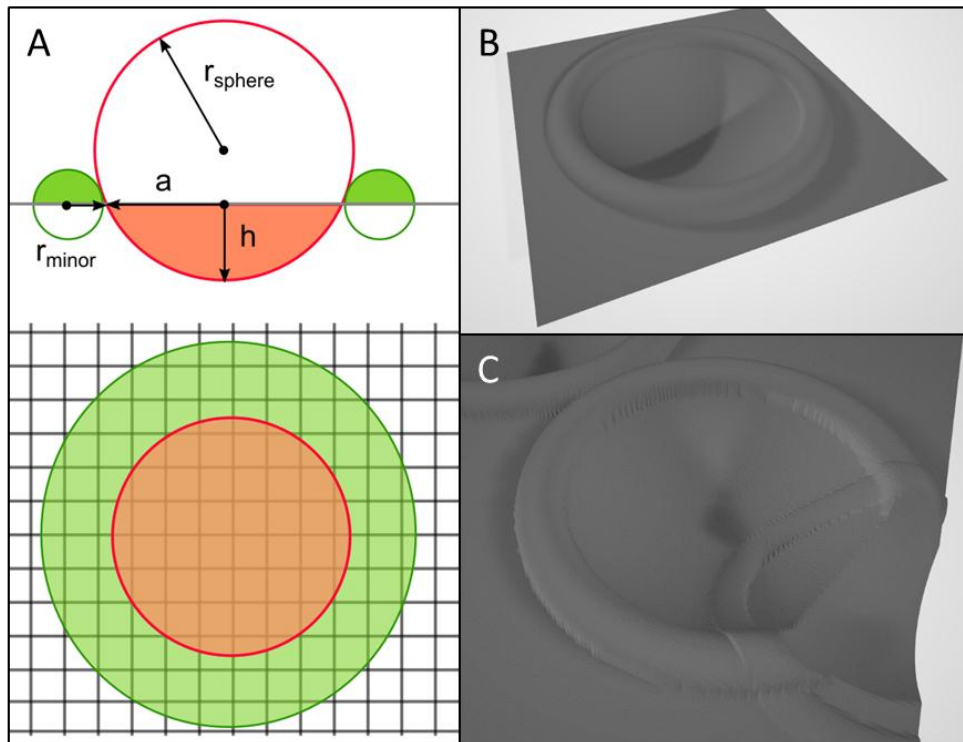


Figure 1 Schematic of combined spherical cap and torus model used for iterative deformation of a metallic surface. A) Top: Side view of deformation model, showing areas that are deformed below datum line (larger circle) and above datum line (smaller outer circles). Bottom: Top view of deformation model show areas that are deformed below datum line (inner circle) and above datum line (outer circle). B) 3D-rendering of a single impact. C) 3D-rendering highlighting overlapping behavior.

$$r_{sphere} = \frac{a^2 + h^2}{2h} \#(1)$$

$$V_{spherical\ cap} = \frac{1}{6}\pi h(3a^2 + h^2) \#(2)$$

$$V_{halftorus} = \pi^2 R r_{minor}^2 = \pi^2 (a + r_{minor}) r_{minor}^2 \#(3)$$

$$V_{torus} = F \cdot V_{spherical\ cap} \#(4)$$

Roughness of the initially flat surface was calculated after a certain number of random impacts. Curvatures were also analyzed for the modified virtual surface.

### Roughness evaluation

Roughness parameters were calculated based on the Abbott-Firestone curve for a 2D-surface, as defined by the standard ISO 25178 [12]. Initially the probability density function (PDF) of the material proportion was calculated, and by drawing a tangential line at 40% cumulative material proportion [13], the roughness parameters *Sk*, *Spk*, *Svk*, *Smr1* and *Smr2* were calculated (Table 1).

Table 1 – Surface roughness parameters obtained from an Abbott-Firestone curve, defined by ISO 25178

Parameter	Description
<i>Sk</i>	Surface roughness core profile
<i>Spk</i>	Reduced peak roughness
<i>Svk</i>	Reduced valley roughness
<i>Smr1</i>	Upper material portion
<i>Smr2</i>	Lower material portion

For each iteration, i.e. each impact, an Abbott-Firestone curve was computed and surface roughness parameters were evaluated each decade with intermediate steps 2 and 5, e.g. 1, 2, 5, 10, 20...5 000, 10 000. The changes in these parameters at these intervals were then analyzed.

### Curvature evaluation

Previous reports have calculated the curvatures of a surface in terms of principal curvatures at different scales, such e.g. in [10]. Here, curvature is described as a second order tensor, which is based on the work by Weingarten [14]. The principal, Gaussian and average curvature values can be determined for each point from this tensor. However for this study, not only the principal curvatures are of interest but also the curvatures at a particular point in all directions. For any given point, N number of directions were chosen to analyze curvature. For each direction three points were chosen: the given point, a point L units away in the given direction, and a point L units away in the opposite direction. With these three

points, one can define a circle on a 2D-plane (See Fig. 2). This method is similar to the procedure reported in [15], where calculations are based on Heron's formula.

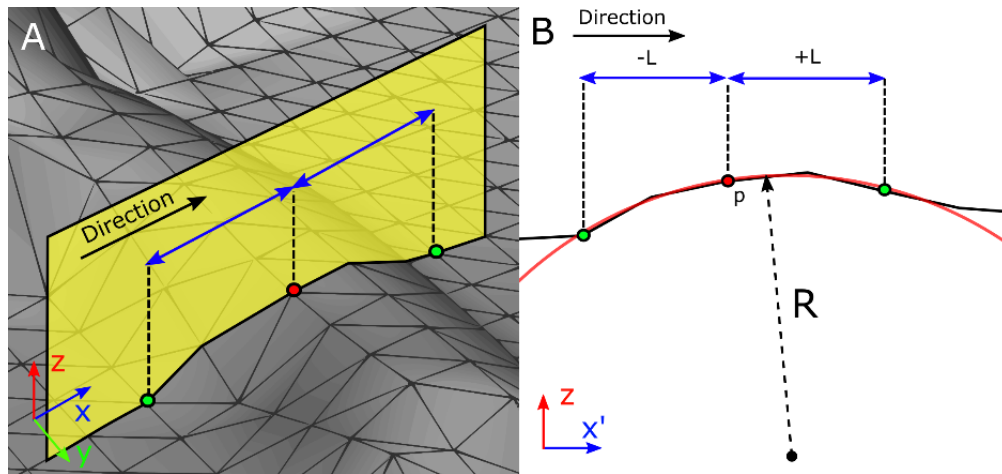


Figure 2 – Schematic of calculating curvature using 3 points on a 2D-plane and inscribing a circle on to it. For any three points  $\in \mathbb{R}^2$  there is only one unique solution to fit a circle. A) Looking at the selected points from the surface. B) Look at the selected points at the cut plane.

Once the coordinates of this set of three points are given, one can inscribe a circle using the steps below.

The three points are defined as:

$$p_1 = (x'_1, z_1), p_2 = (x'_2, z_2), p_3 = (x'_3, z_3)$$

The equation of a circle is described by the equation:

$$Ax'^2 + Az^2 + Bx' + Cz + D = 0$$

Substituting the three points, which lie on the circle, a system of equations is obtained which can be described by the determinant.

$$\begin{vmatrix} x'^2 + z^2 & x' & z & 1 \\ x'^2_1 + z^2_1 & x'_1 & z_1 & 1 \\ x'^2_2 + z^2_2 & x'_2 & z_2 & 1 \\ x'^2_3 + z^2_3 & x'_3 & z_3 & 1 \end{vmatrix} = 0$$

Where,

$$A = \begin{vmatrix} x'_1 & z_1 & 1 \\ x'_2 & z_2 & 1 \\ x'_3 & z_3 & 1 \end{vmatrix}, B = - \begin{vmatrix} x'^2_1 + z^2_1 & z_1 & 1 \\ x'^2_2 + z^2_2 & z_2 & 1 \\ x'^2_3 + z^2_3 & z_3 & 1 \end{vmatrix},$$

$$C = \begin{vmatrix} x'^2_1 + z^2_1 & x'_1 & 1 \\ x'^2_2 + z^2_2 & x'_2 & 1 \\ x'^2_3 + z^2_3 & x'_3 & 1 \end{vmatrix}, D = - \begin{vmatrix} x'^2_1 + z^2_1 & x'_1 & z_1 \\ x'^2_2 + z^2_2 & x'_2 & z_2 \\ x'^2_3 + z^2_3 & x'_3 & z_3 \end{vmatrix}$$

$$r = \sqrt{(x' - x'_1)^2 + (z - z_1)^2} = \sqrt{\frac{B^2 + C^2 - 4AD}{4A^2}}$$

$$K = \frac{1}{r}$$

By taking the inverse of the radius of that circle one determines the curvature in this particular direction. For this analysis L was set to 30 μm. This was repeated for each direction. The number of directions was determined by rotating around the z-axis at the point - 10 degrees for each direction - thus a total of 36 directions. Due to symmetry of the three-point circle calculation, this was reduced to a total of 18 directions. Each point on the surface was evaluated in this manner.

Similar to evaluating the roughness of the surface by computing an analogue to an “Abbott-Firestone” curve, the same principle could be extrapolated to evaluating curvature. Thus curvature parameters for the whole surface were defined, based on the roughness analysis (Table 2). Concavity and convexity refers to positive and negative curvature respectively.

Table 2 – Proposed curvature parameters

Parameter	Description
<i>Kk</i>	Surface curvature core profile
<i>Kpk</i>	Reduced concavity curvature
<i>Kvk</i>	Reduced convexity curvature
<i>Kmr1</i>	Upper material portion
<i>Kmr2</i>	Lower material portion

## RESULTS AND DISCUSSION

### EDM-treated surface and simulated surface comparison

Initial tests of the suitability of the model consisted of comparing a modelled surface with a stainless steel EDM-treated surface (Fig. 3). From the EDM-treated surface, one can clearly see the formation of craters with neighboring ridges. What can also be noted, is that the impact craters appear similar in size and shape. Compared to the simulated surface one can see a clear similarity, and the overlapping behavior from subsequent impacts also are present in the EDM-treated surface. Thus the proposed model was deemed suitable to describe the topographical shape of an EDM-surface.

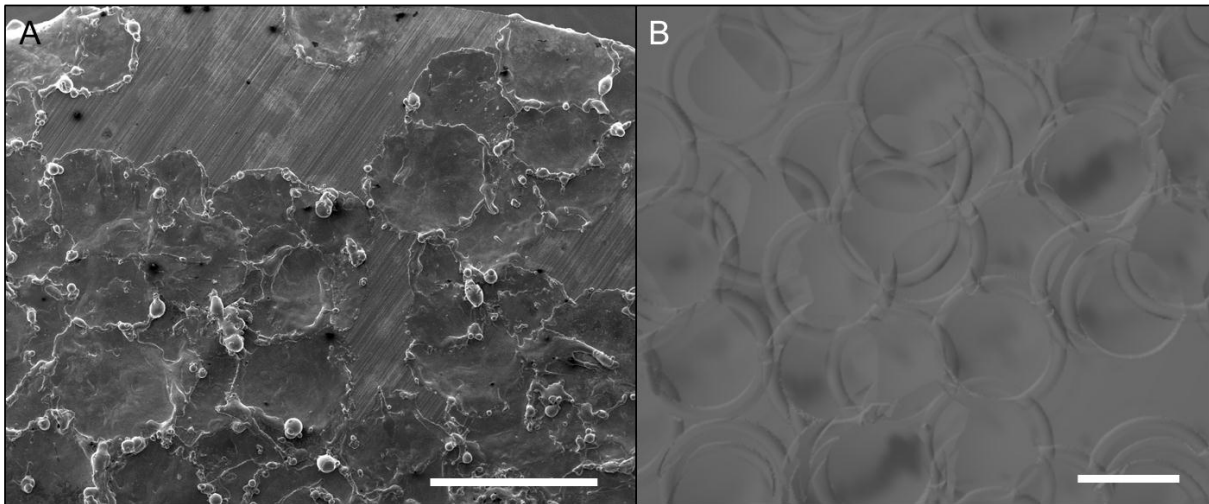


Figure 3 – A) A Scanning Electron Microscopy (SEM) image of a stainless steel EDM treated surface. Scale bar = 1000  $\mu\text{m}$ . B) A surface generated from simulation. Scale bar = 30  $\mu\text{m}$

### Roughness and Curvature analysis

Roughness and curvature analysis were performed after  $n = 1, 2, 5, 10, 20, 50, 100, 200, 500, 1000, 2000, 5000, 10000$  impacts to allow logarithmic plot of the results. The Abbott-Firestone curves for roughness and curvature differ somewhat in shape (Fig. 4). For the roughness analysis, the Abbott-Firestone has a sigmoid shape, as expected, in which the different areas of  $Sk$ ,  $Spk$ , and  $Svk$  are also clearly defined. For the proposed curvature analysis, the Abbott-Firestone has a much sharper appearance, with a plateau in the middle, creating a horizontal tangential line. In addition, the upper and lower material parts are greater for the curvature analysis than for the roughness analysis. This is expected as there are mainly two radii on the surface, that of the crater,  $a$ , and that of the ridge,  $r_{\text{minor}}$ . For a value of  $a = 30 \mu\text{m}$ , the expected curvature from the center going out radially would be  $0.033 \mu\text{m}^{-1}$ , and for a value of  $r_{\text{minor}} = 6 \mu\text{m}$  a curvature of  $0.16 \mu\text{m}^{-1}$ . However there are values out of these regions which can be explained that there are directions that go in all directions, thus if one looks at a point in the crater off-center then the expected curvature values in all directions should differ.

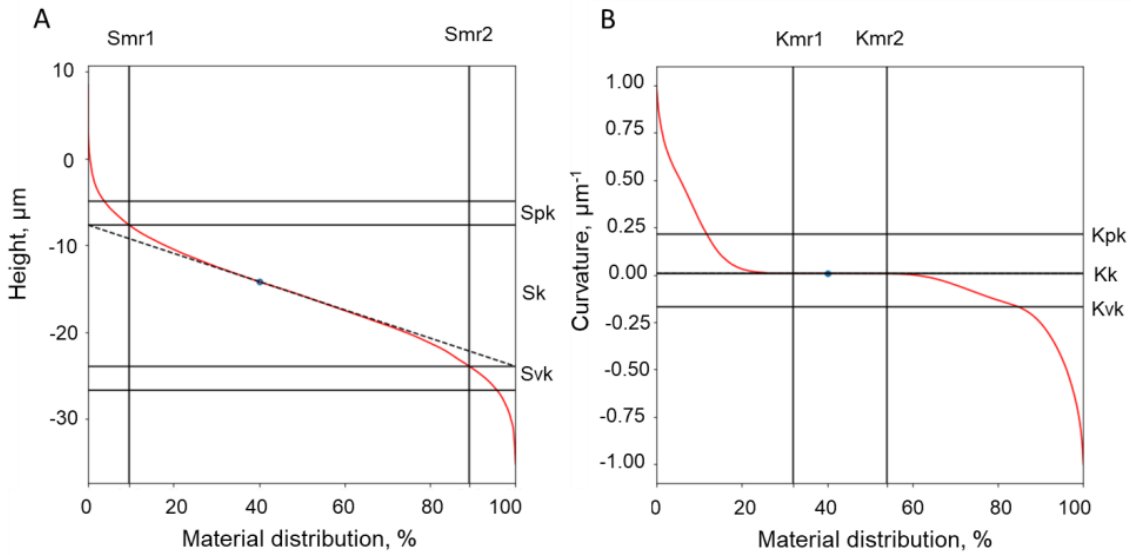


Figure 4. Abbott-Firestone roughness and curvature curves from a surface with the input  $a = 30 \mu\text{m}$  and  $h:a = 0.1$  after 5000 random impacts. The point at 40% material distribution shows at what point the tangential line is drawn, this in turn defined the parameter  $Sk$  and  $Kk$ . A) Abbott-Firestone roughness curve. B) Abbott-Firestone curvature curve

In the interest of predictive modeling, one should try to answer the question of how long a treatment should be conducted to reach a certain roughness value. By looking how the parameters change over time it may give further insight on how to fine tune the input parameters in order to reach the desired properties. For the roughness parameters the core roughness profile,  $Sk$ , gives information of how much the overall roughness changes with each impact, whereas the reduced peak height shows how the number of peaks above the core profile changes with each impact. These graphs are depicted in Fig. 3. From these graphs, it is apparent that  $Sk$  initially changes rapidly and stabilizes with increasing number of impacts. This would mean that after 10,000 impacts the surface does not change significantly.  $Spk$  seems to follow the same trend. Comparing the top and bottom graphs, one sees that the values for both  $Sk$  and  $Spk$  are greater for  $h/a = 0.3$ , which is logical seeing that the depth is greater, and thus for each impact a greater height difference is achieved.

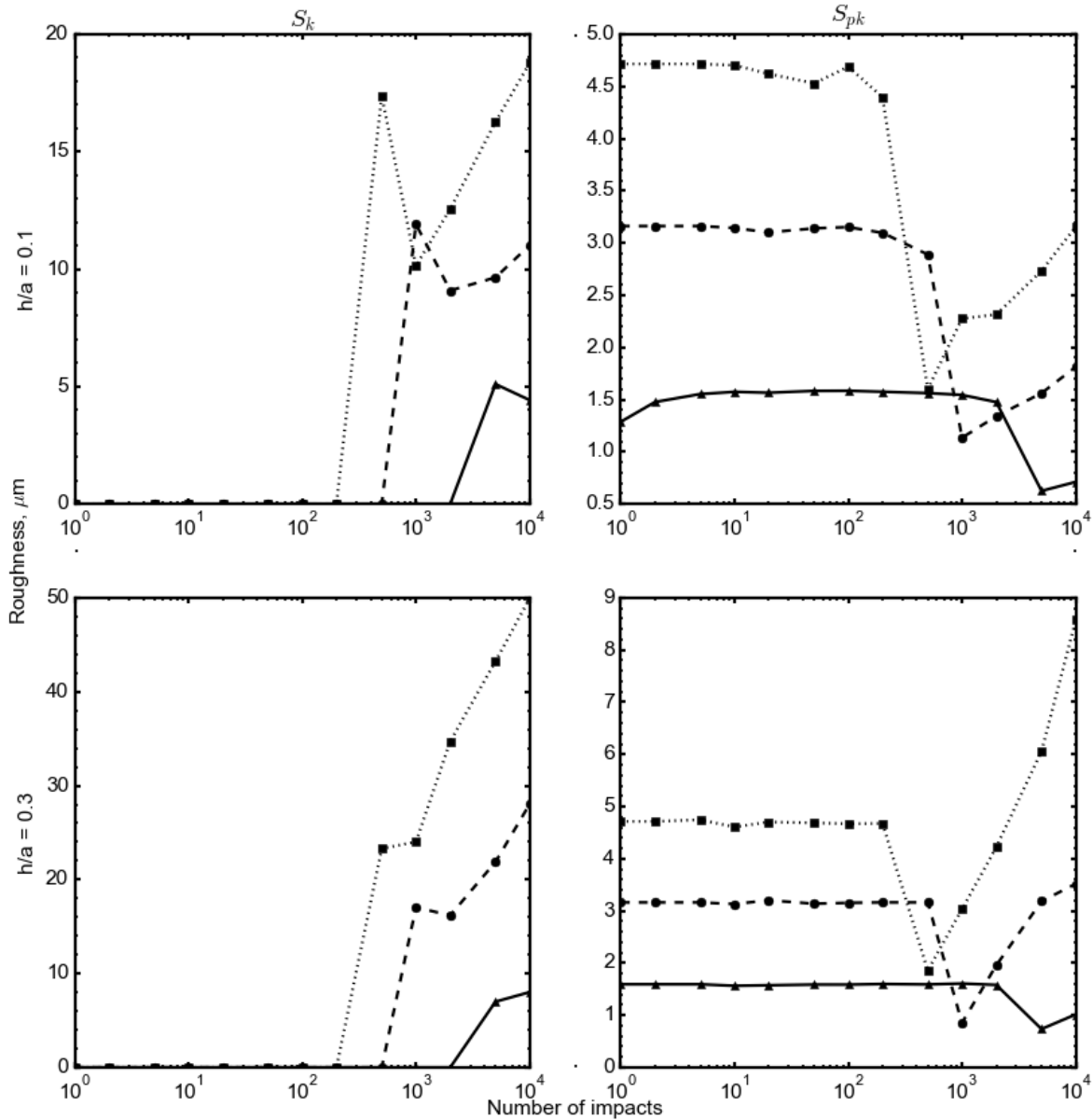


Figure 5 – Graphs of plotting  $S_k$ , core roughness profile (left), and  $S_{pk}$ , reduced peak height (right), as a function of number of impacts. Graphs with  $h/a = 0.1$  (top),  $h/a = 0.3$  (bottom). Lines are shown for impact radius,  $a$ , of 10  $\mu\text{m}$  (line), 20  $\mu\text{m}$  (dashed), and 30  $\mu\text{m}$  (dotted).

On the other hand, there is an apparent difference between the curvature results (see Fig. 5). The core curvature profile appears to increase greatly during the initial phase of impacts, and then switch sporadically from low to high. In contrast, the reduced concavity profile,  $K_{pk}$ , steadily increases until it reaches a final value and plateaus. Also of note, is that the value of  $K_{pk}$  is inversely proportional to  $a$ , since curvature is defined as the reciprocal of the radius of a circle. For any value of  $a$ ,  $K_{pk}$  reaches an equilibrium plateau after a certain number of impacts, which could be due to the curvature values present on the surface are related to  $a$ , and after a certain number of impacts all points on the surface have been deformed at least once, and thus the curvature profile does not



change significantly due to subsequent impacts. What can also be seen is that the greater the value of  $a$ , the quicker the surface reaches its final  $Kpk$  value, which may be explained by the fact that the proportion of the surface deformed with respect to the total surface increases. Comparing the lower and upper graphs, one can see that  $Kpk$  appears to reach equilibrium at a later impact number for  $h/a = 0.3$  compared to  $h/a = 0.1$ , this most notably seen for  $a = 10 \mu\text{m}$ .

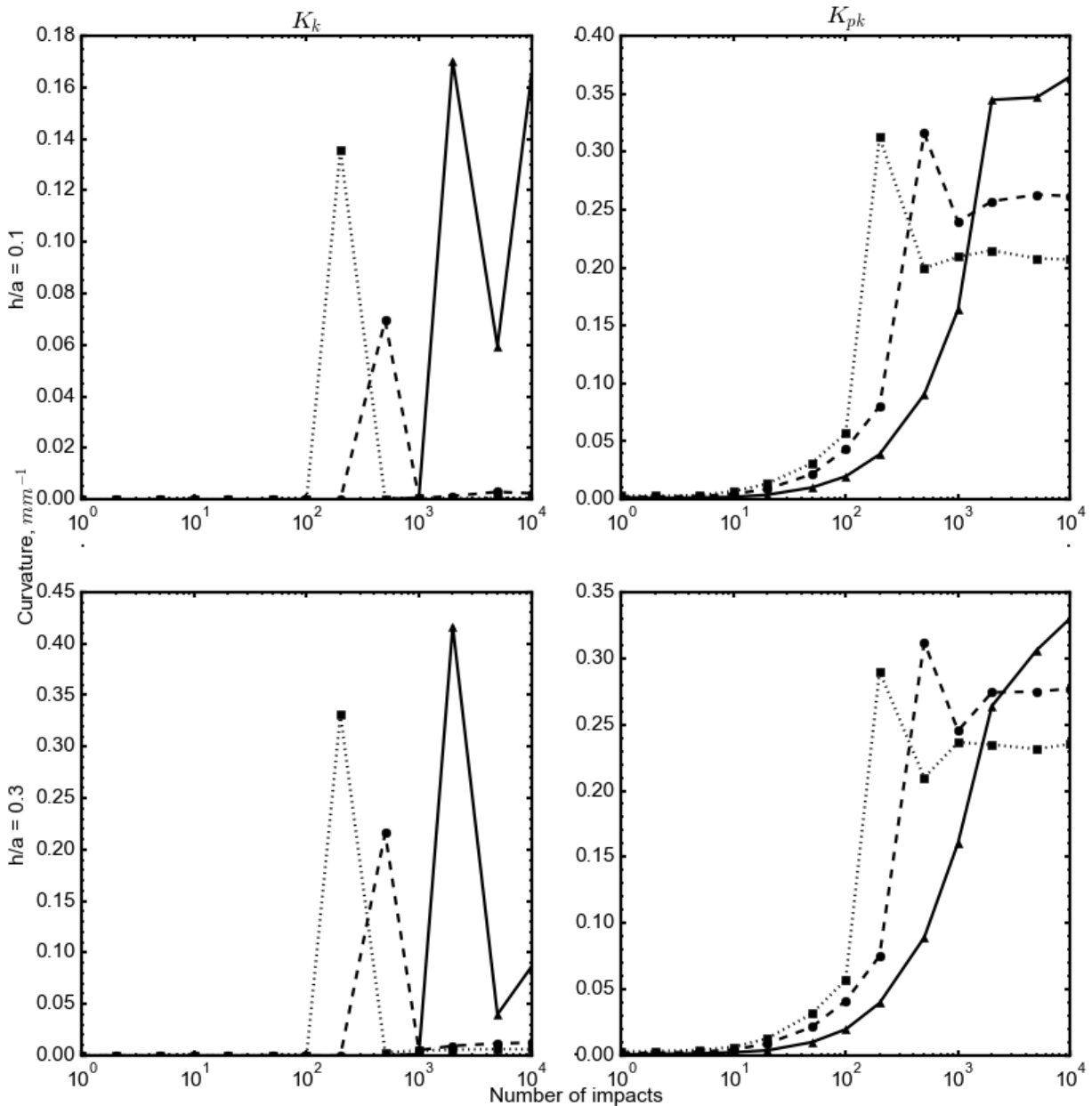


Figure 6 - Graphs of plotting  $K_k$ , core curvature profile (left), and  $K_{pk}$ , reduced curvature concavity profile (right), as a function of number of impacts. Graphs with  $h/a = 0.1$  (top),  $h/a = 0.3$  (bottom). Lines are shown for impact radius,  $a$ , of  $10 \mu\text{m}$  (line),  $20 \mu\text{m}$  (dashed), and  $30 \mu\text{m}$  (dotted).

The values for  $Sk$  as a function of impact number appears to follow an inverse exponential trend, which could be explained by that given that the process is stochastic. The probability of extreme height differences between the lowest and



highest point is small – meaning that the roughness would tend to approach an asymptote at a particular roughness value. For a given impact radius,  $a$ , the strongly concave curvatures will reach its final value at an earlier impact number for a high  $h/a$  ratio compared to a lower one. In addition, a flat surface has no curvature by definition – but at a certain impact number all points are deformed, and each point will have non-zero curvature in all directions. This may seem contrary to the Abbott-Firestone curvature curve (Fig. 4B) as it appears to be a plateau at around  $0 \mu\text{m}^{-1}$ , however these points are in fact weakly concave or convex. This weak concavity and convexity may come from the points on the ridges where the some directions are tangential to the ridges, which are weakly concave. The same is true for the off-centre points in the craters.

In this work, a length of  $30 \mu\text{m}$  was selected to define three points in order to define the curvature for a given point in a given direction. Changing the value of this length will have a direct impact on the curvature calculation and on the “Abbott-Firestone” curves. In our future work we will consider multi-scale curvature analysis [4, 14] and further topographical analysis [16].

It can be assumed from a comparing real and computed surfaces in Fig. 6 that the formation of globules in the real surface is not replicated in the simulated surface. This was omitted, since the modelling of such a variant structure needs more careful analysis of the sizes of such globules, similar to the method reported in [11].

## CONCLUSION

In this study the EDM process was modeled using a combined spherical cap and torus model which was deemed suitable for the purposes of fabrication design by comparing the results to an EDM-treated stainless steel surface. As the surface underwent this treatment as function of impact number, its  $Sk$  value followed an inverse exponential trend, which was as expected due to its stochastic nature. Furthermore, it was shown that one can control the strongly concave and strongly convex regions by reaching a certain impact number, however more simulations are needed in order to define the core curvature profile through varying more input parameters.

## ACKNOWLEDGEMENTS

This work was financially supported by the Helmholtz-Association of German Research Centers (through program-oriented funding, and through the Helmholtz Graduate School of Macromolecular Bioscience [MacroBio], grant no. VH-GS-503).




## REFERENCES

- [1] S. Kumar, R. Singh, T.P. Singh, and B.L. Sethi, *J. Mater. Process. Technol.* **209**, 3675 (2009).
- [2] M. Gostimirovic, P. Kovac, M. Sekulic, and B. Skoric, *J. Mech. Sci. Technol.* **26**, 173 (2012).
- [3] Z. Yu, K.P. Rajurkar, and J. Narasimhan, *ASPE Precis. Mach. Annu.* Portland, OR (2003).
- [4] M. Vulliez, M.A. Gleason, A. Souto-Lebel, Y. Quinsat, C. Lartigue, S.P. Kordell, A.C. Lemoine, and C.A. Brown, *Procedia CIRP* **13**, 308 (2014).
- [5] J. George and M. Chandrasekaran, in *Asp. Mech. Eng. Technol. Ind.* (Nirjuli, India, 2014), pp. 278–284.
- [6] A.A. Aliyu, A.M. Abdul-Rani, T.L. Ginta, C. Prakash, E. Axinte, M.A. Razak, and S. Ali, *Adv. Mater. Sci. Eng.* **2017**, (2017).
- [7] H. Ding, X. Li, X. Wang, L. Guo, and L. Zhao, in *Proc. 2nd Int. Conf. Adv. Mech. Eng. Ind. Informatics (AMEII 2016)* (Atlantis Press, Paris, France, 2016), pp. 1316–1320.
- [8] X. Yang, J. Guo, X. Chen, and M. Kunieda, *Precis. Eng.* **35**, 51 (2011).
- [9] J. Tao, J. Ni, and A.J. Shih, *J. Manuf. Sci. Eng. Trans. ASME* **134**, 1 (2012).
- [10] T. Bartkowiak and C.A. Brown, *J. Manuf. Sci. Eng.* **140**, (2018).
- [11] S. Arooj, M. Shah, S. Sadiq, S.H.I. Jaffery, and S. Khushnood, *Arab. J. Sci. Eng.* **39**, 4187 (2014).
- [12] ISO CD 25178-2:2012 “Geometrical Product Specification (GPS) – Surface Texture: Areal – Part 2: Terms definitions and surface texture parameters,” Geneva Int. Organ. Stand. (2012).
- [13] R. Laheurte, P. Darnis, N. Darbois, O. Cahuc, and J. Neauport, *Opt. Express* **20**, 13551 (2012).
- [14] J. Weingarten, *J. Für Die Reine Und Angew. Math.* **59**, 382 (1861).
- [15] M.A. Gleason, S. Kordell, A. Lemoine, and C.A. Brown, in *14th Int. Conf. Metrol. Prop. Eng. Surfaces, Taipei, Taiwan, Pap. TS4-01* (2013).
- [16] C.A. Brown, H.N. Hansen, X.J. Jiang, F. Blateyron, J. Berglund, N. Senin, T. Bartkowiak, B. Dixon, G. Le Goïc, Y. Quinsat, W.J. Stemp, M.K. Thompson, P.S. Ungar, and E.H. Zahouani, *CIRP Ann.* **67**, 839 (2018).

## **Appendix II Bio-inspired and computer-supported design of modulated shape changes in polymer materials**



## Bio-inspired and computer-supported design of modulated shape changes in polymer materials

Johan Bäckemo , Yue Liu , Andreas Lendlein , Institute of Active Polymers, Helmholtz-Zentrum Hereon, Kantstr. 55, 14513 Teltow, Germany; Institute of Chemistry, University of Potsdam, 14476 Potsdam, Germany

Address all correspondence to Andreas Lendlein at [Andreas.Lendlein@hereon.de](mailto:Andreas.Lendlein@hereon.de)

(Received 21 April 2021; accepted 8 June 2021; published online: 20 July 2021)

### Abstract

The Venus flytrap is a fascinating plant with a finely tuned mechanical bi-stable system, which can switch between mono- and bi-stability. Here, we combine geometrical design of compliant mechanics and the function of shape-memory polymers to enable switching between bi- and mono-stable states. Digital design and modelling using the Chained Beam Constraint Model forecasted two geometries, which were experimentally realized as structured films of cross-linked poly[ethylene-co-(vinyl acetate)] supported by digital manufacturing. Mechanical evaluation confirmed our predicted features. We demonstrated that a shape-memory effect could switch between bi- and mono-stability for the same construct, effectively imitating the Venus flytrap.

### Introduction

In nature, evolution has had millions of years to develop some of the most ingenious solutions for survival. The carnivorous Venus flytrap (*Dionaea muscipula*) comprises of two trap lobes, which upon stimulation of its inner spikes slams shut to trap prey inside. It is with this snap-through behavior, which is occurring within 300 ms,<sup>[1]</sup> that is of particular interest for biomaterial applications. Previously, the mechanism has inspired the invention of pressure-dependent multi-stable origami cells<sup>[2]</sup> and was implemented as a bi-stable reversible hydrogel construct.<sup>[3]</sup> Many researchers have speculated what processes are behind the quick actuation of closing the trap lobes. Water displacement from the inner surface of the lobes to the external surface plays a critical role,<sup>[4]</sup> but pre-stress is important for the speed with which the lobes are closed.<sup>[5]</sup> In its open position, the lobes of the Venus flytrap are concave [Fig. 1(a)] and when activated and stimulated the displacement of water acts as an actuation of the lobes from a concave to a convex configuration. The switching between an open and closed lobe position, can be seen from a mechanical perspective as a bi-stable system—such a system has per definition at least two stable states that remain unchanged until further activation. These positions are points of local energy minima, or in other words where the static forces are balanced. Bi- or meta-stable systems are also present in the field of compliant mechanisms. They are defined as flexible entities that transmit motion through elastic body deformation.<sup>[6]</sup> In comparison to classical mechanisms, e.g. barrel hinges, which require a minimum of three parts; two leaves and a pin connector, a compliant mechanism should enable the same motion in one single part. The benefit is minimized abrasion, since no parts

are grinding against each other, and no need for assembly.<sup>[7]</sup> With the advance of digital manufacturing such as Fused Deposition Modelling (FDM), Multi-Jet Printing (MJP), and Stereolithography (STL), the ability to design and manufacture complex single-part objects have become easier and require less processing time. Mechanisms with bi-stable behavior can be used in a range of applications, including the design of Microelectromechanical Systems (MEMS),<sup>[8]</sup> animatronics,<sup>[9]</sup> or grippers for soft robotics.<sup>[10]</sup> The forecasting of the behavior for such a design is non-trivial and requires analysis and computation by non-linear models. The two major models are the Pseudo Rigid Body Model (PRB)<sup>[11]</sup> by Larry L. Howell and the Beam Constraint Model (BCM)<sup>[12]</sup> from Shorya Awtar, both of which are developed with the intention of incorporating the effects of load stiffening, kinematic and elastokinematic effects while still accessible enough to be used as design tools. This paper incorporates the Chained Beam Constraint Model (CBCM) which is a further improved BCM model proposed by Chen et al.<sup>[13]</sup> To add another degree of functionality, we investigate how one can modulate bi-stable behavior, turning it on or off. The conception of switching between bi-stable and mono-stable states was achieved by active materials, which are well known in the fields of robotics, sensors and autonomous processes.<sup>[14–16]</sup> Here, a thermally responsive shape-memory polymer (SMP) was chosen, as they can shift between preprogrammed and original geometries under certain temperatures governed by melting transition.<sup>[17, 18]</sup> It is the combination of geometrical features, the shape of the lobes, and material properties, the displacement of water that have enabled the Venus flytrap to develop its “snap-through” mechanism. Similarly, by combining compliant mechanisms and the shape-memory effect

J. Bäckemo and Y. Liu contributed equally to this work.

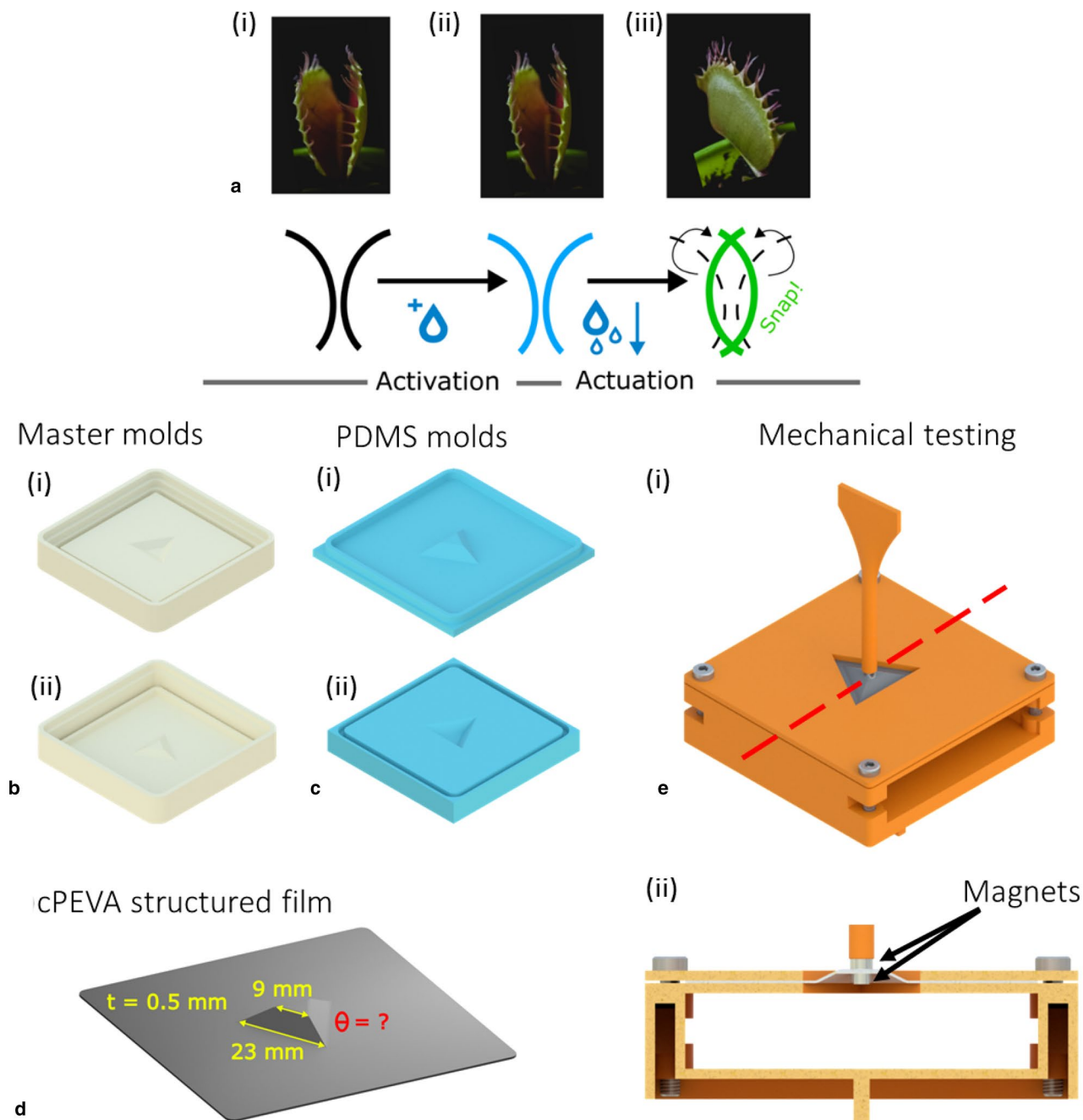


**Figure 1.** (a) The closing “snap-through” mechanism of the Venus flytrap. (i) In its dehydrated state the Venus flytrap is unlikely to snap when stimulated. (ii) When hydrated it is in its activated state, “ready-to-snap”, and upon stimulating its inner spikes (iii) a rapid displacement of water leads to a configuration change of the lobes from concave to convex and thus shuts close. (Photos with permission of Izabella Bedő, Pexels GmbH.) (b) 3D-printed master molds for PDMS mold creation. (i) and (ii) are combined and casted with PDMS to create the top PDMS mold in c(i). Subsequently a casting step is performed with c(i) to create the negative mold c(ii) by PDMS. By combining the PDMS molds c(i) and c(ii) with a PEVA film through hot embossing the final structured cPEVA structure is manufactured (d). The mechanical testing setup (e) shows how the cPEVA films are tested. Here, 3D-printed heat-resistant parts were printed which are able to sustain temperatures up to 200°C shown in orange. The red-dashed line in e(i) shows the plane cut for the cross-section in e(ii). The cPEVA film is clamped down by two opposing plates with a hole in the shape of the truncated tetrahedron. Two magnets on the top and bottom of the cPEVA film respectively couples the mechanical probe and the sample, as can be seen in cross-section in e(ii) indicated by the black arrows.

(SME) we hypothesized that we could create the same effect controlled by temperature instead of humidity.

We explore the design, realization, and characterization of switching between bi-stable states on and off in 3D-structured films prepared from cross-linked poly[ethylene-*co*-(vinyl acetate)] (cPEVA).<sup>[19]</sup> A truncated tetrahedron structure was designed and simulated to predict bi-stable or mono-stable states by varying geometrical parameters. The predicted structures were created through a two-step manufacturing method: (i) master molds were 3D-printed to cast the PDMS molds and (ii) the cPEVA films were created through hot embossing in the PDMS molds. The programming of the cPEVA film was achieved by first compressing the film between the PDMS molds of the targeted shape at the melting temperature and then fixing the temporary shape by cooling to a low temperature.

## Experimental details

### Modelling

Modelling was carried out using the equations for the Chained Beam Constraint Model (CBCM) as outlined in the previously reported publication by Chen et al.<sup>[20]</sup> The relevant equations are outlined in the supporting info as a supporting method. Each beam was subdivided into 15 elements. The solution of the non-linear models were carried out through Python 3.8 using the packages NumPy, SciPy, Pandas, and Matplotlib as part of the Anaconda Distribution (Anaconda, Inc., Austin, USA). The Young's modulus,  $E$ , used for the modelling was set to 40 MPa (Storage modulus  $E' = 44$  MPa, and loss modulus  $E'' = 6.4$  MPa at 25°C as reported by Liu et al.<sup>[21]</sup>).

### Materials

Poly[ethylene-*co*-(vinyl acetate)] with a vinyl acetate content of 18 wt% (PEVA18) was obtained from DuPont de Nemours (Neu-Isenburg, Germany). Crosslinking agent dicumyl peroxide (DCP) was purchased from Sigma-Aldrich Chemie GmbH (Taufkirchen, Germany) and Sylgard™ 184 silicone elastomer kit from Dow Corning Corp. (Midland, USA). All chemicals were used as received. The 3D printing materials used are VeroWhite™ and HighTemp™ (Stratasys, Rehovot, Israel) and printed with the Stratasys Connex 3 Objet 260 Polyjet printer (Stratasys, Rehovot, Israel).

### Preparation of 3D films

The master molds to create the PDMS molds were first designed in Autodesk Inventor (Autodesk, San Rafael, USA) and printed with VeroWhite™ [See Fig. 1(b)] using the Stratasys Connex 3 Objet 260 Polyjet printer (Stratasys, Rehovot, Israel). To ensure good demolding Ease Release™ 200 (Smooth-On, Inc., Macungie, USA) was applied before PDMS casting. The PDMS soft molds were then replicated from the 3D-printed master molds [see Fig. 1(c)] and synthesized from a precursor mixture of 90 wt% prepolymer sylgard 184 and 10 wt% curing

agent by polymerizing at 40°C for 24 h. The PDMS molds were further cured at 80°C for 2 h after removed from the 3D-printed master molds. The cPEVA precursors were prepared by mixing 196 g PEVA18 and 4 g DCP in a twin-screw extruder (Euro-PrismLab, Thermo Fisher Scientific) at 110°C and 50 rpm. The blends were compression molded into films with a 0.5 mm thickness and ready for further molding and crosslinking into defined 3D structures. Finally, for synthesizing the cPEVA 3D films, the PEVA blended films were sandwiched between the pair of PDMS molds and clamped between two metal plates, which was heated in the oven at 200°C for one hour. Then, the resulted 3D film [Fig. 1(d)] was separated from the molds after cooling.

### Mechanical testing

To characterize the bi-stable behavior of the cPEVA 3D film, a Zwick Z1.0 tensile test machine for mechanical testing (Zwick, Ulm, Germany) equipped with a thermo-chamber and temperature controller (Eurotherm Regler, Limburg, Germany) was used. For testing the structure a custom-made test jig was produced [Fig. 1(e)]. The components of the jig were printed with high temperature resistant material (HighTemp™, Stratasys, Rehovot, Israel) using Stratasys Connex 3 Objet 260 Polyjet printer (Stratasys, Rehovot, Israel). These parts are heat resistant up to 230°C (Heat deflection of 0.45 MPa at 230°C), which was sufficient for our testing. Here, two flat plates having triangle holes with side length of 30 mm were designed to clamp and fix the film, which only allows freedom at the location of the truncated tetrahedron structures. Ample space was made below the film to allow the truncated tetrahedron to deform. To apply force on top of the truncated tetrahedron, a cylindrical probe with a diameter of 5 mm was designed and clamped to the top clamp. A pair of magnets, one fixed at the end of probe and the other touching the underside of the truncated tetrahedron, was used to keep the probe in contact with the sample to track the force during on- and off-loading. The force curves of compression on the truncated tetrahedrons of original, programmed and recovered samples were measured at room temperature. The recovery of the programmed sample was achieved by heating to 100°C in the chamber and cooled down to room temperature before measurements.

### Optical microscopy

The optical microscopy of the cPEVA 3D film was measured by DVM6 microscope (Leica Microsystems, Wetzlar, Germany) with the objective PLANAPO FOV 43.75. Each sample was measured by  $\times 50$  magnification with 20 to 48 pictures. The Z dimension was stacked with 14 to 20 steps. The 3D image was integrated and the critical angles of the pyramid structures at three sides were analyzed by software Leica Applications Suite X (LASX, Version 3.0.14). Each side was measured at three positions.



## Programming and fixing

The programming was achieved by compression between PDMS molds with the targeted angle. The cPEVA 3D films were aligned with the pyramid molds and sandwiched between two metal plates and compressed with four clamps. The whole device was put in the oven at 70°C for 1 hour during the programming. Finally, the programmed sample was accomplished by cooling in the fridge at 5°C for 1 hour before being removed from the molds.

## Results and discussion

For a typical bi-stable structure, the definition as hinted in the name is that it has two stable positions, i.e., two stable equilibrium points. At these stable points, the structure will remain unchanged until further acted upon. Figure 2(a) shows the typical behavior of a mono-stable and a bi-stable structure. The requirement for a bi-stable structure is that at some point in the force–displacement curve the force reaches zero at some displacement  $d > 0$ . In a mono-stable structure this does not occur. The critical forces acting on the structure switching between the two stable points in a bi-stable structure are

called the *snap-through force* ( $F_{\max}$ ) and *snap-back force* ( $F_{\min}$ ), respectively.<sup>[20]</sup> As the force  $F$  acting upon the structure reaches the critical value  $F_{\max}$  the structure will “snap” to the second stable position, as this is more energetically favorable. Similarly, this occurs when switching back to the original position with  $F_{\min}$ . These structures are mainly fabricated as 2D-planar structures.<sup>[8, 22–24]</sup> Here, we create a 3D structure with modulated bi-stability, i.e. a structure that could switch from being mono- to bi-stable. We devised a stable structure in CAD, which could later be evaluated with a mechanical tester. The design was settled on a truncated tetrahedron, a “pyramid-like” structure [Fig. 1(d)]. The truncation allows for an area load, which is more stable than a point load. Here, we left it open to see what slope angle  $\theta$  of the sides of the tetrahedron would lead to a mono-stable and bi-stable structure. The side of the tetrahedron has a “sigmoid” like shape and could be modelled as a beam with a fixed and a free end. This allows the structure to be modelled with non-linear beam models. The previously reported Chained Beam Constraint Model (CBCM) was implemented.<sup>[13]</sup> The computational model predicted that a slope angle  $\theta$  of 30° and 45° would show a mono- and bi-stable behavior, respectively [Fig. 2(b) and Supplementary videos S1

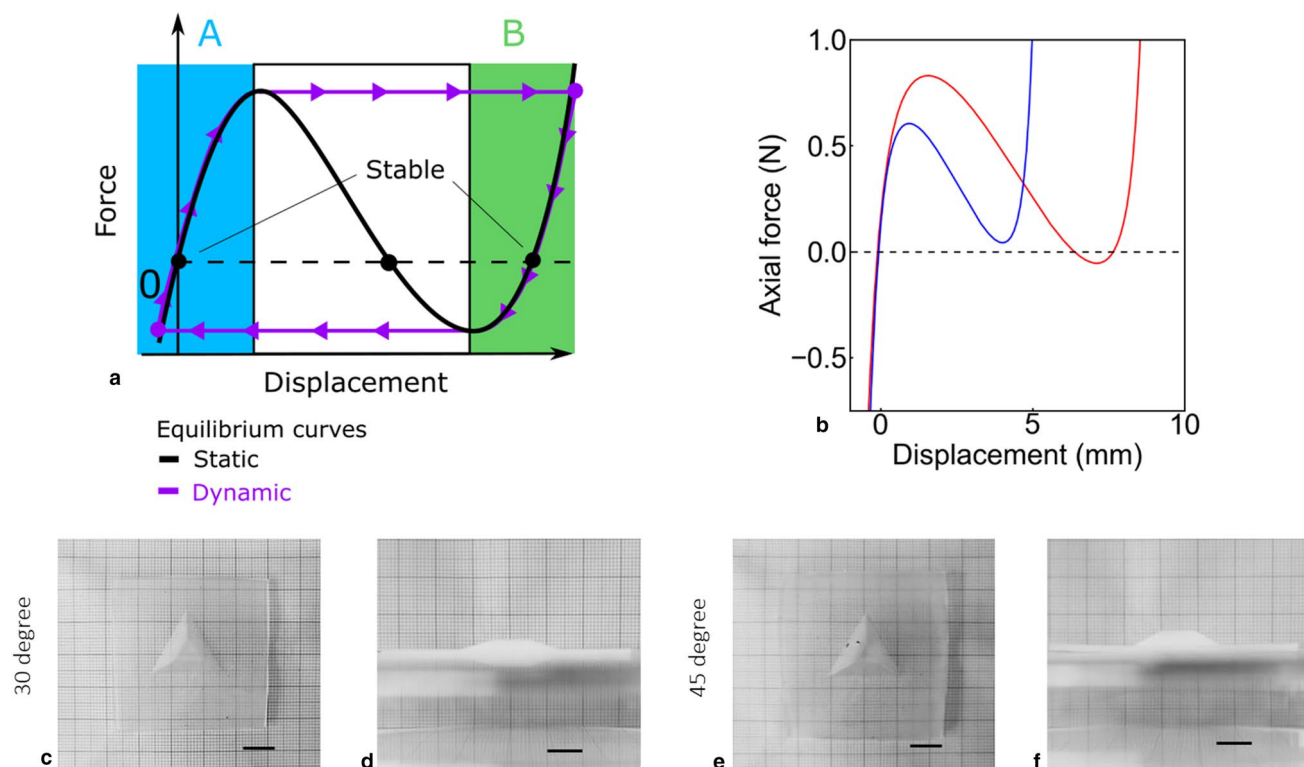


**Figure 2.** (a) A typical mechanical bi-stability diagram showing the static equilibrium curve (black) and dynamic equilibrium curve (purple). Here, three equilibria can be identified (black points) but only where the static and dynamic equilibrium passes through are stable; i.e. only two. The areas in which the structure would return to an equilibrium point is indicated in the areas A (blue) and B (green). The third equilibrium in the middle is unstable and will fall back into a stable equilibrium if only a slight disturbance occurs. (b) Modelled behavior using the CBCM model for slope angles  $\theta$  of 30° (blue) and 45° (red). The structure for a truncated tetrahedron with a slope angle  $\theta$  of 45° shows bi-stable behavior. (c–f) Photos of prepared cPEVA 3D films with pyramid slope angles of 30° (c, d) and 45° (e, f) from top view (c, e) and side view (e, f). The scale bar in each picture is 10 mm.

and S2]. In order to, in the same structure, switch between a mono-stable and a bi-stable structure we needed an active material. We show here how the use of an SMP can achieve this. To fabricate these structures we decided to cast cPEVA using PDMS molds instead of directly using 3D-printed molds due to three considerations. First, the PDMS mold is stable at this high curing temperature of cPEVA (200°C), compared to the 3D-printed mold made from VeroWhite™, which has a low heat deflection temperature (HDT) of 60°C. Second, the PDMS has low surface potential and is chemically inert to the crosslinking reaction of PEVA, while the 3D-printing material is more reactive to the polymerization of PEVA. Third, the PDMS mold is more elastic than the rigid 3D-printed mold and the elasticity is helpful to peel the mold off from the structured cPEVA films. Therefore, a pair of 3D-printed master molds was created with the design of truncated tetrahedron structures, as shown in Figure S1a, b and a pair of PDMS molds

(Fig. S1c,d) were replicated from the 3D-printed counterparts. Then, the cPEVA films with truncated tetrahedron structures [Fig. 2(c)–(f)] were successfully fabricated by soft lithography approach using PDMS molds (Fig. S1e,f). The slope angle of the truncated tetrahedrons were measured by an optical microscope and calculated to be  $29.2^\circ \pm 3.3^\circ$  for the  $30^\circ$  tetrahedron and  $39.3^\circ \pm 1.3^\circ$  for the  $45^\circ$  tetrahedron. The results prove a success of the molding approach and reveal a slightly higher difference for the  $45^\circ$  tetrahedron to the realized sample.

To mechanically test these films, a custom-made test jig was created from high-temperature-resistant material for insertion into a mechanical tester [Figs. 1(ei), 3(a)]. To measure the force throughout the displacement of the structure two magnets were used to couple the mechanical probe to the cPEVA film; one affixed onto the probe and one underneath the cPEVA film at the truncation of the tetrahedron [Figs. 1(eii), 3(b)–(d)]. From the mechanical testing it was

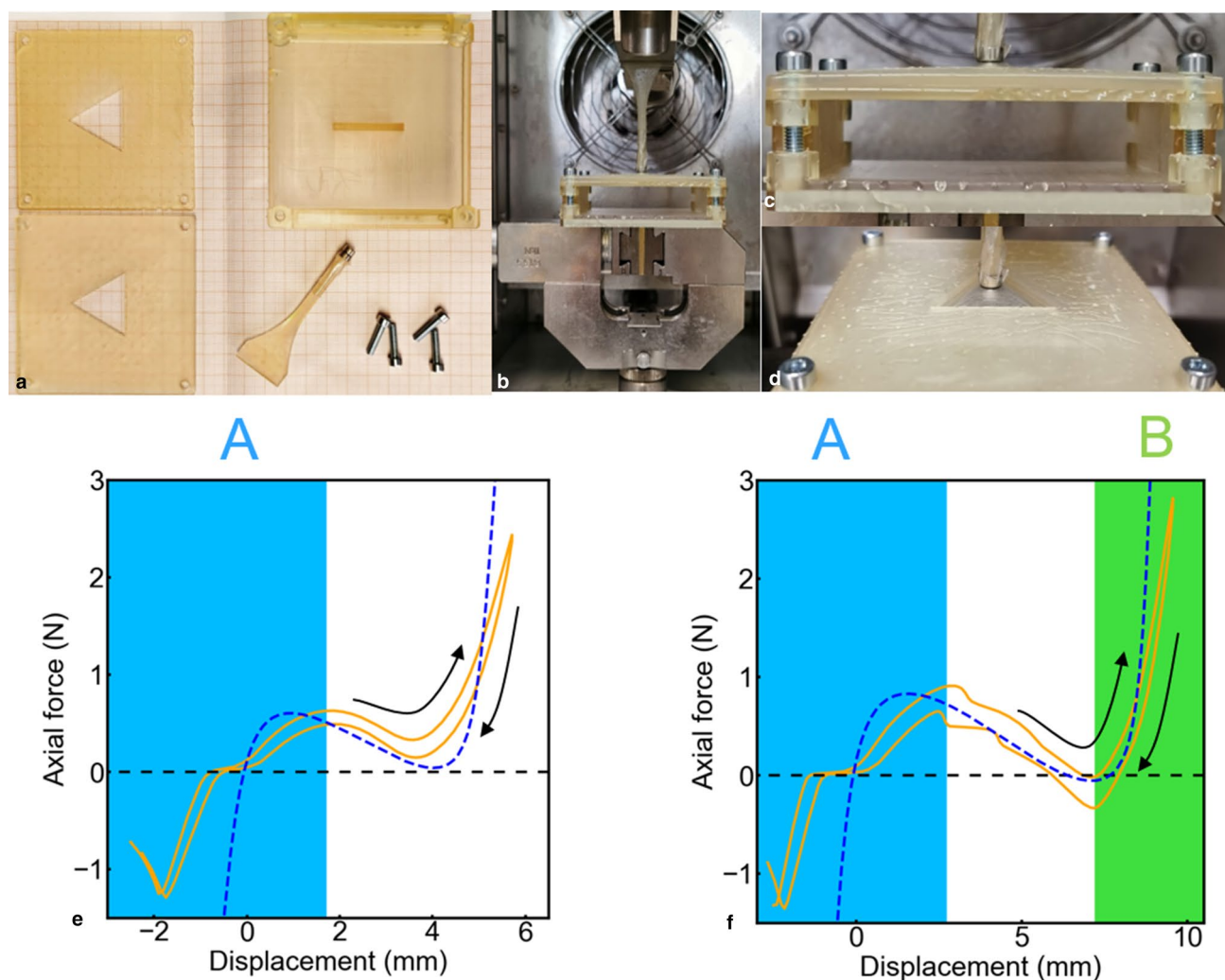


**Figure 3.** (a) Photos of 3D-printed parts used for mechanical test. (b) Photos of assembled self-built device for bi-stable test (c-d). Photos of self-built device working in the tensile test machine. Force–displacement curve of (e)  $30^\circ$  and (f)  $45^\circ$  truncated tetrahedron samples. CBCM model prediction (blue dashed line); mechanical test curve (orange). The black arrows indicate on- and off-loading directions. Areas A (blue) and B (green) indicate stable domains for each construct.



confirmed that the 30° truncated tetrahedron sample showed a mono-stable behavior and that the 45° truncated tetrahedron sample showed a bi-stable behavior, and was in good agreement with the predicted models [Fig. 3(e), (f)]. Additionally, there was some hysteresis present comparing the on- and off-loading curves, due to the viscoelastic nature of cPEVA. Therefore, the *snap-through force* was measured from the on-loading curve, and the *snap-back force* was measured from the off-loading curve. From the evaluation, it is also apparent that the 45° sample required a greater *snap-through force* ( $0.90 \pm 0.13$  N,  $n=3$ ) than the 30° sample ( $0.41 \pm 0.19$  N,  $n=3$ ), and that the *snap-back force* for the 30° was positive ( $0.06 \pm 0.08$  N,  $n=3$ ) and negative for the 45° sample ( $-0.29 \pm 0.08$  N,  $n=3$ ). This granted us to move on to the

next step to create a structure that could switch between mono- and bi-stable modes.

Here, a structured cPEVA film with 30° truncated tetrahedron was programmed by compression between PDMS mold with 45° truncated tetrahedron structure at 70°C and fixation at 5°C, as shown in Fig. 4(a). At room temperature the programmed sample showed a slope angle of  $42.6 \pm 0.9^\circ$  and when the temperature was increased to 100°C the slope angle recovered back to  $27.4 \pm 0.8^\circ$ , as confirmed by the optical microscopy [Fig. 4(b)–(f)]. To confirm the switching between a mono- and bi-stable structure the programmed sample was tested at room temperature, then heated up to 100°C and cooled down to room temperature to be tested again [Fig. 4(g)]. From the results it is apparent that we were able to switch between these two modes, and that the sample

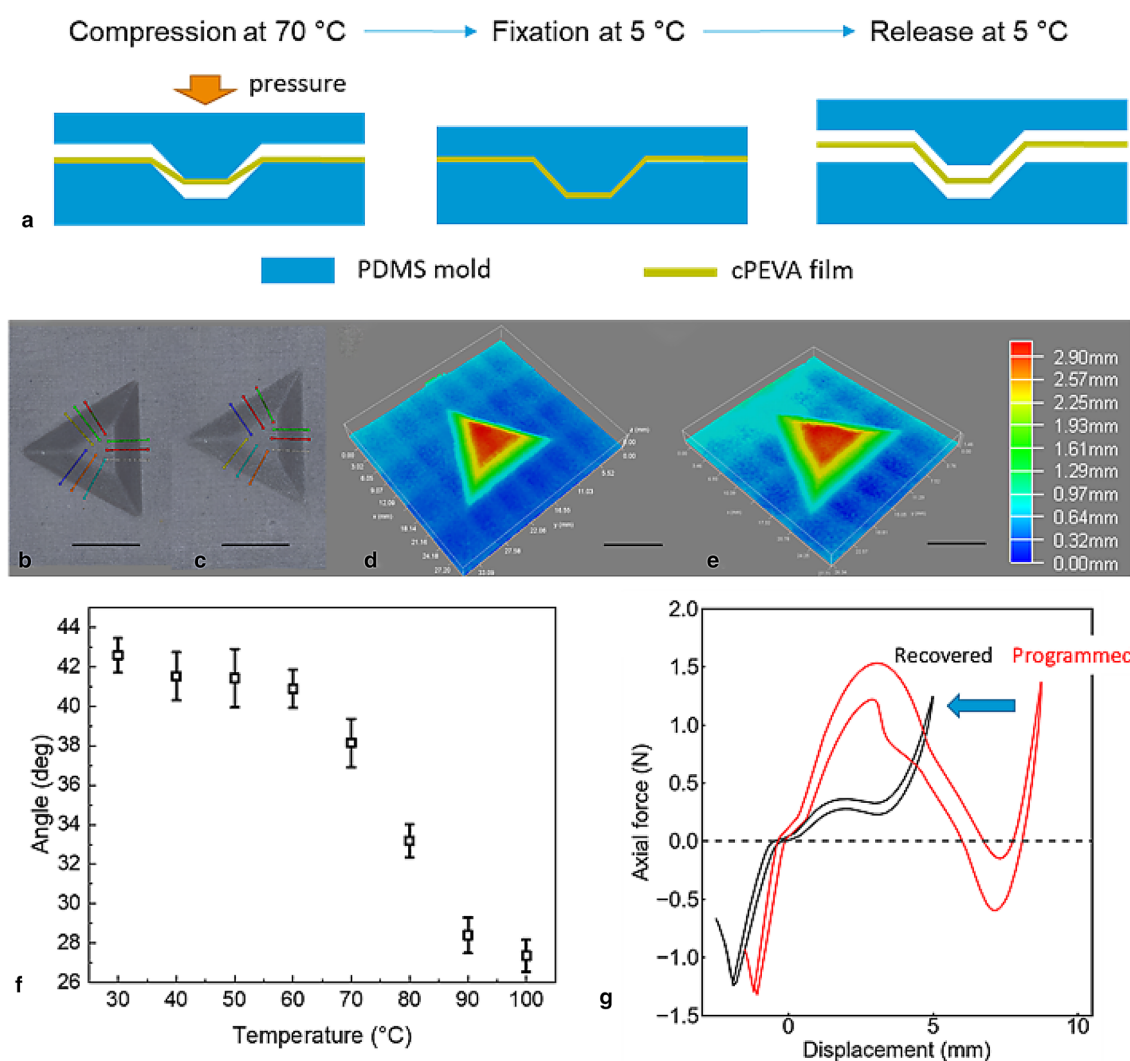


**Figure 4.** (a) Schematic showing of programming of the structured cPEVA film using PDMS molds. (b–e) 3D stacking optical images of cPEVA 3D films in the programmed state (b, d) and recovered state (c, e). The scale bar in each picture is 10 mm. The blue, red and green lines are the markers of positions where the cross-sections were measured; (f) The recovery curve and slope angles with increasing temperatures from 30 to 100°C; (g) Axial force vs. Displacement curve of programmed and recovered truncated tetrahedron sample.

in its programmed state showed a larger force than in its recovered state, i.e. amplification. Finally, we further test the reconfiguration behavior of the programmed sample starting from the second stable state by first compressing on the truncated tetrahedron structure to the other side. Then, when the temperature increased to 80°C, the programmed sample recovered from bi-stable to mono-stable. The losing of bi-stability introduced a snap movement on the structure, as shown in supplementary video S3. By combining the SME and bi-stable property, a shape recovery with higher magnification was achieved.

This mechanism could be thought of as being implemented as a safety switch, which turns off the moment a critical temperature has been reached—and will remain off until reset. It could also be thought of as a dynamic energy storage in which a structure is activated by a mechanical force and the stored energy is released by an increase in temperature. cPEVA is a relatively soft polymer with a Young's modulus of  $E \approx 40$  MPa at room temperature, which shows some viscoelastic behavior.<sup>[21]</sup> This explains the hysteresis in the on- and off-loading curves during mechanical testing. As an outlook, it may be an interesting development to make use of the viscoelastic behavior, which would add another dimension of functionality of the structures in terms of time. Here, one could devise a structure with a highly viscoelastic behavior that is bi-stable only if held at a certain force for a given amount of time, and for transient forces it is mono-stable.

## Conclusion

In this paper, digital methods for design and manufacturing played a key role in the technical realization. We report on the implementation of modelling of beams using the CBCM model as an important tool in the computational design process for compliant mechanisms. It was shown that a truncated tetrahedron structure with a slope angle of 30° showed no mono-stable behavior, and such a structure with a slope angle of 45° did show bi-stable behavior. Furthermore, it successfully realized to switch between these two structures using cPEVA as an SMP. The modulation of compliant mechanisms by the SME of a polymer is an example for a bio-inspired function, which is derived from the switch-like mechanism of the Venus flytrap.

## Acknowledgments

Prof. Dr. Thomas Speck, University of Freiburg, is acknowledged for his helpful insights in the mechanics of the Venus flytrap. This work is financially supported by the Helmholtz Association of German Research Centers through program-oriented funding and through Helmholtz Graduate School for Macromolecular Bioscience (MacroBio, VH-GS-503) and received funding from the European Union's Horizon 2020

research and innovation program under Grant Agreement No. 824074 (GrowBot).

## Funding

Open Access funding enabled and organized by Projekt DEAL.

## Data availability

The datasets generated during and/or analysed during the current study are available from the corresponding author on reasonable request.

## Declarations

### Conflict of interest

The authors have no relevant financial or non-financial interests to disclose.

## Open Access

This article is licensed under a Creative Commons Attribution 4.0 International License, which permits use, sharing, adaptation, distribution and reproduction in any medium or format, as long as you give appropriate credit to the original author(s) and the source, provide a link to the Creative Commons licence, and indicate if changes were made. The images or other third party material in this article are included in the article's Creative Commons licence, unless indicated otherwise in a credit line to the material. If material is not included in the article's Creative Commons licence and your intended use is not permitted by statutory regulation or exceeds the permitted use, you will need to obtain permission directly from the copyright holder. To view a copy of this licence, visit <http://creativecommons.org/licenses/by/4.0/>.

## Supplementary Information

The online version contains supplementary material available at <https://doi.org/10.1557/s43579-021-00056-6>.

## References

1. Y. Forterre, Slow, fast and furious: understanding the physics of plant movements. *J. Exp. Bot.* **64**, 4745 (2013)
2. S. Li, K.W. Wang, Fluidic origami with embedded pressure dependent multi-stability: a plant inspired innovation. *J. R. Soc. Interface* **12**, 20150639 (2015)
3. Q. Zhao, X. Yang, C. Ma, D. Chen, H. Bai, T. Li, W. Yang, T. Xie, A bioinspired reversible snapping hydrogel assembly. *Mater. Horiz.* **3**, 422 (2016)
4. S. Poppinga, M. Joyeux, Different mechanics of snap-trapping in the two closely related carnivorous plants *Dionaea muscipula* and *Aldrovanda vesiculosa*. *Phys. Rev. E* **84**, 041928 (2011)
5. R. Sachse, A. Westermeier, M. Mylo, J. Nadasdi, M. Bischoff, T. Speck, S. Poppinga, Snapping mechanics of the Venus flytrap (*Dionaea muscipula*). *Proc. Natl. Acad. Sci. USA* **117**, 16035 (2020)
6. H.L. Larry, Compliant mechanisms, in *21st Century Kinematics*. ed. by J.M. McCarthy (Springer, London, 2013)
7. H.L. Larry, *Handbook of Compliant Mechanisms* (Wiley, West Sussex, 2013)

8. B. Jensen, L. Howell, L. Salmon, Design of two-link, in-plane, bistable compliant micro-mechanisms. *J. Mech. Des.* **121**, 416–423 (1999)
9. V. Megaro, J. Zehnder, M. Bächer, S. Coros, M. Gross, B. Thomaszewski, A computational design tool for compliant mechanisms. *ACM Trans. Graph.* **36**, 1 (2017)
10. M. Cianchetti, C. Laschi, A. Menciassi, P. Dario, Biomedical applications of soft robotics. *Nat. Rev. Mater.* **3**, 143 (2018)
11. L.L. Howell: *A Generalized Loop-Closure Theory for the Analysis and Synthesis of Compliant Mechanisms*. (1993).
12. S. Awatar, S. Sen: A generalized constraint model for two-dimensional beam flexures, in *International Design Engineering Technical Conferences and Computers and Information in Engineering Conference* (2009), pp. 345.
13. F. Ma, G. Chen: Chained beam-constraint-model (CBCM): a powerful tool for modeling large and complicated deflections of flexible beams in compliant mechanisms, in Vol. 5A: *38th Mechanisms and Robotics Conference* (2014).
14. L. Hines, K. Petersen, G.Z. Lum, M. Sitti, Soft actuators for small-scale robotics. *Adv. Mater.* **29**, 1603483 (2017)
15. S. Palagi, P. Fischer, Bioinspired microrobots. *Nat. Rev. Mater.* **3**, 113 (2018)
16. T. Li, Y. Li, T. Zhang, Materials, structures, and functions for flexible and stretchable biomimetic sensors. *Acc. Chem. Res.* **52**, 288 (2019)
17. A. Lendlein, Fabrication of reprogrammable shape-memory polymer actuators for robotics. *Sci. Robot.* **3**, eaat9090 (2018)
18. A. Lendlein, O.E.C. Gould, Reprogrammable recovery and actuation behaviour of shape-memory polymers. *Nat. Rev. Mater.* **4**, 116 (2019)
19. M. Behl, K. Kratz, U. Noechel, T. Sauter, A. Lendlein, Temperature-memory polymer actuators. *Proc. Natl. Acad. Sci. USA* **110**, 12555 (2013)
20. G. Chen, F. Ma, G. Hao, W. Zhu, Modeling large deflections of initially curved beams in compliant mechanisms using chained beam constraint model. *J. Mech. Robot.* **11**, 011002 (2019)
21. Y. Liu, M.Y. Razzaq, T. Rudolph, L. Fang, K. Kratz, A. Lendlein, Two-level shape changes of polymeric microcuboids prepared from crystallizable copolymer networks. *Macromolecules* **50**, 2518 (2017)
22. S. Henning, S. Linß, P. Gräser, R. Theska, L. Zentner, Non-linear analytical modeling of planar compliant mechanisms. *Mech. Mach. Theory* **155**, 104067 (2021)
23. G. Chen, F. Ma, Kinetostatic modeling of fully compliant bistable mechanisms using timoshenko beam constraint model. *J. Mech. Des.* **137**, 022301 (2015)
24. G.L. Holst, G.H. Teichert, B.D. Jensen, Modeling and experiments of buckling modes and deflection of fixed-guided beams in compliant mechanisms. *J. Mech. Des.* **133**, 051002 (2011)

Supporting Information for

# Bio-inspired and Computer-Supported Design of Modulated Shape Changes in Polymer Materials

J. Bäckemo<sup>1,2,a</sup>, Y. Liu<sup>1,2,a</sup>, A. Lendlein<sup>1,2,\*</sup>

<sup>1</sup>Institute of Active Polymers, Helmholtz-Zentrum Hereon, Kanststr. 55, 14513 Teltow, Germany;

<sup>2</sup>Institute of Chemistry, University of Potsdam, 14476 Potsdam, Germany

<sup>a</sup> both co-authors contributed equally

\*corresponding author: [Andreas.Lendlein@hereon.de](mailto:Andreas.Lendlein@hereon.de)

## Supporting method

The equations used to calculate the deformation of the already curved beams were taken from Chen et al. <sup>1</sup>. Here a beam is divided into N subdivisions. Through the Curved Beam Constraint Model (CBCM) equations below it describes the bending shape of the beam and resulting forces involved. The equations used are for the beams where curvature is not constant along the whole beam, which requires each subdivision of the length of the beam,  $L_i$ , to be computed, i.e. unequal discretization. Thus only equations 21-36 are quoted below, as this describes the whole system of non-linear equations.

The y-coordinate defined by the x-coordinate defined by some function

$$22. y_i = f(x_i)$$

The slope,  $\beta_i$

$$23. \beta_i = \arctan f'(x_i)$$

Curvature,  $K_i$

$$24. K_i = \frac{f''(x_i)}{[1+f'^2(x_i)]^{3/2}}$$

The length of each element,  $L_i$

$$25. L_{xi} = x_{i+1} - x_i, L_{yi} = y_{i+1} - y_i$$

$$26. L_i = L_{xi} \cos \beta_i + L_{yi} \sin \beta_i$$

Thickness and approximate curvature normalized to  $L_i$

$$27. t_i = \frac{T}{L_i}, \kappa_i \approx \frac{K_i + K_{i+1}}{2} L_i$$

Here  $P_i, F_i, M_i, \Lambda_i, \Delta_i$  and  $\alpha_i$  are the radial force, tangential force, moment, tangential deflection, radial deflection and the end slope. The lowercase variables  $p_i, f_i, m_i, \lambda_i, \delta_i$ , and  $\alpha_i$  correspond to their non-dimensionalised forms.

$$28. p_i = \frac{P_i L_i^2}{EI}, f_i = \frac{F_i L_i^2}{EI}, m_i = \frac{M_i L_i}{EI}, \lambda_i = \frac{\Lambda_i}{L_i}, \delta = \frac{\Delta_i}{L_i}, \alpha_i = \alpha_i$$

Beam constraint model equations (3N equations)

$$29. \begin{bmatrix} f_i \\ m_i \end{bmatrix} = \begin{bmatrix} 12 & -6 \\ -6 & 4 \end{bmatrix} \begin{bmatrix} \delta \\ \alpha \end{bmatrix} + p_i \begin{bmatrix} \frac{6}{5} & -\frac{1}{10} \\ -\frac{1}{10} & \frac{2}{15} \end{bmatrix} \begin{bmatrix} \delta \\ \alpha \end{bmatrix} + p_i^2 \begin{bmatrix} -1/700 & 1/1400 \\ 1/1400 & -11/6300 \end{bmatrix} \begin{bmatrix} \delta \\ \alpha \end{bmatrix} + p_i \begin{bmatrix} \kappa/2 \\ \kappa/12 \end{bmatrix}$$

$$30. \lambda_i = \frac{t_i^2 p_i}{12} - \frac{\kappa_i}{2} \delta_i - \frac{\kappa_i}{12} \alpha_i - \frac{1}{2} [\delta_i \quad \alpha_i] \begin{bmatrix} \frac{6}{5} & -\frac{1}{10} \\ -\frac{1}{10} & \frac{2}{15} \end{bmatrix} \begin{bmatrix} \delta_i \\ \alpha_i \end{bmatrix} - p_i [\delta_i \quad \alpha_i] \begin{bmatrix} -\frac{1}{700} & \frac{1}{1400} \\ \frac{1}{1400} & -\frac{11}{6300} \end{bmatrix} \begin{bmatrix} \delta_i \\ \alpha_i \end{bmatrix} + p_i \frac{\kappa}{360} \alpha_i + p_i \frac{\kappa_i^2}{720}$$

Static equilibrium equations (3N equations)

$$31. P_0 = \frac{p_1 EI}{L_1^2}, F_0 = \frac{f_1 EI}{L_1^2}, P_0 = \frac{m_N EI}{L_N}$$

$$32. \begin{bmatrix} \cos \theta_i & \sin \theta_i & 0 \\ -\sin \theta_i & \cos \theta_i & 0 \\ (1 + \lambda_i) & -(0.5\kappa_i + \delta_i) & 1 \end{bmatrix} \begin{bmatrix} f_i \\ p_i \\ m_i \end{bmatrix} = \begin{bmatrix} \frac{f_1 L_i^2}{L_i^2} \\ \frac{p_1 L_i^2}{L_i^2} \\ \frac{m_{i-1} L_i}{L_{i-1}} \end{bmatrix}$$

$$33. \theta_1 = 0, \theta_i = \beta_1 + \sum_{k=1}^{i-1} \alpha_k \quad (i = 2, 3, \dots, N)$$

Geometric constraint equations (3 equations)

$$34. \sum_{i=1}^N [(1 + \lambda_i) L_i \cos \theta_i - (0.5\kappa_i + \delta_i) L_i \sin \theta_i] = X_0$$

$$35. \sum_{i=1}^N [(1 + \lambda_i) L_i \sin \theta_i + (0.5\kappa_i + \delta_i) L_i \cos \theta_i] = Y_0$$

$$36. \beta_{N+1} + \sum_{i=1}^N \alpha_i = \theta_0$$

Through these 6N + 3 equations and given three of the six parameters  $p_0, f_0, m_0, x_0, y_0$ , and  $\theta_0$ , one could solve for the other three parameters. For the modelling in the manuscript,  $x_0, y_0$  and  $\theta_0$  were used as inputs to solve for the other variables  $p_0, f_0, m_0$ . The values for the axial force given in the manuscript is  $F_0$ .

1. G. Chen, F. Ma, G. Hao and W. Zhu: Modeling Large Deflections of Initially Curved Beams in Compliant Mechanisms Using Chained Beam Constraint Model. *Journal of Mechanisms and Robotics* **11**, 011002 (2019).

## Supporting figures

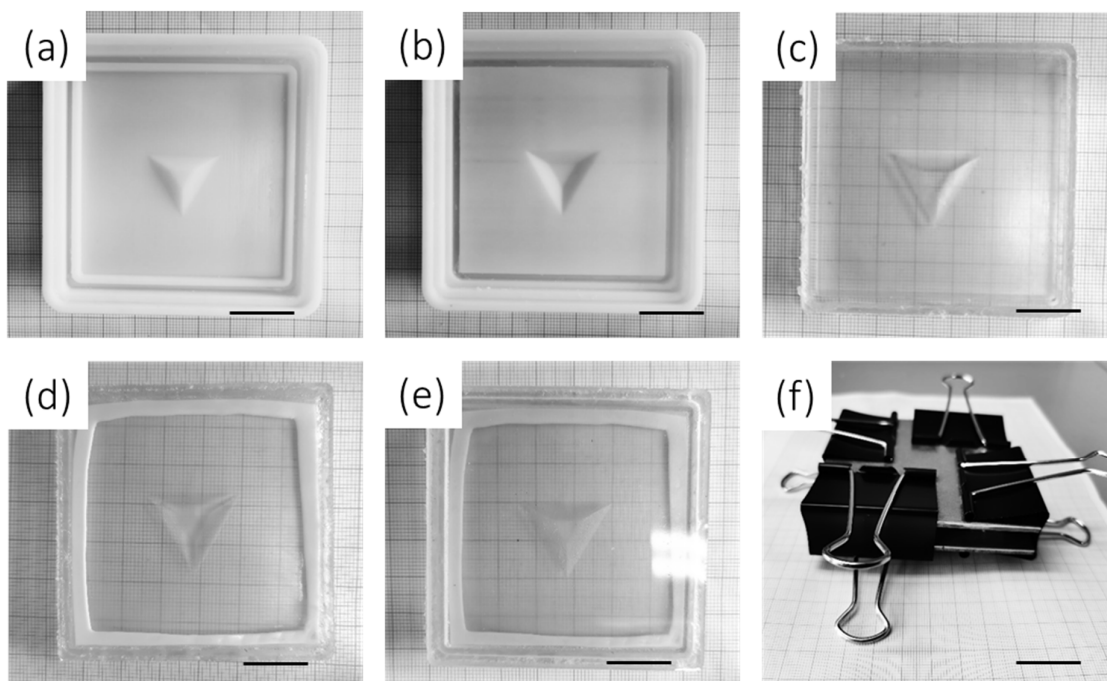


**Figure S1** - Photos of different molds and casting device. (a, b) 3D printed counter parts for casting PDMS molds. (c, d) PDMS molds replicated from 3D printed counter parts. A Teflon spacer of 0.5 mm thickness was attached to one of the PDMS molds (d), in order to create the desired thickness of the cPEVA film. (e) PDMS molds sandwiched with PEVA blended film. (f) Casting device: sandwiched PDMS molds compressed between two metal clamps and fixed with four clamps. The scale bar in each picture is 20 mm.

## Supporting videos

**Supplementary video S1** – A Video of the digital model of the 30 degree truncated tetrahedron. (Left) The undeformed beam (black) and deformed beam (blue). (Right) The force-displacement curve with respect to the deformed beam. The parameters used for the digital modelling: Number of elements,  $N = 15$ ; Deformation step,  $\Delta Y = 0.05$  mm; Young's modulus = 40 MPa; Width = 7.215 mm; Thickness = 0.5 mm

**Supplementary video S2** – A Video of the digital model of the 45 degree truncated tetrahedron. (Left) The undeformed beam (black) and deformed beam (blue). (Right) The force-displacement curve with respect to the deformed beam. The parameters used for the digital modelling: Number of elements,  $N = 15$ ; Deformation step,  $\Delta Y = 0.05$  mm; Young's modulus = 40 MPa; Width = 7.215 mm; Thickness = 0.5 mm

**Supplementary video S3** – A video showing the temperature-activated snapping movement by pushing a programmed sample from shape A to shape B and resetting the structure by heating up the temperature to 80 °C

## **Appendix III A Biomimetic Alternative bi-modular bi-stable fixation Device (BAFD)**



# A Biomimetic Alternative bi-modular bi-stable fixation Device (BAFD)

J. Bäckemo<sup>1,2,\*</sup>, M. Reinthaler<sup>1,3</sup> A. Lendlein<sup>1,2</sup>,

<sup>1</sup>Institute of Active Polymers, Helmholtz-Zentrum Hereon, Kanststr. 55, 14513 Teltow, Germany;

<sup>2</sup>Institute of Chemistry, University of Potsdam, 14476 Potsdam, Germany

<sup>3</sup>Department of Cardiology, Campus Benjamin Franklin, Charité Berlin, Berlin, Germany

\*corresponding author: [publications@hereon.de](mailto:publications@hereon.de)

ORCID-ID

JB: 0000-0001-6721-8109

AL: 0000-0003-4126-4670

## 1 Background

### 1.1 Biological Inspiration

With the ever-advancing pursuit of new technologies within energy, transport, and medicine it may appear that utilizing the latest digital tools and features are the starting points for any type of technical development. Humans have amassed a copious amount of knowledge within a relatively short time, looking evolutionary. However, because of the advantage of time, mother nature has managed to come up with some brilliant solutions to intricate problems. Some scientists and engineers have observed nature and been inspired from it, in awe of what it is capable of. A historical example is that of George de Mestral. He is said to have come up with the hook-and-loop fastener system while on a stroll with his dog. He observed that burdock burrs managed to stick to the fur of his and to his own clothing and were intertwined with the hairs [1]. Later, he came up with the well-known attachment system devised by one layer containing the fabric “loops”, and the other layer containing the fabric

“hooks”. This novel idea has since its invention been used to fasten shoes, close bags, attach tools to name a few, and is known world over by its tradename: Velcro®. More recent examples are the invention of new adhesives inspired from the setae structure of gecko feet working through van der Waal’s forces [4], or the development of super-hydrophobic substrates based on the pearling effect on water from lotus leaves [5]–[7]. These examples illustrate that nature is a cornucopia of yet to be discovered inventions. However, the strategy to disclose the mechanisms behind these ingenious solutions is not trivial and requires a high level of curiosity, careful considerations of material and geometrical choices and the right analytical tools. By utilizing methods, such as non-linear modelling of beams, functional programming, Computer Aided Design (CAD), Finite Element Analysis (FEA), and Additive Manufacturing (AF) one can forecast, analyse, and implement the mechanisms identified from a specific species (**Fig. 1**). Using these approaches, we lay out a strategy in this manuscript to design a new mechanism inspired by the tapeworm attachment system to attach minimally invasive devices to biological tissues, and how to optimize these mechanisms using non-linear methods.



**Fig. 1 Bioinspiration and Digital Engineering combinatorial approach**

## 1.2 Clinical aspect

In medicine the safety of the patient is of the utmost importance, and therefore should the risk-benefit ratio of any intervention should outweigh the natural course of any given disease or complication. The last few decades have seen a remarkable development for interventional procedures, and particularly for laparoscopic surgeries, or its more descriptive term “key-hole surgery”. For such procedures the clinician, rather than opening up a particular part of the body locally, one or several small incisions are made to insert long thin instruments, often guided by a camera. This approach is widely applied for procedures ranging from appendectomy, cholecystectomy (removal of gall bladder), oesophageal surgery, and many more [9], [10]. One of the latest and most complex developments in this field is minimally invasive cardiac surgery [10]. Traditionally, open heart surgery is performed by opening the chest via a procedure called sternotomy, where the sternum (breastbone) is cracked open after a longitudinal incision. Furthermore, during the procedure the heart of the patient is arrested and the circulation is sustained by connecting the patient to an artificial pump - the heart lung machine. These operations such as valve replacement or bypass surgery therefore constitute a significant risk especially for the typically multimorbid cardiovascular patient. [11]. More recently a new field in cardiovascular medicine, using trans-catheter approaches has emerged. These interventions are characterized by a transluminal (transvenous or transarterial) access without the need of a heart lung machine (“beating heart” procedures). Many of the former surgical domains like heart valve replacement or bypass surgery are slowly getting replaced by these new procedures which can be performed at a lower risk for the patient [12]. An overview of common interventional procedures is given in **Fig. 2**.

Usually a so-called sheath is used, through which a catheter is placed at a certain area within the heart to deliver a device, designed to fulfil a certain purpose. This means that the device itself needs to be foldable, or crimped, so that they fit through such a catheter. This puts a significant design restriction on the design of such implants. One of these limitations is to ensure safe and sufficient attachment of these devices to certain cardiac structures which may result in device embolization. To address these apparent issues, looking at nature for inspiration may provide interesting design rationales.

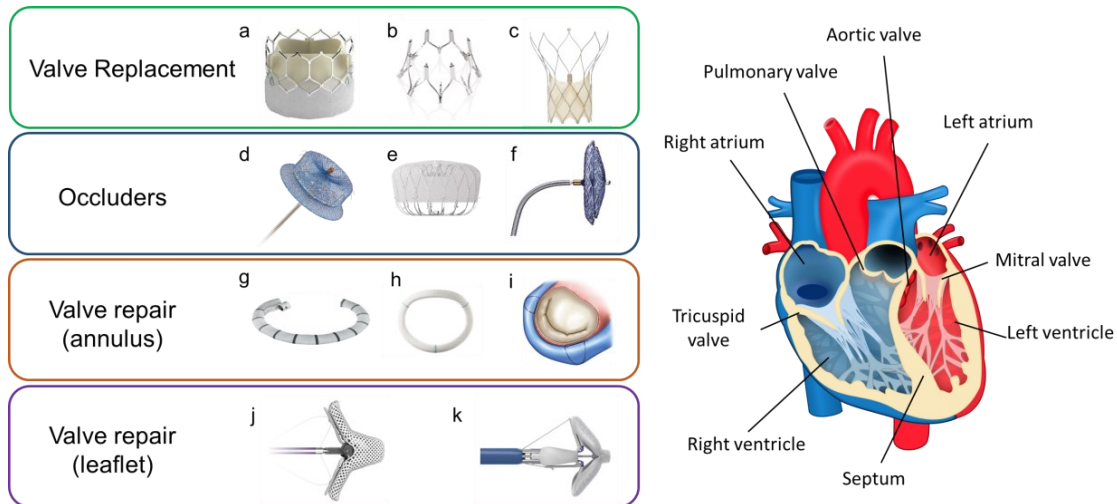


**Fig. 2 Overview of common interventional cardiac devices.** **a** Sapein 3 Ultra Valve (Edwards Lifesciences, Irvine, USA). **b** Millipede Transcatheter Mitral Annuloplasty System (Boston Scientific, Marlborough, USA). **c** Portico™ aortic valve replacement (Abbott Laboratories, Chicago, USA). **d** Amplatzer Amulet LAA Occluder (Abbott Laboratories, Chicago, USA). **e** Watchman Occluder (Boston Scientific, Marlborough, USA). **f** Amplatzer PFO occluder (Abbott Laboratories, Chicago, USA). **g** Cardioband Tricuspid Valve Reconstruction System (Edwards Lifesciences, Irvine, USA). **h** Carpentier-Edwards Physio II Annuloplasty ring (Edwards Lifesciences, Irvine, USA). **i** Carillon Mitral Contour System (Cardiac Dimensions Inc., Kirkland, USA). **j** Pascal System (Edwards Lifesciences, Irvine, USA). **k** Mitraclip® (Abbott Laboratories, Chicago, USA). **l** Diagram adapted from “Heart Diagram” by ZooFari licensed under CC BY-SA 3.0.

### 1.3 Decoding nature

When looking at biology to seek for potential organic solutions, one starting point is to see what different attachment modalities there are and what constitutes their physical principles. In nature, to attach or adhere to other substrates serves a natural purpose – whether it is for sustaining nutrition, defending against intruders, for hunting prey, locomotion, or simply to stabilize their position. Geckos have seen much interest in recent years due to their ability to climb vertical and inclined surfaces with ease. The physical principle that underlies this attachment is van der Waal’s forces which are long-range forces that act between two opposing surfaces which decrease in magnitude with increasing distance between the two surfaces [24]. The feet of Gecko, and Hexapods, have architectural structures known as setae which are microscopic hair-like protrusions which increases the interaction between its feet and the opposing substrate [25]. Species that use suction cups, such as octopi or tapeworms, rely on the use of a soft structure that is able to undergo volumetric contraction and expansion. For octopi, there is a structure known as the *acetabulum* which is a cavity that contracts to form a vacuum, and the loose epithelium at the edges of the sucker enables a proper seal [26]. For the tapeworm, the sucker surface is instead covered in *scopulate spinitriches*, a hair-like structure only a

few micrometres long, which presumably enables a seal through van der Waal's forces [27]. Then there are attachment systems with the intent of staying attached permanently, like for barnacles and ivies. Barnacles often attach themselves to cliffs and rockfaces by the ocean and needs to be stable in a turbulent environment. They achieve this by depositing a cement-like substance rich in proteins which is also only a few micrometres thick [28]. For the plant group of ivies, which are commonly found climbing up walls and rocks, they secrete nanoparticles compounds which contain oxygen, nitrogen, and sulphur which aids in hydrogen bonding [29]. Another, more invasive form of attachment is tissue penetration either through fangs like in spiders, or stingers for bees, or porcupine quills. Although trivial, all penetration devices are usually high aspect ratio structures, meaning long and thin, and either have a curved geometry like a scorpion stinger [30], or a straight geometry, like a bee stinger [31]. The use for these modes may be for feeding like for the spider, for fending off other animals like the scorpion, or for permanent attachment like in the tapeworm [32]. A summary of the mentioned modes of attachment and their underlying physical principles can be seen in Table 1.

**Table 1. A summary of different attachment systems in nature**

Species / Bioinspiration	Physical principle	Function	Properties
Gecko feet [33]	Van der Waal's forces	Attachment and locomotion on dry surfaces	Reversible; non-invasive; must be in a dry environment
Hexapod feet[34]	Van der Waal's forces, friction	Attachment and locomotion	Reversible; quick detachment
Octopus sucker [35]–[37]	Suction	Attachment to seafloor; grabbing prey; locomotion	Reversible; non-invasive
Tapeworm suckers [38]	Suction	Temporary attachment; locomotion	Reversible; non-invasive
Barnacle glue [39]–[41]	Chemical bond to substrate	Long-term attachment on wet surfaces	Long-term; wet environment
Ivy rootlets [42]	Chemical bond to substrate	Long-term attachment	Long-term; non-reversible
Sundew [43]	Chemical bond to substrate	Capture of prey	Strong
Frog toe pads[44]	Capillary effect between pads and substrates	Attachment to wet substrates	Non-invasive

Scorpion stinger [30], [32]	Penetration	Defence; hunting prey	Quick actuation; invasive; curved geometry
Wild boar tusks [32]	Penetration	Defence;	Mechanically stable; invasive; curved geometry
Tape worm hooks [32]	Penetration	Attachment in intestine	Long-term attachment; invasive; curved geometry
Spider fangs [45]	Penetration	Hunting prey	Damage resilience; invasive; curved geometry
Wasp and bee stingers[31]	Penetration	Defence; hunting prey	Invasive; curved geometry (wasps), straight geometry (bees)
Porcupine [46]	Penetration	Defence	Invasive; straight geometry

When considering the different modes of attachment, their physical principles and their purpose on species sticks out: the tapeworm. There are many different species considered tapeworms, and they come in many forms that either only have suckers as their mode of attachment or a combination of suckers and hooks. *Cyclophyllidea* is an order of tapeworms which all share the characteristics of having four suckers located on their *scolex* (head), and their body are composed of proglottid segments that give them a “ribbon”-like look (see **Fig. 3**). The *Taeniidae* family of tapeworms include some common varieties that occur in cattle and farm animals, such as the *Taenia Solium* (pork tapeworm), *Taenia saginata* (beef tapeworm). With the suckers the tapeworm can temporarily attach itself to host tissue, presumably to probe a potential landing location. For certain species there are also hooks located on the rostellum, which can either be invaginated or evaginated. The mechanism with which the tapeworm attaches is a result of specifically designed hooks coordinated by a fine-tuned muscular system. The rostellum can be described as a muscular pouch which comprises circular muscle fibres which are located a small distance above the suckers. This forms a sphincter which is believed to be contracted when the hooks are invaginated keeping them inert. This sphincter is located above the hooks when they are invaginated and below the hooks inside the scolex when they are evaginated. The rostellum is also separate from the rest of the scolex tissue by the rostellar capsule

[47]. Analysing the attachment steps of the tapeworm one can conclude that once roaming the host in the gastro-intestinal (GI) tract, one can see that initially the tapeworm may probe probable locations for attachment by using its suckers. Once such a location is deemed suitable for the tapeworm it evaginates its hooks and penetrates the mucosal wall. It has been observed that the latter mode of attachment is irreversible, meaning that this attachment serves as an anchoring mechanism [48] - the tapeworm would spend the rest of its life cycle firmly attached to the GI tract of its host. Seeing that these species are present in the small intestine, their inherent design is suited for attachment to soft tissue. *T. Solium* has gone through an evolutionary process in which the suckers and hooks are designed to attach to one or more villi simultaneously [49], which are lamellar structures in the duodenum that creates cavities in between them. There are many varied species in the *Cyclophyllidae* order, and by searching the literature for morphological characteristics such as hook length and sucker diameter, there is a great variation (see **Table 2**). By comparing the hook length to the sucker diameter, one gets a ratio of 10:1 for the family of *Raillietina* which are commonly found in birds, a ratio of 1:1 for *Taenia Pisiformis* which are regularly found in house cats, and a ratio of 3:1 for *Taenia Solium* which are found in pigs. By extracting these pieces of information for attachment mentioned above the order of *Cyclophyllidea* serves a blueprint for a new medical device.

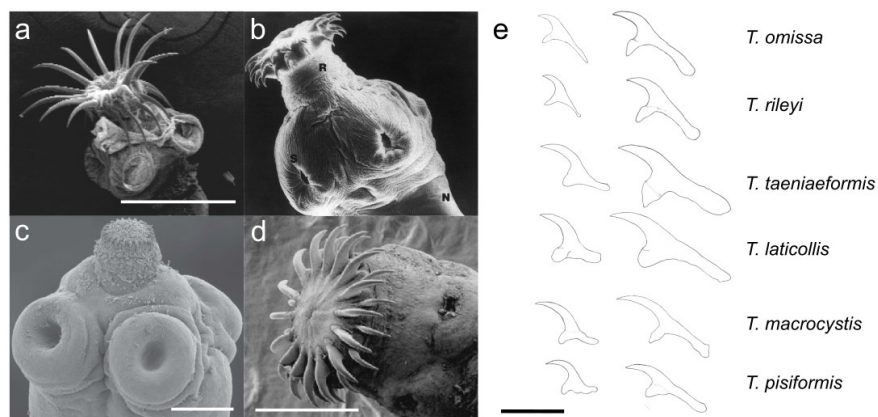


**Fig. 3 Attachment structures of tapeworms of the order *Cyclophyllidea*.** a-d Scolex (head) of some common tapeworms. a *Paradilepis cf. minima*, scale bar 200 µm, b *T. Solium*, no scale bar, c *Hymenolepis microstoma*, scale bar 50 µm, d *T. Solium* scale bar 500 µm. e Hook morphology of a selection of the family *Taenia*, scale bar 200 µm. (Images from a [27], b [50], c [51], d [52], e [53]).

**Table 2 Morphological features of some common tapeworms of the order Cyclophyllidea.**

Species	Hook length		Blade		Sucker	Source
	Large	Small	Large	Small		
<i>T. solium</i>	159 - 166	118 - 127			411	[54]
	140 - 180	110 - 140				[55]
	105 - 130	168 - 174				[56]
<i>T. solium</i> (Thailand strain)	17	11			144	[57]
<i>Cysticercus cellolusae</i>	179 - 186	127 - 129			526	[55]
<i>T. saginata</i>	24	10			203 -	[58]
					258	
<i>T. taeniaeformis</i>	380 - 400	250 - 260	180 - 190	140 - 150		[53]
	360 - 440	250 - 270				[60]
<i>T. laticollis</i>	380 - 400	210	170	140		[53]
<i>T. macrocystis</i>	320 - 340	190	160	120 - 130		[53]
<i>T. pisiformis</i>	240 - 290	130 - 170	90 - 130	60 - 100		[61]
	250 - 270	140 - 150	90 - 100	80 - 90		[53]
	235	140			300	[61]
<i>T. serialis</i>	145.3	86.4			268	[62]
<i>T. omisssa</i>	240 -280	180 -210	110	90 - 100		[53]
<i>T. rileyi</i>	220 - 240	160 - 170	11 - 110	70		[53]
<i>Sobolevitaenia moldavica</i>	45 - 47	40 - 42			126 -	[63]
					145	
<i>S. japonensis</i>	48 - 50	43 - 45			118 -	[62]
					120	
<i>Paradilepis cf. minima</i>	157 - 186	111 - 128	105 - 124	74 - 86	86.4 -	[27]
					97.9	
<i>Cotugnia polyacantha</i>	9 - 11				90 - 100	[63]
<i>Raillietina echninobothrida</i>	8 - 14				50 - 100	[63]
<i>R. tetragona</i>	4 - 8				80	[63]
<i>R. tunetensis</i>	7				35	[63]
<i>R. Skrjabinia cesticiullus</i>	7 - 12					[63]



## 1.4 Design transferral

The tapeworm attachment can be separated into two modes of attachment: temporary, through suction, and permanent, through the penetration of hooks. The cylindrical shape of the tapeworm is due to its natural habitat in the crypts of Lieberkühn between the villi in the small intestine of humans and mammals. The tapeworm secures itself into the mucosal wall of the microvilli using their suckers, and then anchors themselves using their hooks (**Fig. 4**). The rostellar pad, with which it ejects its hooks, could be likened to a curved dome that turns inside out. The actualizing mechanism is governed by a finely tuned system of oblique and radial muscle fibres [27]. One approach to convert these mechanisms, may be to use suction to also initiate hook release into tissue. The switching between temporary and permanent attachment, could then be achieved through a mechanically bi-stable system. In such a system, there are two energy minima at which the structure will not deform unless further acted upon – much like a ball in a valley. The ball remains at rest until acted further upon, and reaching a critical energy barrier will make the ball move to another valley, i.e. another energy minimum. Designing such a mechanism is non-trivial and is governed by non-linear phenomena, such as stress relaxation, creep, and load stiffening [64]. To forecast such behaviour is challenging, and common models used in Finite Element Analysis (FEA) usually produce erroneous results. Models that have been developed to forecast such behaviours include the Pseudo-Rigid Body Model (PRBM) [64], [65] and the Beam Constrain Model (BCM)[66]. In this work we chose to implement the Chained Beam Constraint Model (CBCM)[67] which is discretization development of the BCM model to forecast structure for bi-stability, which has also been used in our previous work [68].

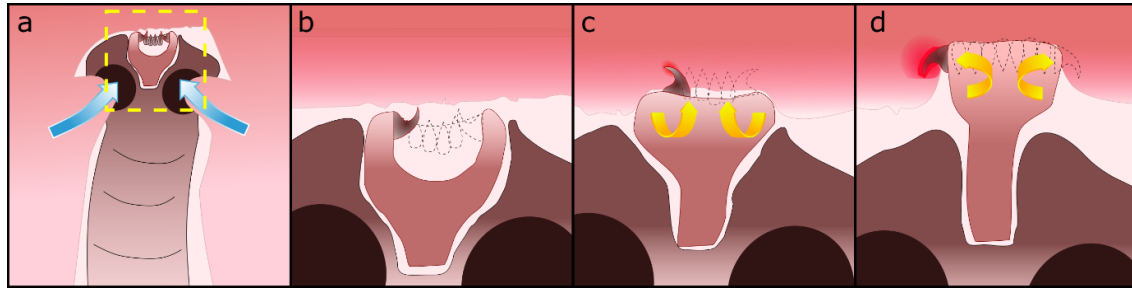


**Fig. 4 Attachment mechanism of the tapeworm in the small intestine.** **a** The tapeworm situates itself into the crypts of Lieberkühn in the small intestine. Its suckers stabilises the body by attaching itself to the epithelial wall. **b – d** Rostellum evagination (zoomed in from yellow rectangle in **a**). **b** The anchoring mechanism of the rostellum in its invaginated state. The hooks are not in contact with the intestinal wall. **c** As the rostellum is being evaginated the rostellum pad is turning inside out to create a moment to drive the hooks into the intestinal wall. **d** Once completed the tapeworm is completely anchored to the wall.

## 2 Methods

### 2.1 Modelling

To forecast the bending behavior of the bi-stable column, and to identify the relevant equilibria, the Chained Beam Constraint Model (CBCM) developed by Chen et al. was applied [21]. The relevant equations were applied and executed through Python programming as described in our previous work [20]. The modelling results were compared to Nastran In-CAD non-linear static simulation with a linear material model (Autodesk, San Rafael, USA) using an applied downward displacement of 8 mm and a step increment of 0.1 mm between each subsequent step. The logarithmic equation developed by Qi et al. to convert Shore A hardness to Young's modulus was applied for the used material [22].

$$E_0 = 0.0235 * S - 0.6403$$

Where  $E_0$  is the estimated Young's modulus, and  $S$  is the Shore A durometer hardness. The estimated moduli for the materials tested are outlined in the supplementary information. These moduli were used in CBCM and NASTRAN™ modelling.

### 2.2 3D-Design

The design of all components were designed using Autodesk Inventor Pro 2019 (Autodesk, San Rafael, USA). The devised design can be seen in Fig. 8.

### 2.3 Materials

The 3D-printing materials used are VeroWhite™ (Stratasys, Rehovot, Israel) and printed with the Stratasys Connex® 3 Objet 260 Polyjet printer (Stratasys, Rehovot, Israel). The materials were mixed as digital materials with the two last digits indicating the Shore A durometer material stiffness: FLX9895, FLX9885, FLX9870, FLX9860, FLX9850, FLX9840. After printing the samples were post-processed with a water jet cleaning station. The porcine tissue used for the pressure tests were obtained from a local butcher.

### 2.4 Mechanical testing

To characterize the bi-stable behavior of the printed columns, a Zwick Z1.0 tensile test machine (Zwick, Ulm, Germany) for mechanical testing was used. For testing the structure a custom-made test jig was produced. The components of the jig were printed with VeroWhite™ (Stratasys, Rehovot, Israel) using Stratasys Connex 3 Objet 260 Polyjet printer (Stratasys, Rehovot, Israel). The test jig was designed in such a way to allow for deformation of the bi-stable column. The Young's modulus for VeroWhite is 2.5 GPa which significantly higher than for the materials used for the bi-stable column (~4 – 40 MPa), thus preventing any significant deformation of the test jig during testing. The bi-stable column was attached to the bottom part of the test jig using screws located on the rim, and attached to the top part of the test jig through a central hole (see Fig. 6). By mechanically coupling the bi-stable column the on- and off-loading of the bi-stable column could be measured.

### 2.5 Pressure tests

Pressure tests were performed with the CVC 3000 (Vacuubrand, Wertheim, Germany) control unit and the PC 3004 Vario vacuum pumping unit (Vacuubrand, Wertheim, Germany) which enables

control of the applied vacuum in steps of 100 Pa from ambient pressure (~1000 Pa). The applied pressure was pre-programmed to reach a certain value and was applied when stabilized.

### 3 Results

The tapeworm is a species that are commonly found in farm animals such as pigs, cows, and sheep. They reside in the gastrointestinal tract and attach their head (rostellum) to the mucosal tissue of the small intestine. It does so by using suckers located on the side of their heads. Some species, such as *Taenia Solium* (**Fig. 3b**) that belongs to the family *Cyclophyllidea*, are also equipped with hooks attached to a structure known as the rostellum, which is a movable part of the tapeworm which can in- or evaginate the hooks [50]. In other words, the tapeworm has two modes of attachment: suction and penetration of hooks. The mode with which the tapeworm evaginates its hooks, is through a muscular structure known as the *rostellum* which is actuated with the aid from oblique and radial muscle fibres [27]. In this paper it was interesting to see whether we could create a proof-of-concept device that is able to switch between these two modes. As suction is one of the attachment modes, our hypothesis was to use only pressure (vacuum) to activate both modes of attachment, and to do this sequentially depending on the strength of the vacuum (**Fig. 5**). The question arose how to switch between the two modes only using pressure – and one approach were to make use of bi-stable mechanics.

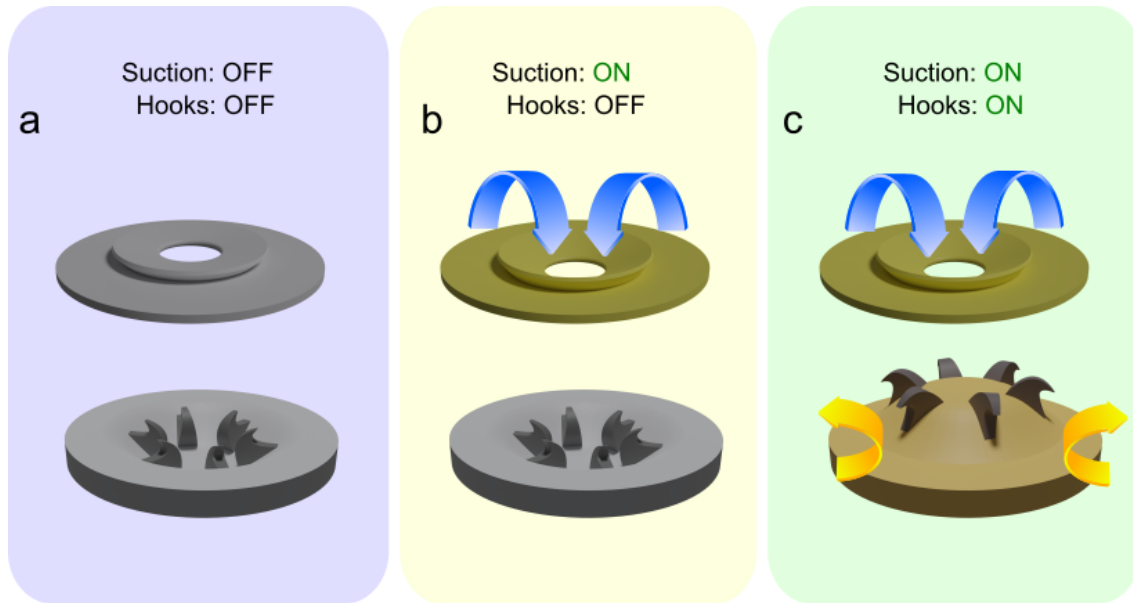


**Fig. 5 Attachment principle for BAFD.** **a** in the inactivated state neither suction nor hook penetration is activated. **b** Upon suction activation below a certain critical pressure, only suction is activated and the hooks are yet to be evaginated. **c** After the critical pressure has been reached, the rostellar pad is inverted and the hooks are evaginated.

Bi-stable mechanics are defined by their two stable points during deformation upon which all static forces are balanced. In our previous work we investigated a design for a beam profile that may exhibit bi-stable behaviour and found that a beam with a  $45^\circ$  slope angle would show such behaviour when deformed in-plane to the beam [68]. For this paper we wanted to investigate further how the material stiffness, Young's modulus, and the thickness of the beam would impact the behaviour and if there would be any non-linear effects to take into consideration. The design we came up with was cone-like shape (**Fig. 6a-b**) which consists of the soft material, a digital mixture of VeroWhite+™ and TangoBlackPlus™, and a hard material, VeroWhite+™. The beam profile follows the design which was previously modelled with the CBCM. The Young's moduli used for each material is listed in Supplementary Table S1. We decided to test three thicknesses (0.5, 1.0, and 1.5 mm) and the six different material mixes for the digital material (FLX9840, FLX9850, FLX9860, FLX9870, FLX9885, FLX9895). This gave us a total of 18 different combinations to tune the bi-stability behaviour. In addition to material and geometric effects, we decided to investigate the non-linear effects by evaluating the bi-stable switches at four different strain rates  $0.01 \text{ s}^{-1}$ ,  $0.1 \text{ s}^{-1}$ ,  $1 \text{ s}^{-1}$ , and  $10 \text{ s}^{-1}$ . The strain rate,  $\dot{\epsilon}$ , was defined as the crosshead speed,  $v$ , divided by the thickness of the bi-stable

switches,  $t$ :  $\dot{\epsilon} = \frac{v}{t}$ . A test jig was designed for accurate testing of the bi-stable columns to ensure that the applied axial force was centered (**Fig. 6c**)

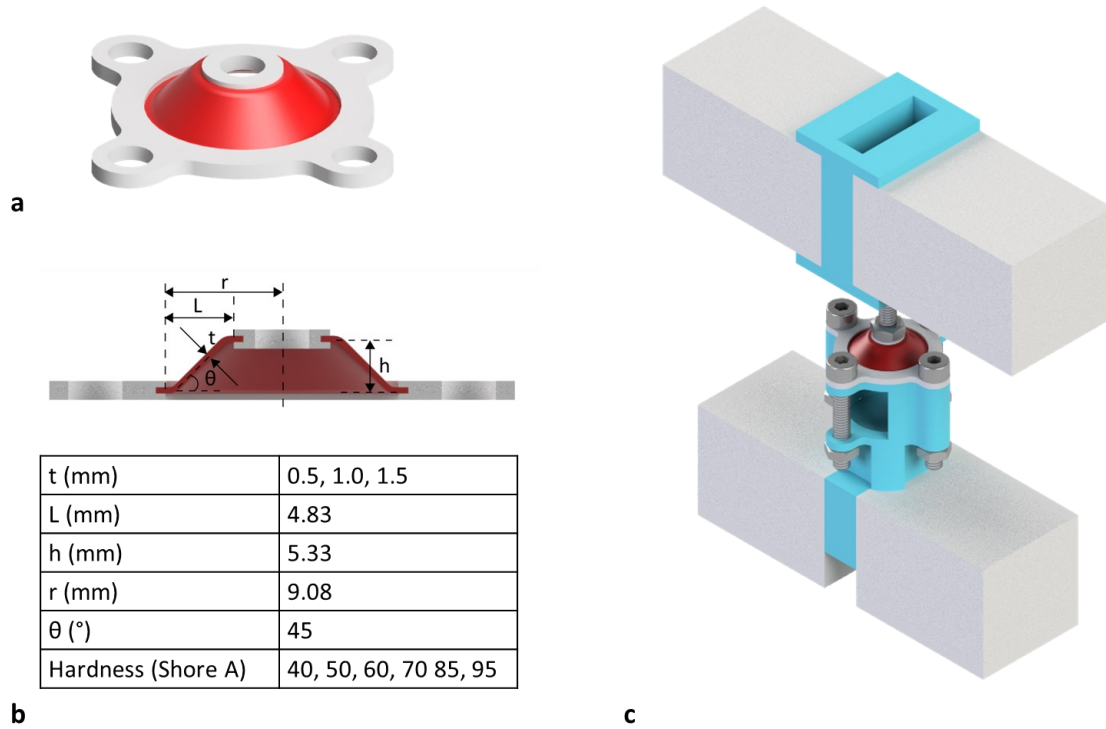


**Fig. 6 Bi-stable column and test jig design.** **a** Bi-stable column with stiff (gray) and soft (red) material parts. **b** Cross-section of the bi-stable column and a table of the design parameters. **c** Bi-stable attached to the test contraction (blue) attached to the upper and lower cross-heads of the mechanical tester (gray).

Each bi-stable column was printed successfully without any structural damages and was post-processed without any visible scarcities. After post-processing the bi-stable columns were inserted into the mechanical tester together with the bespoke test jig and evaluated (**Fig. 7a**). The mechanical testing results were compared to the estimated modelled behaviour by the CBCM model and the NASTRAN simulation. An example for the FLX9840 material can be seen in **Fig. 7b**. What can be seen is that the non-linear static NASTRAN simulation fails to correctly simulate the second bi-stable point, and failed after an applied displacement of 7.33 mm. The CBCM model accurately predicts the general shape of the bi-stable test curve, however the resulting  $F_{\min}$  and  $F_{\max}$  values are overestimated. In **Fig. 7c-d**  $F_{\max}$  and  $F_{\min}$  are plotted respectively for each material against the applied strain rate  $\dot{\epsilon}$ . All mechanical testing results can be seen in Supporting Figures S1-S3. Considering thickness, it was

found that for the material configurations with a thickness of 1.5 mm showed inconsistencies during testing, especially for lower strain rates ( $0.01 \text{ s}^{-1}$ ) and higher strain rates ( $10 \text{ s}^{-1}$ ) (Fig. S4b,d). In contrast the material configurations with a thickness of 0.5 mm all tested well, but the measured magnitudes for the forces  $F_{\max}$  and  $F_{\min}$  were deemed low for strain rates at  $1 \text{ s}^{-1}$  ( $< 1 \text{ N}$ ) and not suitable for applying vacuums (Fig. S4a,c). In addition, a thickness of 0.5 mm was rendered the samples fragile and prone to tears. Thus for subsequent pressure tests the material configurations with a thickness of 1.0 mm were used.

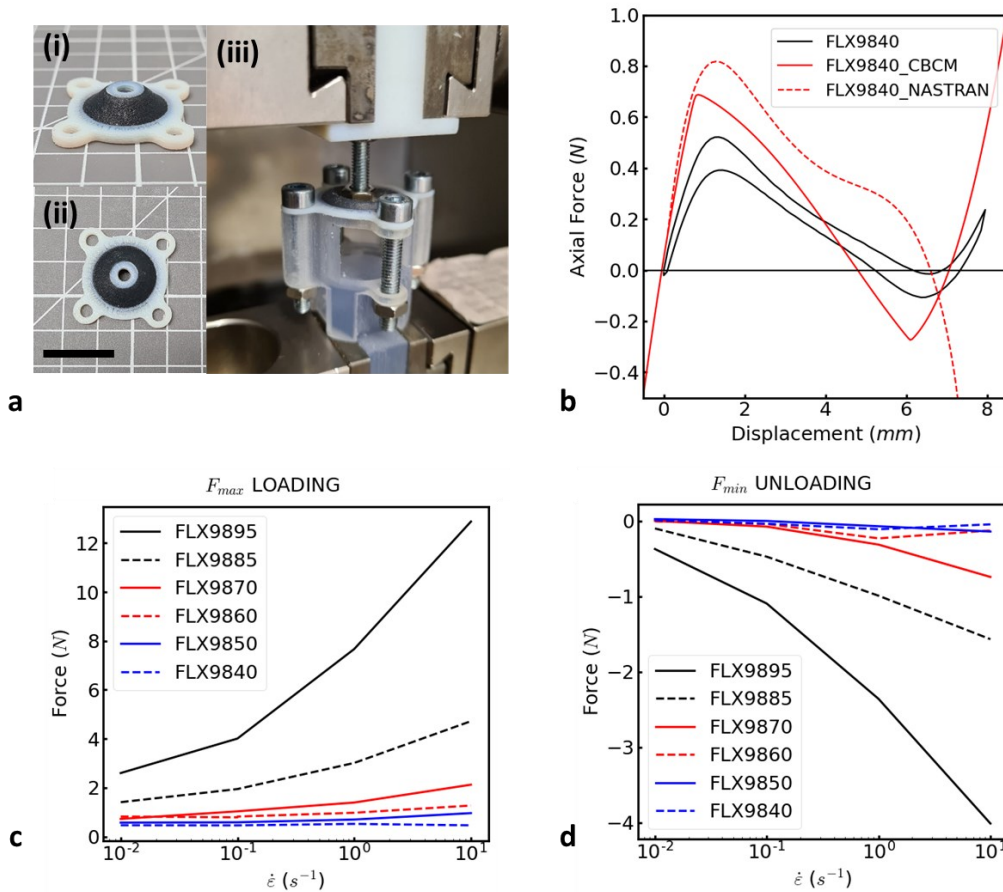


**Fig. 7 Mechanical testing of bi-stable columns.** **a** Photo showing the bi-stable column being deformed in the mechanical tester. **b** A comparison between the CBCM (red) the non-linear NASTRAN analysis (dashed red) and obtained data for FLX9840 (black; thickness = 1 mm). **c** The snap-through force ( $F_{\max}$ ) for the bi-stable columns with varying material stiffness (thickness = 1.0 mm). **d** The snap-back force ( $F_{\min}$ ) for the bi-stable columns with varying material stiffness (thickness = 1.0 mm).

In order to test the proof of principle a scaled-up model was created. For designing the BAFD the limiting factor was to manufacture the hooks which is the smallest component, and seeing that the 3D-printer was able to create components down to 0.5 mm this became the critical parameter for the hook tip. Following the natural shape of the tapeworm hooks resulted in a hook size length of 2.5 mm. The hook size to sucker diameter was 3:1 for *T. Solium* which is commonly found in pigs, which have a similar physiology to humans - thus a hole diameter of 7.5 mm was chosen. These critical design parameters chosen for the prototype manufactured resulted in a scale-up model with a scale of 1:20 compared to the parameters from *T. Solium*. In addition it was decided to create a hook construct consisting of 6 hooks arranged centro-symmetrically in one row **Fig. 8ai,aiv**, as more hooks would have resulted in hooks crashing into each other during actuation. The bi-stable column was modified for this design change and the inner diameter was increased to 17.5 mm **Fig. 8aiii**. The printed BAFD prototype can be seen in **Fig. 8b**. The suction inlet is located on the bottom, as shown in the cross-sectional view in **Fig. 8aiii**. To ensure that the printed prototype was hermetically sealed, an O-ring was designed into the bottom plate (**Fig. 8biii-biv**). In order to validate the mechanical tests conducted previously the pressure tests were conducted with the different material configurations inserted into a BAFD prototype with covered suction holes, in order to remove the effect of an insufficient seal on the top. As expected, the applied vacuum  $\Delta P$  increased with material stiffness (**Fig. 8c**) for all materials except FLX9895, with which the top layer ruptured before collapsing the column. For the demonstrative tests it was noticed that at an applied pressure of 15 – 20 kPa a good seal was detected. For the materials FLX9840 and FLX9850 due to a pressure <15 kPa to collapse the column were deemed unfit to be implemented in the prototype. To prevent that  $F_{\min}$  should increase while applying the pressure which may be equivalent to deforming the structure at a strain rate  $\dot{\epsilon} = 10\text{s}^{-1}$ , as seen for FLX9840 and FLX9860 (**Fig. 7d**), FLX9870 was ultimately chosen to be the bi-stable switch to be incorporated into the BAFD prototype. Attachment tests were performed with porcine tissue using the BAFD prototype with the FLX9870 bi-stable column [See Supplementary video S1]. At an applied vacuum of  $\Delta P = 20$  kPa suction was applied without collapsing the column. The difference between the collapsing column tests and the porcine tissue test may be due to insufficient seal and that the vacuum pump needs to reach a consistent value of 20 kPa, which may



have led to the bi-stable column requiring a greater applied vacuum for collapse. Increasing the applied vacuum of  $\Delta P = 50$  kPa touching the BAFD prototype with the top of the porcine tissue initiated suction and subsequently the ejection of the hooks (**Fig. 8di**). To ensure that the hooks were in fact penetrating the tissue, the sample was slowly peeled of (**Fig. 8dii-diii**) to expose the hooks, and after complete removal showed an imprint into the porcine tissue (**Fig. 8div**).

## 4 Discussion

Bioinspiration is a powerful tool to design new interventions that may be used in interventional medicine. This work demonstrates how a concept taken from nature can be decoded and implemented into a design for use in cardiovascular medicine, with a new step-controllable attachment principle. In brief our strategy shows the combination of suction and penetration of hooks, and the switch between the two aided by a bi-stable mechanism, is a technical feasibility to be implemented in the design and realization of minimally invasive cardiovascular devices. This concept is important in cardiovascular medicine, as during operation re-positioning of the device may be necessary and a two-step approach would enable this level of control. The approach presented in this work could be implemented for the fixation of transcatheter valves, pacemaker leads, or left atrial appendage occluders (LAAOs).

From mechanical testing of the bi-stable columns the on-loading and off-loading curve are different due to the viscoelastic nature of the FLX digital material mixes and thusly shows hysteresis. As a further remark, the digital material mixes are highly non-linear which can be shown on their dependency on applied strain rate, which other groups have confirmed [69]. Looking at **Fig. 7c,d** what can be deduced is that the faster the switches need to actuate, the more force is required.  $F_{\max}$  and  $F_{\min}$  are thus not only dependent on their design, and applied material, but the speed with which it needs to deform – this is an important factor when considering at what time scale the column should deform. The speed with which a device needs to deform will have consequences for what type of material and geometrical design should be applied. For the production of the BAFD, the hooks are created from a

printed material using the Stratasys Objet 260 in digital material mode. With a resolution of 30 micrometres and an accuracy of 200 micrometres [70] which limits the smallest dimension in the device, the width of the hook tip was set to be 0.5 mm to have at least 15 layers of material. Creating a device with hooks made from a stiffer material and sharper points, i.e., smaller tip widths, would ease the penetration of hooks into the tissue. For the BAFD prototype another consideration to be made is to create a design in which the holes are self-sealing if not touching or congruent with a tissue. This would prevent loss of pressure for the suckers in contact with tissue. Previous attempt to implement a tape-worm inspired design was tried by Yang et al. [5] and Spina et al. [6], but only tested the design of the rostellar hooks on porcine tissue. In our work we show that suction and penetration of hooks can work in succession and the switching between the two can be done through one stimulus. A limitation of the design, is the issue of miniaturization and biocompatibility. The scaled-up model which has a scale of 20:1 and multi-material components requires a very complex manufacturing process, and to simplify the design further may aid in preparing for large scale production. The materials used are acrylate-based and are not biocompatible, here the TangoBlack™ component could be replaced by a thermoplastic polyurethane (TPU) with polylactic acid (PLA) to make the material stronger [71] – and as for VeroWhitePlus™ could be replaced by medical grade poly(methyl methacrylate) or polycarbonate. Furthermore in the case of LAA occluders, there may be a benefit of lower thrombi formation due to the low surface area compared for example the Amplatzer PFO closure device [72]. Being a minimally invasive device, the patients would also be subject to more rapid convalescence, fewer hospital day stays, and a quicker return to normal activities [9].

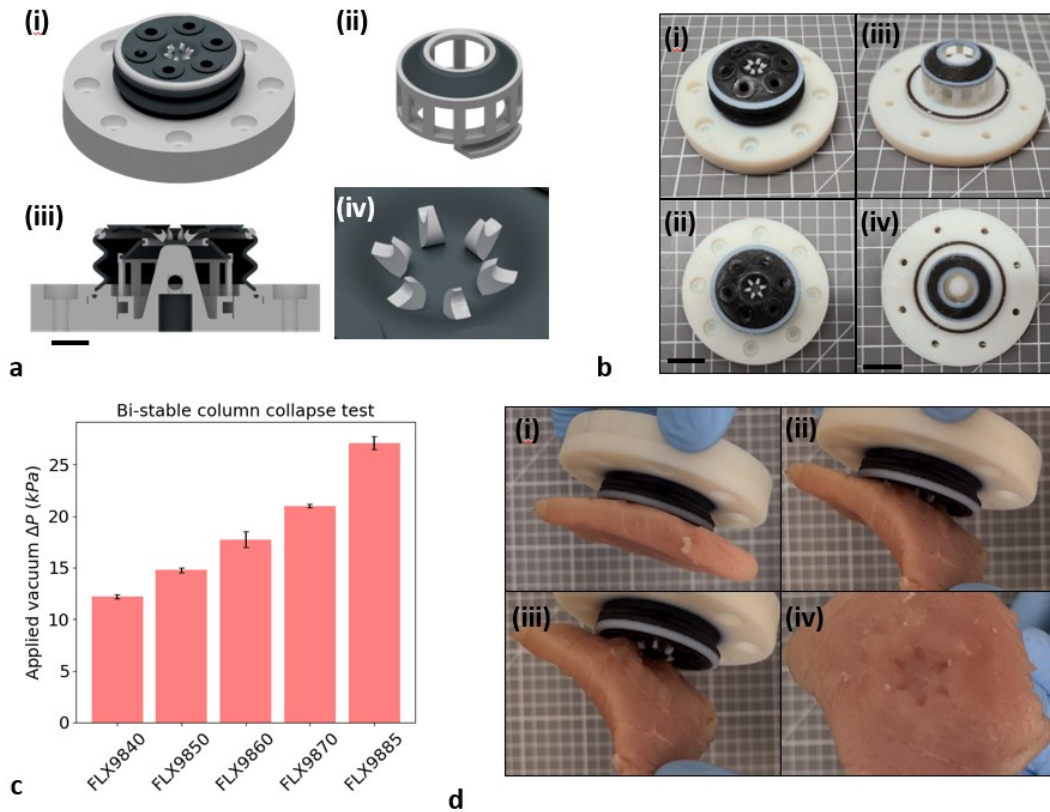


**Fig. 8 Results from prototype manufacturing and testing.** **a** The designed BAFD prototype showing (i) the whole device, (ii) the modified bi-stable column, (iii) cross-section of the BAFD prototype (scale bar = 1 cm), and (iv) the hook construct showing six rostellar hooks. **b** The printed BAFD prototype showing (i-ii) whole device, and (iii-iv) prototype with the top disc removed showing the modified bi-stable column. Scale bar = 2 cm. **c** Bi-stable column collapse test for material configurations FLX9840 – FLX9885\* (Results displayed are average  $\pm$  std. deviation,  $n = 3$ ). **d** BAFD attachment test on porcine tissue. (i) At an applied pressure of 50 kPa the device attached with suction with hooks ejected. (ii-iii) while peeling off the tissue, the hooks exposed show that they are attached and (iv) leave an imprint on the tissue. (\* = The bi-stable column with FLX9895 was too stiff and the top layer of the BAFD ripped in all three tests).

## 5 Conclusion

The research in this paper illustrated how bioinspiration and digital tools can serve to produce innovative and effective new concepts for medical devices, that may not be possible or prove cumbersome to manufacture with traditional subtractive manufacturing methods. Here we show that one can create a device with two modes of attachment: suction, and hook penetration, and that the switch between the two is controlled by the deformation of a mechanically bi-stable switch which can in addition be tuned to switch at a particular applied vacuum. Here a prototype was manufactured which only attached via suction at an applied vacuum of  $\Delta P = 20$  kPa, and when increasing the

vacuum further to  $\Delta P = 50$  kPa subsequently evaginated the hooks to penetrate into porcine tissue. The hooks were found to have penetrated the tissue, validating our hypothesis that a bi-modular bi-stable alternative fixation device can be modelled, designed, and manufactured using digital methods such as modelling and additive manufacturing. For further development, the device needs to be minimized and medical grade polymers need to be incorporated. Projects like these will further improve treatment options and outcome of patients in the near future.

## 6 Acknowledgements

Victor Izraylit is thanked for the use of his vacuum pump, and Mark Schröder, Dr. Manfred Gossen and Prof. Friedrich Jung for their insightful and helpful discussions throughout this work. This work is financially supported by the Helmholtz Association of German Research Centers through program-oriented funding and through Helmholtz Graduate School for Macromolecular Bioscience (MacroBio, VH-GS-503)

### References:

- [1] VELCRO®, “Velcro: Our Story.” <https://www.velcro.com/original-thinking/our-story/> (accessed Oct. 11, 2021).
- [2] S. Hengherr, A. G. Heyer, H. R. Köhler, and R. O. Schill, “Trehalose and anhydrobiosis in tardigrades - Evidence for divergence in responses to dehydration,” *FEBS Journal*, vol. 275, no. 2, pp. 281–288, Jan. 2008, doi: 10.1111/j.1742-4658.2007.06198.x.
- [3] R. O. Schill, B. Mali, T. Dandekar, M. Schnölzer, D. Reuter, and M. Frohme, “Molecular mechanisms of tolerance in tardigrades: New perspectives for preservation and stabilization of biological material,” *Biotechnology Advances*, vol. 27, no. 4, pp. 348–352, Jul. 2009. doi: 10.1016/j.biotechadv.2009.01.011.
- [4] A. Mahdavi *et al.*, “A biodegradable and biocompatible gecko-inspired tissue adhesive,” *Proc Natl Acad Sci U S A*, vol. 105, no. 7, pp. 2307–2312, 2008, doi: 10.1073/pnas.0712117105.

- [5] S. S. Latthe, C. Terashima, K. Nakata, and A. Fujishima, "Superhydrophobic surfaces developed by mimicking hierarchical surface morphology of lotus leaf," *Molecules*, vol. 19, no. 4. Molecular Diversity Preservation International, pp. 4256–4283, 2014. doi: 10.3390/molecules19044256.
- [6] Y. Yu, Z. H. Zhao, and Q. S. Zheng, "Mechanical and superhydrophobic stabilities of two-scale surfacial structure of lotus leaves," *Langmuir*, vol. 23, no. 15, pp. 8212–8216, Jul. 2007, doi: 10.1021/la7003485.
- [7] A. Marmur, "The lotus effect: Superhydrophobicity and metastability," *Langmuir*, vol. 20, no. 9, pp. 3517–3519, Apr. 2004, doi: 10.1021/la036369u.
- [8] A. K. Bastola, N. Rodriguez, M. Behl, P. Soffiatti, N. P. Rowe, and A. Lendlein, "Cactus-inspired design principles for soft robotics based on 3D printed hydrogel-elastomer systems," *Materials and Design*, vol. 202, Apr. 2021, doi: 10.1016/j.matdes.2021.109515.
- [9] A. Buia, F. Stockhausen, and E. Hanisch, "Laparoscopic surgery: A qualified systematic review," *World Journal of Methodology*, vol. 5, no. 4, p. 238, 2015, doi: 10.5662/wjm.v5.i4.238.
- [10] A. Park, D. W. Birch, and P. Lovrics, "Laparoscopic and open incisional hernia repair: a comparison study," *Surgery*, vol. 124, no. 4, pp. 816–822, 1998.
- [11] M. J. Mack, "Minimally invasive cardiac surgery," *Surgical Endoscopy and Other Interventional Techniques*, vol. 20, no. 2 SUPPL. Apr. 2006. doi: 10.1007/s00464-006-0110-8.
- [12] H. Reichenspurner *et al.*, "Port-Access Coronary Artery Bypass Grafting With the Use of Cardiopulmonary Bypass and Cardioplegic Arrest," 1998.
- [13] J. A. Morgan *et al.*, "Robotic techniques improve quality of life in patients undergoing atrial septal defect repair," *Annals of Thoracic Surgery*, vol. 77, no. 4, pp. 1328–1333, Apr. 2004, doi: 10.1016/j.athoracsur.2003.09.044.

- [14] J. Rodés-Cabau, “Transcatheter aortic valve implantation: Current and future approaches,” *Nature Reviews Cardiology*, vol. 9, no. 1. pp. 15–29, Jan. 2012. doi: 10.1038/nrcardio.2011.164.
- [15] G. C. M. Siontis *et al.*, “Transcatheter aortic valve implantation vs. surgical aortic valve replacement for treatment of symptomatic severe aortic stenosis: an updated meta-analysis,” *European Heart Journal*, vol. 40, no. 38, pp. 3143–3153, Oct. 2019, doi: 10.1093/eurheartj/ehz275.
- [16] M. Taramasso *et al.*, “Clinical outcomes of MitraClip for the treatment of functional mitral regurgitation,” *EuroIntervention*, vol. 10, no. 6, Oct. 2014, doi: 10.4244/EIJV10I6A128.
- [17] O. Franzen *et al.*, “MitraClip® therapy in patients with end-stage systolic heart failure,” *European Journal of Heart Failure*, vol. 13, no. 5, pp. 569–576, May 2011, doi: 10.1093/eurjhf/hfr029.
- [18] J. Schofer, K. Bijuklic, C. Tiburtius, L. Hansen, A. Groothuis, and R. T. Hahn, “First-in-Human Transcatheter Tricuspid Valve Repair in a Patient With Severely Regurgitant Tricuspid Valve,” 2015.
- [19] J. Romero, I. E. Perez, A. Krumerman, M. J. Garcia, and R. J. Lucariello, “Left atrial appendage closure devices,” *Clinical Medicine Insights: Cardiology*, vol. 8, pp. 45–52, 2014, doi: 10.4137/CMC.S14043.
- [20] S. H. Kang *et al.*, “Biodegradable-polymer drug-eluting stents vs. bare metal stents vs. durable-polymer drug-eluting stents: a systematic review and Bayesian approach network meta-analysis,” *Eur Heart J*, vol. 35, no. 17, pp. 1147–1158, 2014, doi: 10.1093/eurheartj/ehz570.
- [21] J. B. Masson *et al.*, “Transcatheter Aortic Valve Implantation. Review of the Nature, Management, and Avoidance of Procedural Complications,” *JACC: Cardiovascular Interventions*, vol. 2, no. 9. pp. 811–820, Sep. 2009. doi: 10.1016/j.jcin.2009.07.005.

- [22] G. Ailawadi *et al.*, “One-Year Outcomes after MitraClip for Functional Mitral Regurgitation,” *Circulation*, vol. 139, no. 1, pp. 37–47, Jan. 2019, doi: 10.1161/CIRCULATIONAHA.117.031733.
- [23] J. M. Sinning and E. Grube, “Transcatheter heart valve failure: The sword of Damocles over our heads?,” *European Heart Journal*, vol. 36, no. 21. Oxford University Press, pp. 1284–1287, Jun. 01, 2015. doi: 10.1093/eurheartj/ehu459.
- [24] I. E. Dzyaloshinskii, E. M. Lifshitz, and L. P. Pitaevskii, “The general theory of van der Waals forces,” *Advances in Physics*, vol. 10, no. 38, pp. 165–209, 1961, doi: 10.1080/00018736100101281.
- [25] B. Hayes, “How Gecko Toes Stick,” *Society*, vol. 91, no. 6, pp. 484–488, 2003, doi: 10.1511/2011.89.106.
- [26] W. M. Kier, “The Structure and Adhesive Mechanism of Octopus Suckers,” *Integrative and Comparative Biology*, vol. 42, no. 6, pp. 1146–1153, 2002, doi: 10.1093/icb/42.6.1146.
- [27] B. Presswell, R. Poulin, and H. S. Randhawa, “First report of a gryporhynchid tapeworm (Cestoda: Cyclophyllidea) from New Zealand and from an eleotrid fish, described from metacestodes and in vitro-grown worms,” *Journal of Helminthology*, vol. 86, no. 4, pp. 453–464, 2012, doi: 10.1017/S0022149X11000691.
- [28] K. Kamino, “Mini-review: Barnacle adhesives and adhesion,” *Biofouling*, vol. 29, no. 6. pp. 735–749, Jul. 2013. doi: 10.1080/08927014.2013.800863.
- [29] M. Zhang, M. Liu, H. Prest, and S. Fischer, “Nanoparticles secreted from ivy rootlets for surface climbing,” *Nano Letters*, vol. 8, no. 5, pp. 1277–1280, May 2008, doi: 10.1021/nl0725704.
- [30] Z. L. Zhao, T. Shu, and X. Q. Feng, “Study of biomechanical, anatomical, and physiological properties of scorpion stingers for developing biomimetic materials,” *Materials Science and Engineering C*, vol. 58, pp. 1112–1121, 2016, doi: 10.1016/j.msec.2015.09.082.

- [31] R. Das, R. N. Yadav, P. Sihota, P. Uniyal, N. Kumar, and B. Bhushan, "Biomechanical Evaluation of Wasp and Honeybee Stingers," *Scientific Reports*, vol. 8, no. 1, 2018, doi: 10.1038/s41598-018-33386-y.
- [32] Z. Liu, Y. Zhu, D. Jiao, Z. Weng, Z. Zhang, and R. O. Ritchie, "Enhanced protective role in materials with gradient structural orientations: Lessons from Nature," *Acta Biomaterialia*, vol. 44, pp. 31–40, 2016, doi: 10.1016/j.actbio.2016.08.005.
- [33] Z. Liu, Z. Zhang, and R. O. Ritchie, "Structural Orientation and Anisotropy in Biological Materials: Functional Designs and Mechanics," *Advanced Functional Materials*, vol. 30, no. 10, 2020, doi: 10.1002/adfm.201908121.
- [34] R. G. Beutel and S. N. Gorb, "Ultrastructure of attachment specializations of hexapods (Arthropoda): evolutionary patterns inferred from a revised ordinal phylogeny," *Journal of Zoological Systematics and Evolutionary Research*, vol. 39, no. 4, pp. 177–207, 2001, doi: 10.1046/j.1439-0469.2001.00155.x.
- [35] A. Miserez, T. Schneberk, C. Sun, F. W. Zok, and J. H. Waite, "The transition from stiff to compliant materials in squid beaks," *Science*, vol. 319, no. 5871, pp. 1816–1819, Mar. 2008, doi: 10.1126/science.1154117.
- [36] T. Takahashi, M. Suzuki, and S. Aoyagi, "Octopus bioinspired vacuum gripper with micro bumps," *2016 IEEE 11th Annual International Conference on Nano/Micro Engineered and Molecular Systems, NEMS 2016*, pp. 508–511, 2016, doi: 10.1109/NEMS.2016.7758301.
- [37] W. M. Kier and A. M. Smith, "The Structure and Adhesive Mechanism of Octopus Suckers 1," 2002. [Online]. Available: <http://icb.oxfordjournals.org/>
- [38] T. Scholz, R. Drábek, and V. Hanzelová, "Scolex morphology of Proteocephalus tapeworms (Cestoda: Proteocephalidae), parasites of freshwater fish in the Palaearctic Region.," *Folia parasitologica*, vol. 45, no. 1, pp. 27–43, 1998, [Online]. Available: <http://www.ncbi.nlm.nih.gov/pubmed/9516993>



- [39] D. E. Barlow, G. H. Dickinson, B. Orihuela, J. L. Kulp, D. Rittschof, and K. J. Wahl, "Characterization of the adhesive plaque of the barnacle *Balanus amphitrite*: Amyloid-like nanofibrils are a major component," *Langmuir*, vol. 26, no. 9, pp. 6549–6556, 2010, doi: 10.1021/la9041309.
- [40] K. Kamino, "Underwater adhesive of marine organisms as the vital link between biological science and material science," *Marine Biotechnology*, vol. 10, no. 2, pp. 111–121, 2008, doi: 10.1007/s10126-007-9076-3.
- [41] S. v Dorozhkin and M. Epple, "Biological and medical significance of calcium phosphates," *Angewandte Chemie - International Edition*, vol. 41, no. 17, pp. 3130–3146, 2002, doi: 10.1002/1521-3773(20020902)41:17<3130::AID-ANIE3130>3.0.CO;2-1.
- [42] M. Zhang, M. Liu, H. Prest, and S. Fischer, "Nanoparticles secreted from ivy rootlets for surface climbing," *Nano Letters*, vol. 8, no. 5, pp. 1277–1280, 2008, doi: 10.1021/nl0725704.
- [43] P. M. Favi, S. Yi, S. C. Lenaghan, L. Xia, and M. Zhang, "Inspiration from the natural world: from bio-adhesives to bio-inspired adhesives," *Journal of Adhesion Science and Technology*, vol. 28, no. 3–4, pp. 290–319, 2014, doi: 10.1080/01694243.2012.691809.
- [44] S. B. Emerson and D. Diehl, "Toe pad morphology and mechanisms of sticking in frogs," *Biological Journal of the Linnean Society*, vol. 13, no. 3, pp. 199–216, 1980, doi: 10.1111/j.1095-8312.1980.tb00082.x.
- [45] B. Bar-On, F. G. Barth, P. Fratzl, and Y. Politi, "Multiscale structural gradients enhance the biomechanical functionality of the spider fang," *Nature Communications*, vol. 5, 2014, doi: 10.1038/ncomms4894.
- [46] W. K. Cho *et al.*, "Microstructured barbs on the North American porcupine quill enable easy tissue penetration and difficult removal," *Proceedings of the National Academy of Sciences of the United States of America*, vol. 109, no. 52, pp. 21289–21294, 2012, doi: 10.1073/pnas.1216441109.

- [47] H. Kumazawa and K. Yagyu, "Rostellar gross anatomy and the ultrastructural and histochemical characterization of the rostellar tegument-related structures in *Hymenolepis nana*," *International Journal for Parasitology*, vol. 18, no. 6, pp. 739–746, 1988, doi: 10.1016/0020-7519(88)90113-0.
- [48] N. A. Pospekhova and S. K. Bondarenko, "Morpho-functional characteristics of the scolex of *Wardium chaunense* (Cestoda: Aploparaksidae) penetrated into host intestine," *Parasitology Research*, vol. 113, no. 1, pp. 131–137, 2014, doi: 10.1007/s00436-013-3635-5.
- [49] M. T. Merchant, L. Aguilar, G. Avila, L. Robert, A. Flisser, and K. Willms, "Taenia solium: description of the intestinal implantation sites in experimental hamster infections," *The Journal of parasitology*, pp. 681–685, 1998.
- [50] E. Sciutto *et al.*, "Taenia solium disease in humans and pigs: an ancient parasitosis disease rooted in developing countries and emerging as a major health problem of global dimensions," 2000.
- [51] L. J. Cunningham and P. D. Olson, "Description of *Hymenolepis microstoma* (Nottingham strain): A classical tapeworm model for research in the genomic era," *Parasites and Vectors*, vol. 3, no. 1, 2010, doi: 10.1186/1756-3305-3-123.
- [52] A. Menciassi and P. Dario, "Bio-inspired solutions for locomotion in the gastrointestinal tract: Background and perspectives," *Philosophical Transactions of the Royal Society A: Mathematical, Physical and Engineering Sciences*, vol. 361, no. 1811, pp. 2287–2298, Oct. 2003, doi: 10.1098/rsta.2003.1255.
- [53] N. W. Riser, "The Hooks of Taenioid Cestodes from North American Felids," 1956.
- [54] A. Verster, "Redescription of *Taenia solium* LINNAEUS, 1758 and *Taenia saginata* GOEZE, 1782," 1967.
- [55] E. J. L. Soulsby, "Helminths, arthropods and protozoa of domesticated animals. 1982," *Eastbourne, United Kingdom: Baillière, Tindall & Cassell*, vol. 7, 2015.

- [56] M. E. Boa, A. A. Kassuku, A. L. Willingham, J. D. Keyyu, I. K. Phiri, and P. Nansen, "Distribution and density of cysticerci of *Taenia solium* by muscle groups and organs in naturally infected local finished pigs in Tanzania," *Veterinary parasitology*, vol. 106, no. 2, pp. 155–164, 2002.
- [57] P. C. Fan, W. C. Chung, C. Y. Lin, and C. C. Wu, "Experimental infection of Thailand *Taenia* (Chiengmai strain) in domestic animals," *International Journal for Parasitology*, vol. 20, no. 1, pp. 121–123, Feb. 1990, doi: 10.1016/0020-7519(90)90183-N.
- [58] P. C. Fan, C. Y. Lin, and W. C. Chung, "Experimental infection of philippine *Taenia* in domestic animals," *International Journal for Parasitology*, vol. 22, no. 2, pp. 235–238, Apr. 1992, doi: 10.1016/0020-7519(92)90107-V.
- [59] K. Al-Jashamy and M. N. Islam, "Morphological Study Of *Taenia taeniaeformis* Scolex Under Scanning Electron Microscopy Using Hexamethyldislazane," *ANNALS OF MICROSCOPY*, vol. 7, Apr. 2007.
- [60] E. C. Stevenson and C. C. Engberg, "Variation in the hooks of the dog-tapeworms *Taenia serrata* and *Taenia serialis* with a discussion of the mathematical results," *Studies Zoological Laboratory University of Nebraska*, no. 59, pp. 409–448, 1904.
- [61] K. A. Padgett, S. A. Nadler, L. Munson, B. Sacks, and W. M. Boyce, "Systematics of *Mesocestoides* (Cestoda: Mesocestoididae): Evaluation of Molecular and Morphological Variation among Isolates," 2005. [Online]. Available: [https://www.jstor.org/stable/20059891?seq=1&cid=pdf-reference#references\\_tab\\_contents](https://www.jstor.org/stable/20059891?seq=1&cid=pdf-reference#references_tab_contents)
- [62] "Kugi - 2000 - *Sobolevitaenia japonensis* n. sp. (Dilepididae Dilepidinae) from a dusky thrush, *Turdus naumanni eunomus* Temminck, in Oita".
- [63] C. T. Ba, T. H. Sene, and B. Marchand, "Scanning electron microscope examination of scale-like spines on the rostellum of five *Davaineinae* (Cestoda, Cyclophyllidea) | Observations au microscope ?lectronique ? balayage, d??pines en forme d??cailles sur le rostre de cinq

- Davaineinae (Cestoda, Cy,” *Parasite*, vol. 2, no. 1, pp. 63–67, 1995, doi: 10.1051/parasite/1995021063.
- [64] H. Larry L. and L. L. S. P. M. B. M. O. Howell, *Handbook of Compliant Mechanisms*. West Sussex, United Kingdom: Wiley & Sons, Ltd., 2013.
- [65] L. L. Howell and A. Midha, “A method for the design of compliant mechanisms with small-length flexural pivots,” 1994.
- [66] S. Awtar and S. Sen, “A generalized constraint model for two-dimensional beam flexures,” in *International Design Engineering Technical Conferences and Computers and Information in Engineering Conference*, 2009, vol. 49040, pp. 345–358.
- [67] F. Ma and G. Chen, “Chained beam-constraint-model (CBCM): A powerful tool for modeling large and complicated deflections of flexible beams in compliant mechanisms,” in *Proceedings of the ASME Design Engineering Technical Conference*, 2014, vol. 5A. doi: 10.1115/DETC2014-34140.
- [68] J. Bäckemo, Y. Liu, and A. Lendlein, “Bio-inspired and computer-supported design of modulated shape changes in polymer materials,” *MRS Communications*, vol. 11, no. 4. Springer Nature, pp. 462–469, 2021. doi: 10.1557/s43579-021-00056-6.
- [69] V. Slesarenko and S. Rudykh, “Towards mechanical characterization of soft digital materials for multimaterial 3D-printing,” *International Journal of Engineering Science*, vol. 123, pp. 62–72, 2018, doi: 10.1016/j.ijengsci.2017.11.011.
- [70] Stratasys, “Objet 260 Connex 3 - EN Spec Sheet.” [Online]. Available: <https://support.stratasys.com/en/printers/polyjet/objet260-connex-1-2-3>
- [71] Q. Chen, J. D. Mangadlao, J. Wallat, A. de Leon, J. K. Pokorski, and R. C. Advincula, “3D printing biocompatible polyurethane/poly(lactic acid)/graphene oxide nanocomposites: Anisotropic properties,” *ACS Applied Materials and Interfaces*, vol. 9, no. 4, pp. 4015–4023, Feb. 2017, doi: 10.1021/acsami.6b11793.

- [72] B. Plicht *et al.*, “Risk Factors for Thrombus Formation on the Amplatzer Cardiac Plug After Left Atrial Appendage Occlusion.”

# Supporting info for: A Biomimetic Alternative bi-modular bi- stable fixation Device (BAFD)

J. Bäckemo<sup>1,2,\*</sup>, M. Reinthaler<sup>1,3</sup> A. Lendlein<sup>1,2</sup>,

<sup>1</sup>Institute of Active Polymers, Helmholtz-Zentrum Hereon, Kanststr. 55, 14513 Teltow, Germany;

<sup>2</sup>Institute of Chemistry, University of Potsdam, 14476 Potsdam, Germany

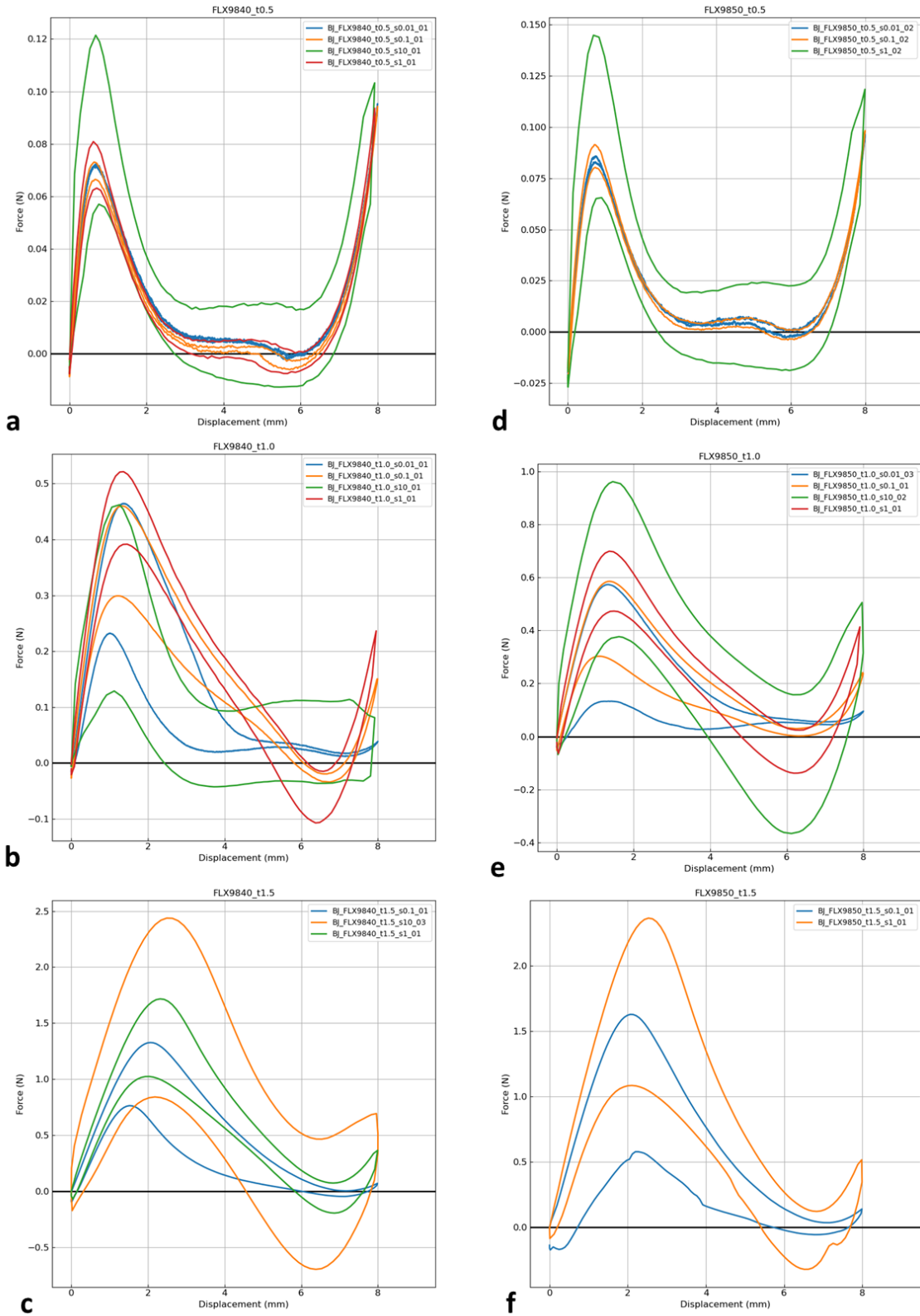
<sup>3</sup>Department of Cardiology, Campus Benjamin Franklin, Charité Berlin, Berlin, Germany

\*corresponding author: [publications@hereon.de](mailto:publications@hereon.de)

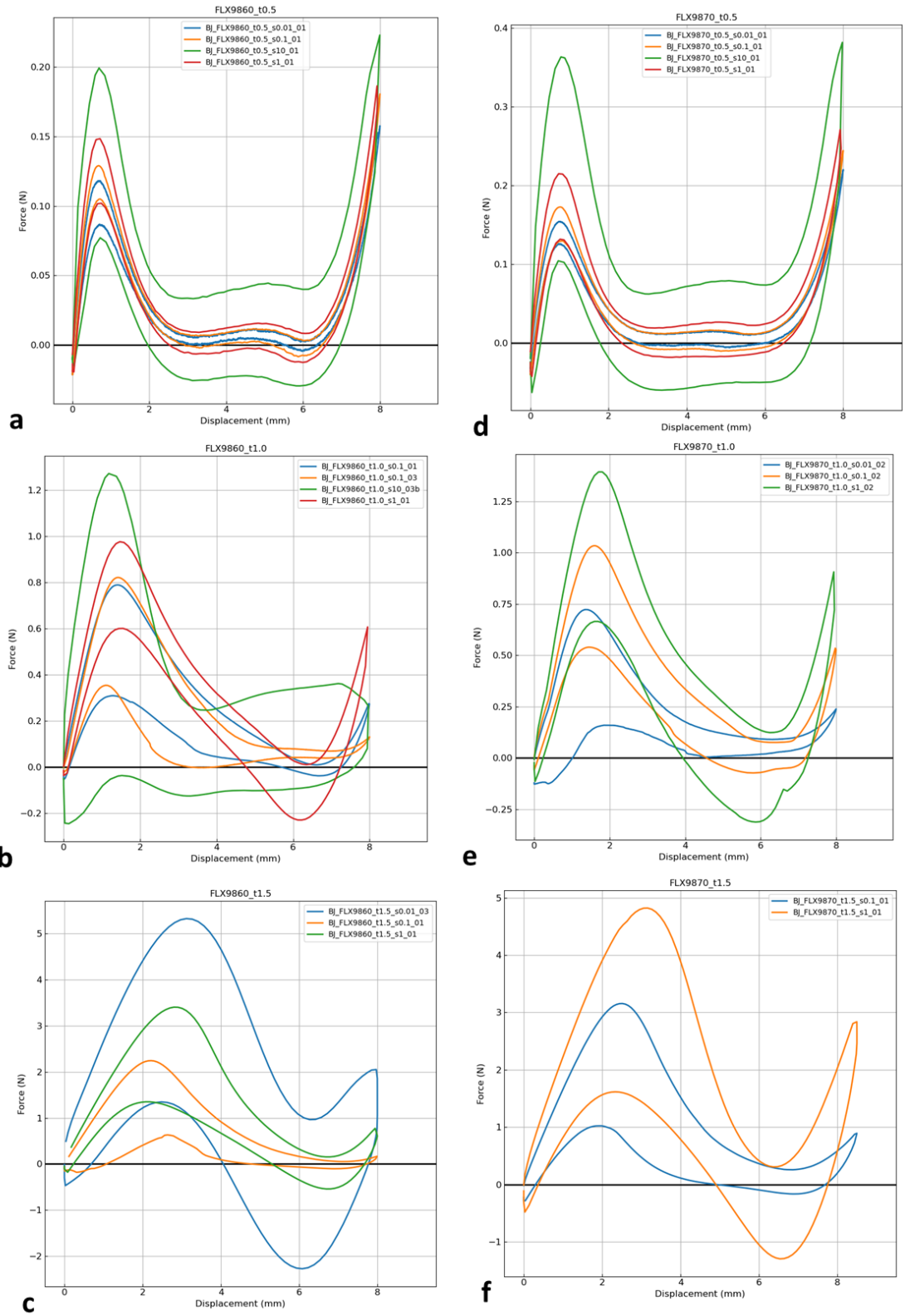
ORCID-ID

JB: 0000-0001-6721-8109

AL: 0000-0003-4126-4670

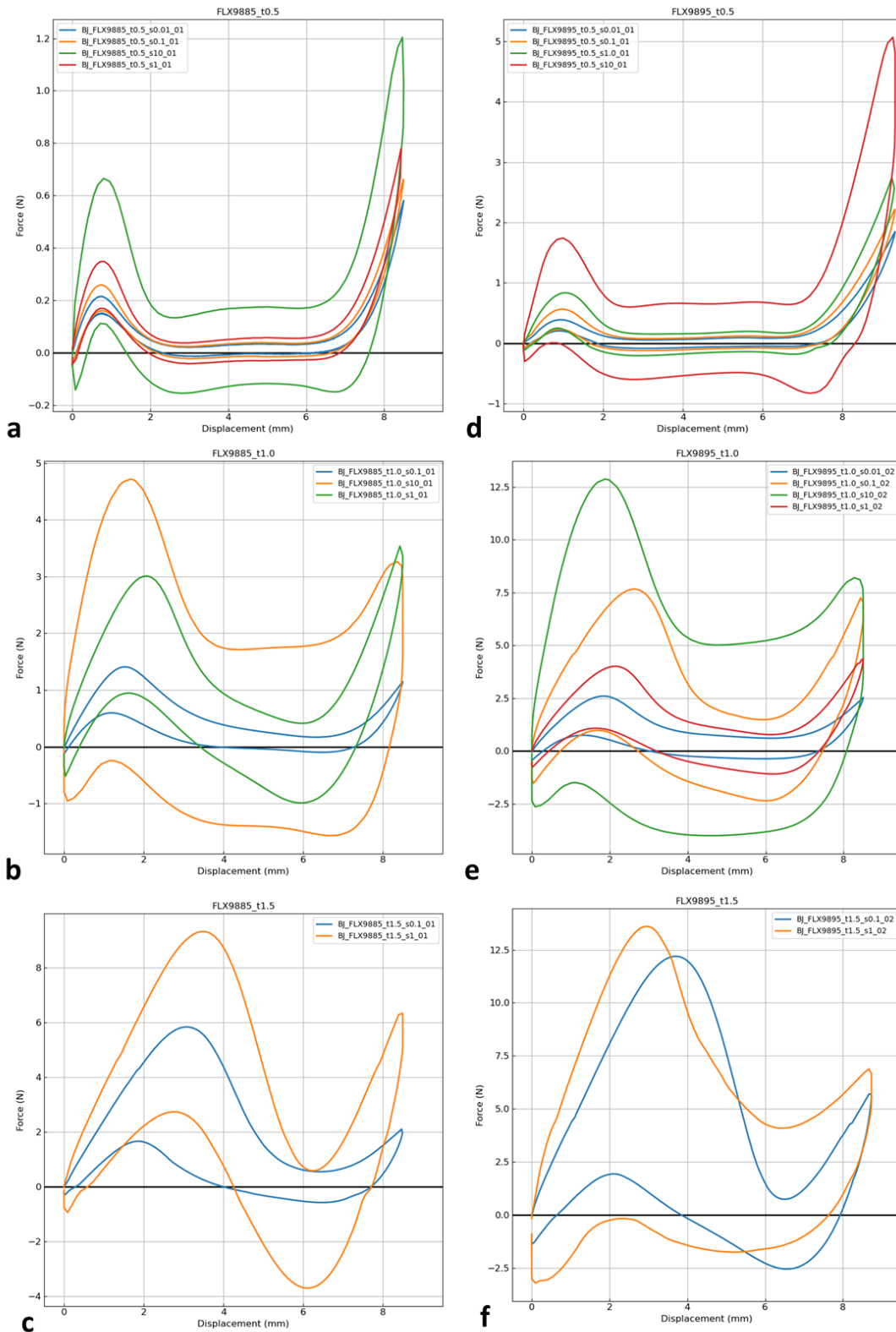


Supporting Figure 1. (a-c) Mechanical testing results with varying strain rate for FLX9840 bi-stable columns with thickness (a) 0.5 mm, (b) 1.0 mm, and (c) 1.5 mm. (d-f) Mechanical testing results with varying strain rate for FLX9850 bi-stable columns with thickness (d) 0.5 mm, (e) 1.0 mm, and (f) 1.5 mm.

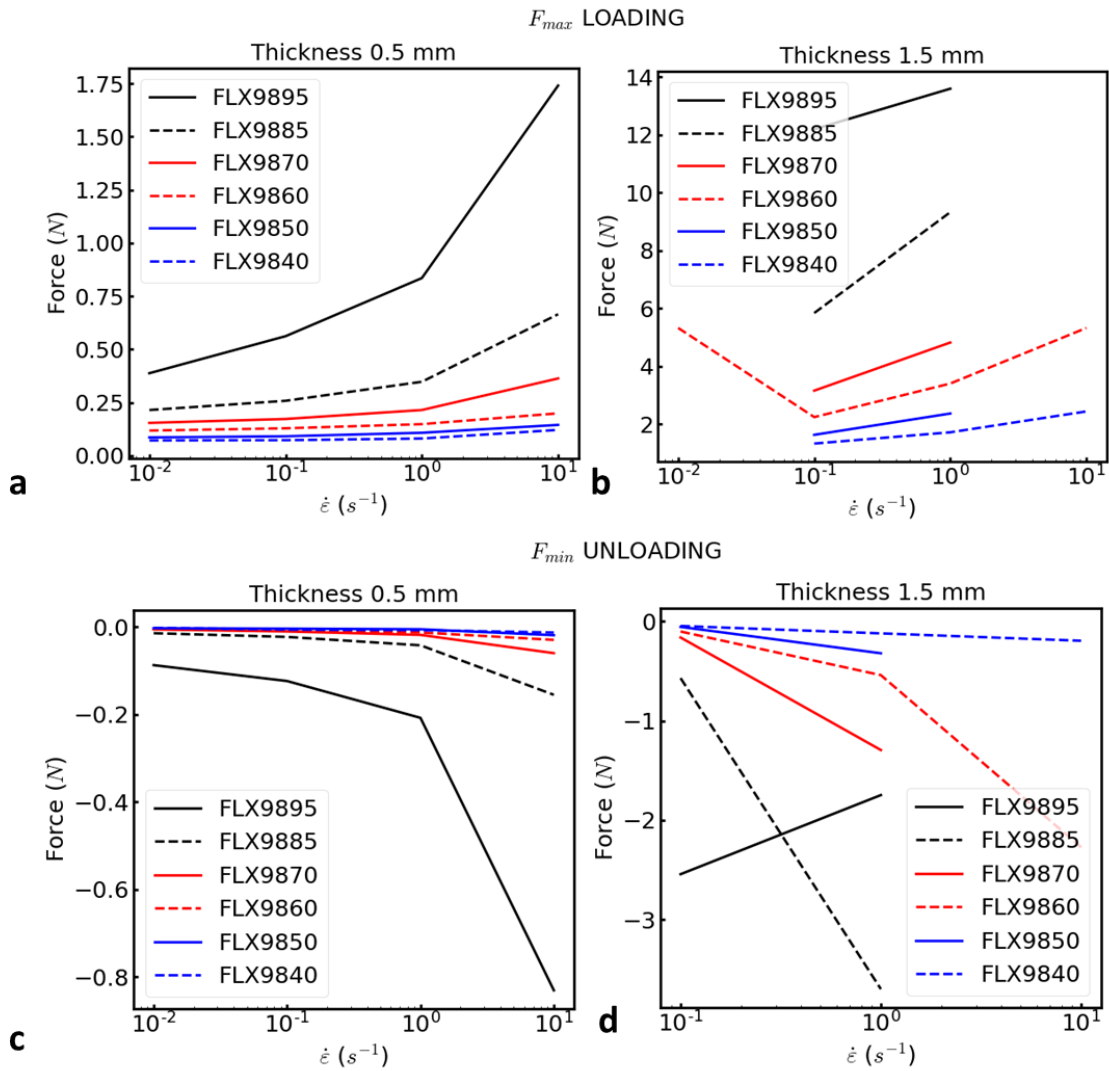


Supporting Figure 2. (a-c) Mechanical testing results with varying strain rate for FLX9860 bi-stable columns with thickness (a) 0.5 mm, (b) 1.0 mm, and (c) 1.5 mm. (d-f) Mechanical testing results with varying strain rate for FLX9870 bi-stable columns with thickness (d) 0.5 mm, (e) 1.0 mm, and (f) 1.5 mm.





Supporting Figure 3. (a-c) Mechanical testing results with varying strain rate for FLX9885 bi-stable columns with thickness (a) 0.5 mm, (b) 1.0 mm, and (c) 1.5 mm. (d-f) Mechanical testing results with varying strain rate for FLX9895 bi-stable columns with thickness (d) 0.5 mm, (e) 1.0 mm, and (f) 1.5 mm.



**Supporting Figure S4.**  $F_{max}$  measurements with varying strain rate for thickness (a) 0.5 mm and (b) 1.5 mm.  $F_{min}$  measurements with varying strain rate for thickness (c) 0.5 mm and (d) 1.5 mm.

**Supplementary Table S1.** Shore A durometer conversion to Young's modulus using the equation

$$E_0 = 0.0235 * S - 0.6403 \text{ from Qi et al. [1]}$$

<b>Material</b>	<b>Youngs modulus, E (Mpa)</b>
FLX9895	39.10
FLX9885	22.76
FLX9870	10.11
FLX9860	5.88
FLX9850	3.43
FLX9840	1.99

**Supplementary Movie S1:** Movie showing the BAFD with the FLX9870 bi-stable column with a thickness of 1 mm being attached to tissue by suction only at an applied vacuum of 20 kPa, and attached through suction and hooks at an applied vacuum of 50 kPa.

1. Boyce, M.C., K. Joyce, and H.J. Qi, *Durometer Hardness and the Stress-Strain Behavior of Elastomeric Materials*. Rubber Chemistry and Technology, 2003. **76**(2): p. 419-435.

## Appendix IV Programmatic implementation

For many of scientific challenges, there is in this day and age a big necessity and focus on computation. Concepts such as machine learning [104], big data [105], and artificial intelligence [106] has seen tremendous leaps in the last two decades which has put a lot emphasis and need on the ability to understand programming. As of 2018, Python was the most popular programming language to program in [107]. It is generally accepted in the scientific community as an "all-round" programming language which is capable of both functional and object-oriented programming. With the advancement of Graphical Processing Unit (GPU)s and computing power, for both technical and scientific applications Python is the preferred language [108]. When it comes especially for large computing tasks, compiled languages such as C, C++ and FORTRAN have much faster processing times [109]. However, many of the most widely used libraries of Python such as NumPy which uses C-like arrays for numerical calculations and matrix operations for numerical computation and matrix operations [110]. Another SciPy is used for scientific computation and is based on NumPy functions. These packages are in turn dependent on internal libraries that are written in C, but when some functionality is not found in these internal libraries the Python interpreter is used and thus more processing time is needed [110]. Another limitation of Python is the inability to natively use Graphical Processing Unit (GPU)s, but there are packages that can interpret the code to be used on GPUs and implement parallelization, such as Numba [111]. It allows Python to convert marked functions to so-called Compute Unified Device Architecture (CUDA) cores for the Nvidia GPU, which are normally designed for C, C++, and FORTRAN. This thesis uses Python and the application of CUDA cores in order to solve the mathematical equations and matrix operations needed for all three projects.

## Appendix V CV

*This section includes personal data and was removed from the dissertation*

*Dieser Teil enthält persönliche Daten und wurde aus der Dissertation entfernt*

## Appendix VI List of Publications

**Bäckemo, J.**, Liu, Y. & Lendlein, A. Bio-inspired and computer-supported design of modulated shape changes in polymer materials. MRS Communications (2021).

**Bäckemo, J.**, Heuchel, M., Reinthaler, M., Kratz, K. and Lendlein, A., 2020. Predictive topography impact model for Electrical Discharge Machining (EDM) of metal surfaces. MRS Advances, 5(12), pp.621-632.

Braune, S., **Bäckemo, J.**, Lau, S., Heuchel, M., Kratz, K., Jung, F., Reinthaler, M. and Lendlein, A., 2020. The influence of different rewetting procedures on the thrombogenicity of nanoporous poly (ether imide) microparticles. Clinical Hemorheology and Microcirculation, (Preprint), pp.1-14.

Reinthaler, M., **Johansson, J.B.**, Braune, S., Al-Hindwan, H.S.A., Lendlein, A. and Jung, F., 2019. Shear-induced platelet adherence and activation in an in-vitro dynamic multiwell-plate system. Clinical hemorheology and microcirculation, 71(2), pp.183-191.

Reinthaler, M., Ozga, A.K., Sinning, D., Curio, J., Al-Hindwan, H.S., **Johansson, J.B.**, Jung, F., Lendlein, A., Rauch, G. and Landmesser, U., 2018. Revival of transcatheter PFO closure: A meta-analysis of randomized controlled trials-impact of shunt size and age. American heart journal, 201, pp.95-102.

Curio, J., Reinthaler, M., Kasner, M., Al-Hindwan, H.S.A., **Baeckemo-Johansson, J.**, Neumann, T., Jacobs, S., Lauten, A. and Landmesser, U., 2018. Repeated MitraClip procedure in patients with recurrent MR after a successful first procedure: limitations and outcome. Journal of interventional cardiology, 31(1), pp.83-90.

Braune, S., Basu, S., Kratz, K., **Johansson, J.B.**, Reinthaler, M., Lendlein, A. and Jung, F., 2016. Strategy for the hemocompatibility testing of microparticles. Clinical hemorheology and microcirculation, 64(3), pp.345-353.